

**THE BIOGEOCHEMICAL CYCLING AND ANTHROPOGENIC INPUTS OF
CADMIUM AND SILVER IN THE STRAIT OF GEORGIA, BRITISH COLUMBIA**

by

Cheng Kuang

B.Sc., The University of British Columbia, 2017

A THESIS SUBMITTED IN PARTIAL FULFILLMENT OF
THE REQUIREMENTS FOR THE DEGREE OF

MASTER OF SCIENCE

in

THE FACULTY OF GRADUATE AND POSTDOCTORAL STUDIES

(Oceanography)

THE UNIVERSITY OF BRITISH COLUMBIA

(Vancouver)

December 2019

© Cheng Kuang, 2019

The following individuals certify that they have read, and recommend to the Faculty of Graduate and Postdoctoral Studies for acceptance, a thesis/dissertation entitled:

The biogeochemical cycling and anthropogenic inputs of cadmium and silver in the Strait of Georgia, British Columbia

submitted by Cheng Kuang in partial fulfillment of the requirements for

the degree of Master of Science

in Oceanography

Examining Committee:

Roger Francois

Supervisor

Maria T. Maldonado

Supervisory Committee Member

Kristin Orians

Additional Examiner

Additional Supervisory Committee Members:

Urs Hafeli

Supervisory Committee Member

Abstract

We present the temporal and spatial variations of two toxic trace metals, cadmium (Cd) and silver (Ag) in the Salish Sea, with a focus on the southern Strait of Georgia (SoG). Our results from field measurements and a box model application show that conservative mixing between riverine discharge and oceanic input largely governs the distribution of dissolved Cd, and anthropogenic influence is negligible. Conservative mixing between low-Cd river water and high-Cd Pacific water largely governs the spatial distribution and temporal variability of dissolved Cd in the Salish Sea. Spatially, concentrations decrease as the Pacific source water flows from the deep basin of Juan de Fuca Strait (818 ± 6 pmol/kg) towards the SoG basin (maximum of 717 pmol/kg) due to riverine dilution. Time-series sampling in the southern SoG between 2017 and 2018 reveals a small but significant decrease of dissolved Cd concentrations (17 ± 7 pmol/kg) in deep waters during the winter. We attributed the decline to a downward flux of dissolved Cd across the sediment-water interface due to Cd sulfide precipitation in sediment porewaters. In addition, enrichment of particulate Cd at 50 m in the water column of the southern SoG may be reflective of sulfide formation within anaerobic microenvironments associated with sinking particles, potentially released from municipal effluent.

There is a scarcity of data on dissolved Ag in the open ocean and coastal waters due to analytical challenges in the quantitative determination of its extremely low concentrations in pristine environments. This study provides the first water column measurements of dissolved Ag in the SoG, using a commercially available seawater preconcentration system (*seaFAST*, Elemental Scientific) combined with analysis on an inductively coupled plasma mass spectrometer (ICP-MS). Dissolved Ag concentrations are variable with depth and season, ranging from 3.4 pmol/kg to 12.8 pmol/kg in the southern SoG. Results suggest that incorporation of dissolved Ag into sinking particles and subsequent desorption in deep waters play an important role in its biogeochemical cycling. Anthropogenic Ag loadings from three major sewage outfalls located in the Metro Vancouver and Capital Regional District are low compared to riverine and oceanic inputs.

Lay Summary

Cadmium and silver are naturally present at trace concentrations in the global oceans, yet they can be highly toxic to aquatic organisms at elevated levels. The overarching goal of this study is to understand the modes of addition, transport, and fate of cadmium and silver in the Strait of Georgia, as well as in the larger estuarine system of the Salish Sea. To achieve this goal, concentrations of dissolved and particulate cadmium and silver were analyzed in samples collected from the southern Strait of Georgia in different seasons between 2017 – 2018. Additional sampling was conducted across the Salish Sea in the summer of 2018 to determine the spatial distributions of dissolved cadmium and silver. Results of this study shed light on the physical, chemical, and biological processes that govern the distributions of cadmium and silver in the coastal waters off British Columbia.

Preface

Chapter 2

The Salish Sea Box Model was published by Wang, Pawlowicz, and Sastri (2019) in *the Journal of Geophysical Research: Oceans*, 124. <https://doi.org/10.1029/2018JC014766>. The model has been modified by Samuel Stevens (UBC) and used by me for interpretation of dissolved trace metal data collected in the Salish Sea.

Chapter 3 and 4

Municipal effluent samples were provided by Metro Vancouver and Capital Regional District every two months between 2017 and 2018. I collected dissolved and particulate trace metal samples in the Salish Sea aboard the CCGS Siyay, Moytel, and Vector from 2017 to 2018. I performed all sample preparation, ICP-MS measurements, and analysis of trace metal data. Salish Sea nutrient samples were collected by me and Iselle Flores Ruiz in the field and analyzed by Chris Payne (UBC) in the lab. Chlorophyll-a concentrations were collected and measured by Iselle Flores Ruize (UBC). Jay Cullen's lab shared dissolved trace metal samples collected at station P4 in the 2018 September Line P cruise. Robyn Taves collected and acidified the samples, and I processed them for analysis on the ICP-MS.

I generated all figures and tables (unless otherwise referenced) and wrote the main text of this thesis. Roger Francois provided important suggestions for revision and also edited the chapters. Maria T. Maldonado gave valuable feedbacks and edits for the chapters.

Table of Contents

Abstract	iii
Lay Summary.....	iv
Preface	v
Table of Contents.....	vi
List of Tables.....	xi
List of Figures	xiv
List of Symbols.....	xxi
List of Abbreviations	xxii
Acknowledgements	xxiii
Chapter 1: General introduction.....	1
1.1 Metro Vancouver’s Georgia Strait Ambient Monitoring Program	1
1.2 Environmental setting.....	1
1.3 Water circulation	2
1.4 Primary productivity.....	5
1.5 Municipal effluent discharge into the Salish Sea	6
1.6 Contribution of thesis to the Metro Project	6
Chapter 2: Materials and methods	8
2.1 Sampling locations and methods	8
2.1.1 Water column sampling in the Salish Sea	8
2.1.2 Municipal effluent sampling.....	10
2.2 Analytical methods.....	11

2.2.1	Dissolved Cd and Ag in seawater.....	11
2.2.2	Particulate Cd and Ag in seawater.....	15
2.2.3	Dissolved and total Cd and Ag in municipal effluent	16
2.2.4	Salish Sea Box Model.....	17
Chapter 3: Biogeochemical cycling and anthropogenic input of cadmium in the Strait of Georgia		19
3.1	Introduction	19
3.1.1	Sources of Cd in the environment	19
3.1.2	Biogeochemical cycling of Cd in the ocean	19
3.1.3	Previous information on Cd in the SoG.....	21
3.2	Results	22
3.2.1	Temporal variations of water properties in the southern SoG.....	23
3.2.1.1	Temperature, salinity, and density.....	23
3.2.1.2	Oxygen concentration and apparent oxygen utilization	25
3.2.1.3	Macronutrients and chlorophyll-a	26
3.2.1.4	Dissolved Cd concentrations	28
3.2.2	Spatial distributions of water properties in the Salish Sea	29
3.2.2.1	Temperature, salinity, and density in the Salish Sea	29
3.2.2.2	Dissolved Cd concentrations in the Salish Sea.....	31
3.2.3	Particulate Al, P, and Cd in the southern SoG.....	32
3.2.4	Concentrations and fluxes of dissolved and total Cd in municipal effluent.....	34
3.3	Discussion.....	36
3.3.1	Natural sources of dissolved Cd to the Salish Sea.....	36

3.3.1.1	Freshwater end member.....	37
3.3.1.2	Pacific end member	41
3.3.1.3	Box model application for spatial distributions of dissolved Cd.....	42
3.3.2	Anthropogenic input of Cd to the Salish Sea	45
3.3.3	Temporal variations of dissolved Cd in the southern SoG.....	48
3.3.3.1	Surface layer (0 – 50 m).....	48
3.3.3.2	Intermediate layer (50 – 200 m).....	51
3.3.3.3	Deep layer (> 200 m).....	54
3.3.4	Particulate Cd concentrations in the southern SoG	58
3.3.4.1	Sources of particulate Cd.....	58
3.3.4.2	Particulate Cd enrichment in particle microenvironment.....	61
3.3.5	Seawater – particle – sediment interactions and the decoupling between dissolved Cd, NO ₃ ⁻ , and PO ₄ ³⁻ in the water column of SoG.....	64
3.3.6	Cd mass balance in the SoG	67
3.4	Conclusions for Cd.....	69

Chapter 4: Biogeochemical cycling and anthropogenic input of silver in the Strait of

Georgia	71	
4.1	Introduction	71
4.1.1	Sources of Ag in the environment	71
4.1.2	Biogeochemical cycling of Ag in the ocean.....	72
4.1.3	Previous information on Ag in the SoG	74
4.2	Results	75
4.2.1	Temporal and spatial variations of dissolved Ag in the Salish Sea.....	75

4.2.2	Particulate Ag concentrations in the southern SoG	77
4.2.3	Concentrations and fluxes of dissolved and total Ag in municipal effluents	78
4.3	Discussion.....	80
4.3.1	Ag inputs from natural and anthropogenic sources	80
4.3.1.1	Dissolved Ag input from continental runoff.....	80
4.3.1.2	Dissolved Ag input from the Pacific Ocean	84
4.3.1.3	Anthropogenic input of Ag from municipal effluent.....	85
4.3.2	Temporal variations and spatial distributions of dissolved Ag	86
4.3.2.1	Temporal trends of dissolved Ag in the southern SoG.....	86
4.3.2.2	Spatial distributions of dissolved Ag in the Salish Sea	89
4.3.2.3	Propagation of seasonal variations of dissolved Ag.....	90
4.3.3	Sources of particulate Ag in the southern SoG.....	95
4.4	Conclusions for Ag.....	101
Chapter 5: Conclusions		103
5.1	Major findings of study	103
5.1.1	Biogeochemical cycling of Cd in the SoG	103
5.1.2	Distribution of dissolved Ag in the SoG	104
5.2	Future studies.....	104
Bibliography.....		106
Appendices		111
Appendix A. Supplementary figures		111
Appendix B. Supplementary tables		113

Appendix C. Preliminary laboratory experiments to determine dissolved Ag uptake rates by SoG calanoid copepods (*Metridia pacifica*) and by a model diatom (*Thalassiosira oceanica*) 124

C.1. Uptake of dissolved Ag by calanoid copepods in the SoG..... 124

C.2. Uptake of dissolved Ag by marine phytoplankton 126

List of Tables

Table 2.1 Seawater sampling locations, water depths, and time of sampling in the Salish Sea....	10
Table 2.2. Average procedural blanks and detection limits for three analytical runs utilizing the seaFAST sample preconcentration system followed by ICP-MS. Detection limits are calculated as three times the standard deviation of the procedural blank. *The Ag blank and detection limit reported for the 1 st run are likely overestimates of the true values due to suspected contamination.	14
Table 2.3. Summary of repeated measurements (± 1 SD) of certified reference material CASS-6 purchased from the National Research Council Canada in all three analytical runs.....	15
Table 2.4. Summary of repeated measurements (± 1 SD) of a sample collected from 600 m at Ocean Station Papa (OSP) during the August 2013 Line P cruise in all three analytical runs. Sample was provided by Dr. Kristin Orian’s research group (UBC), courtesy of Nari Sim.	15
Table 3.1. Concentrations of total and dissolved Cd in wastewater samples measured in influent and effluent from the Iona WWTP, and screened samples from Macaulay Point and Clover Point outfalls. Particulate Cd* is calculated by subtracting measured concentrations of dissolved Cd from the total. Red indicates values that exceed the BC Water Quality Guidelines for total Cd in marine waters (1060 pM) without dilution.....	35
Table 3.2. Average concentrations and annual fluxes of total, dissolved, and particulate Cd measured between 2017 and 2018 from three outfalls (Iona WWTP, Macaulay Point, and Clover Point). Particulate Cd* is calculated by subtracting measured concentrations of dissolved Cd from the total. Total annual flow rates are reported for 2018 (Metro Vancouver and Capital Regional District, personal communication).....	36

Table 3.3. Model outputs for dissolved Cd with various Pacific input (which requires a unit in pM) . * indicates that June 2018 is an exception, where model output is greater than the average dissolved Cd concentration measured in the upper 50 m of SoG.....44

Table 3.4. Volume fluxes, average concentrations and loadings of dissolved Cd in effluent discharged from the Iona WWTP, from riverine input (mainly Fraser River), and from the upwelled Pacific water. Volume flux from the Iona WWTP is based on the 2018 flow data (Metro Vancouver, personal communication). Box model outputs are indicated by asterisk (*). 48

Table 3.5. Concentrations of pCd, pAl, pP measured in the water column of station S4-1.5 in December 2017. The lithogenic fraction of P and Cd is calculated based on the molar crustal ratio of P/Al (0.008) and Cd/Al (3E-7), respectively (Taylor & McLennan, 1995). The biogenic fraction of P is calculated as the difference between the total and the lithogenic P concentrations. The ratios between pCd and biogenic P are shown to compare with the average phytoplankton Cd: P quota (0.21 pmol/nmol; Ho et al., 2013).59

Table 3.6. Concentrations of pCd, pAl, pP measured in the water column of station S4-1.5 in April 2018. The lithogenic fraction of P and Cd is calculated based on the molar crustal ratio of P/Al (0.008) and Cd/Al (3E-7), respectively (Taylor & McLennan, 1995). The biogenic fraction of P is then calculated as the difference between the total and the lithogenic concentrations. The ratios between pCd and biogenic P are also shown to compare with the average phytoplankton Cd: P quota (0.21 pmol/nmol; Ho et al., 2013).60

Table 4.1. Concentrations of total and dissolved Ag in wastewater samples measured in influent and effluent from the Iona WWTP, and screened samples from Macaulay Point and Clover Point outfalls. Red indicates levels that exceed the BC Water Quality Guidelines for total Ag in marine waters (27.8 nM) without dilution.....79

Table 4.2. Average concentrations and annual fluxes of total, dissolved, and particulate Ag measured between 2017 and 2018 from three outfalls (Iona WWTP, Macaulay Point, and Clover Point). Particulate Ag* is calculated by subtracting measured values of dissolved Ag from the total. Total annual flow rates reported for the year of 2018 (Metro Vancouver and Capital Regional District, personal communication).....80

List of Figures

Figure 1.1. A map of the Salish Sea, which is comprised of the Strait of Georgia, Juan de Fuca Strait, and Puget Sound and all adjoining waters.	2
Figure 1.2. Schematic circulation in the Salish Sea taken from Pawlowicz et al., (2019). a) Summer circulation when the deep water of the SoG is being renewed. b) Circulation during the rest of the year when deep water is stagnant.	3
Figure 2.1. Locations of municipal sewage outfalls (black triangles) and water column sampling stations (red diamonds) in the Salish Sea. Stations P4 and JF2 (red circle) along the Line P transect sample the oceanic source water that fuels the Salish Sea.	9
Figure 2.2. Post-column extraction standard curves for a surface sample (10 m) and a deep sample (100 m) collected in June 2018. The counts of Ag-107 are normalized by the internal standard (In-115).	13
Figure 2.3. Relationship between sample salinity and the slope of post-column standard curves for Ag analysis in coastal seawater collected in the Salish Sea.	13
Figure 2.4. Box model schematic diagram modified from Wang et al., (2019). The system has 3 basins: Strait of Georgia (SoG), Haro Strait (HS), and Juan de Fuca Strait (JF). Each basin is divided into an upper layer (0-50m) and a lower layer (50 m to bottom). River discharge is denoted by \tilde{F} (m^3/s). Q_g and Q_h represent the volume flux (m^3/s) between the upper boxes of HS & SoG, and HS & JF, respectively. The thick arrows between upper and lower boxes in the three basins denote vertical mixings.	18

Figure 3.1. Depth profiles of temperature and salinity in the water column (A: top 50 m; B: 50 – bottom waters) of the southern Strait of Georgia at station S4-1.5 from September 2017 to August 2018.....23

Figure 3.2. Depth profiles of density (sigma-theta) in the water column (A: top 50 m; B: 50 – bottom waters) of the southern Strait of Georgia at station S4-1.5 from September 2017 to August 2018.....24

Figure 3.3. Depth profiles of dissolved oxygen and apparent oxygen utilization (AOU) in the water column of the southern Strait of Georgia at station S4-1.5 from September 2017 to August 2018. AOU is calculated as the difference between oxygen at saturation (determined by in-situ water temperature and salinity), and measured oxygen concentrations.26

Figure 3.4. Concentrations of macronutrients (nitrate, phosphate, silicic acid) measured in the water column of the southern Strait of Georgia at station S4-1.5 from September 2017 to August 2018.27

Figure 3.5. Chlorophyll-a concentrations measured in the upper 30 m at station S4-1.5 from September 2017 to August 2018.27

Figure 3.6. Depth profiles of dissolved Cd at station S4-1.5 from Sep. 2017 to Aug. 2018. Error bars for dissolved Cd concentrations represent one standard deviation of analytical uncertainty.28

Figure 3.7. Depth profiles of temperature, salinity, and density at stations located in the northern strait (NG), southern strait (S4-1.5), Haro Strait (HS), and Juan de Fuca Strait (JF2) in August 2018. Salinity data at station P4 were obtained from the Line P program data archived for the September 2018 cruise (Institute of Ocean Sciences, 2019).30

Figure 3.8. Depth profiles of dissolved Cd in the Salish Sea at stations located in the northern strait (NG), southern strait (S4-1.5), Haro Strait (HS), and Juan de Fuca Strait (JF2) in August 2018. Dissolved Cd concentration were also measured in four samples collected at station P4 during the September 2018 Line P cruise (samples were provided by Dr. Jay Cullen’s lab in University of Victoria).....32

Figure 3.9. Depth profiles of particulate Al, P, and Cd at station S4-1.5 in December 2017 and April 2018. Error bars represent one standard deviations of analytical uncertainty.33

Figure 3.10. Percentage of transmission based on in-situ CTD measurements in the water column at station S4-1.5 in December 2017 and April 2018.34

Figure 3.11. Time series (2011-2018) of freshwater discharge, dissolved Cd concentration, and dissolved Cd flux. Discharge is based on measurements from Fraser River at Hope and Englishman River by Water Survey of Canada. Dissolved Cd concentrations were obtained from the Fraser River Water Quality Buoy located in the Main Arm of the river (Environment and Climate Change Canada, 2018).....39

Figure 3.12. Total river discharge rate (top), dissolved Cd concentrations measured in the Fraser River Main Arm (centre), and dissolved Cd fluxes from rivers (bottom) all plotted against months. Black empty circles are data shown in Figure 3.11. Orange filled squares are calculated averages ± 1 SD for each time interval with relatively constant river discharge and dissolved Cd concentration.40

Figure 3.13. A) Salinity profiles at stations JF2 (red) and P4 (black) on the Line P cruise track in February (dash line) and September (solid line) 2018. Hydrographic data were obtained from the Line P program online data archive (Institute of Ocean Sciences). B) Dissolved Cd profiles for

the entire water column at station P4 during the August 2012 cruise (Janssen et al., 2017), and selected samples (25 m – 400 m) measured from the September 2018 cruise.....42

Figure 3.14. Modelled vs measured salinity in the Strait of Georgia upper (SoGu), Strait of Georgia lower (SoGl), Haro Strait upper (HSu), Haro Strait lower (HSl), Juan de Fuca Strait upper (JFu), and Juan de Fuca Strait lower (JFl) boxes. Upper boxes represent water column from the surface to 50 m, and lower boxes are 50 m to the bottom. Filled and empty circles represent the average salinity in the upper (0 – 50 m) and lower (50 m – bottom) boxes, respectively, based on CTD profiles collected at station S4-1.5 (Strait of Georgia) between February 2017 to August 2018, as well as at stations JF2 (Juan de Fuca Strait) and HS (Haro Strait) in August 2018.....43

Figure 3.15. Modelled vs measured dissolved Cd concentrations in the Strait of Georgia upper (SoGu), Strait of Georgia lower (SoGl), Haro Strait upper (HSu), Haro Strait lower (HSl), Juan de Fuca Strait upper (JFu), and Juan de Fuca Strait lower (JFl) boxes. Upper boxes represent water column from the surface to 50 m, and lower boxes are 50 m to the bottom. Model results are based on the best fit Pacific input (650 + 300 pM; Table 3.3). Filled and empty circles are field measurements for dissolved Cd in the upper (average concentrations between 0 and 50 m) and lower (average concentrations below 50 m) boxes, respectively.45

Figure 3.16. Box model outputs for the Pacific and freshwater volume fluxes into the Salish Sea.47

Figure 3.17. Temporal variations of salinity measured at 50 m, 100 m and 200 m from all CTD casts done at station S4-1.5.....53

Figure 3.18. Bottom current speed (green curves) and seawater densities (red curves) at Ocean Networks Canada’s Central node (49.0423°N 123.3171°W, water depth 300 m; Ocean Networks

Canada) in the Strait of Georgia in 2017 (A) and 2018 (B). Grey shaded regions are periods of weak tidal mixing based on tidal predictions. Black arrows indicate deep water renewal seasons. Figure and caption are modified from the UBC-Metro 2018 report (Pawlowicz, Francois, & Maldonado, 2018).....55

Figure 3.19. Concentrations of dissolved Cd plotted against salinity for December 2017 samples (> 0 m) and two bottom samples in April 2018 (exact depths: 239 m and 287 m). A linear fit for the December 2017 data (11 depths in total, excluding the 0 m sample) is used as the winter mixing line between SoG and riverine input.57

Figure 3.20. Depth profiles of total particulate Cd concentrations measured in April 2018 at station S4-1.5. The biogenic fraction of particulate Cd is estimated based on the phytoplankton dCd: PO₄³⁻ uptake ratio (0.04 pmol/nmol) in April. The lithogenic fraction is calculated using the crustal abundance of Cd/Al (3×10^{-7} mol pCd per mol of pAl).61

Figure 3.21. Depth profiles of the estimated authigenic pCd concentrations in marine particles collected in December 2017 and April 2018 at station S4-1.5.....63

Figure 3.22. Depth profiles of dissolved oxygen (CTD), N*, Cd* at station S4-1.5 in December 2017 and April 2018.66

Figure 3.23. Modelled vs measured dissolved Cd concentrations in the Strait of Georgia upper (SoGu), Strait of Georgia lower (SoGl), Juan de Fuca Strait upper (JFu), and Juan de Fuca Strait lower (JFl) boxes. Filled and empty circles are field measurements for dCd in the upper and lower boxes, respectively. Red circles represent average dCd concentrations measured in the SoG, while green circles represent Juan de Fuca Strait measurements. Uncertainties in the modelled data are illustrated by the upper and lower boundaries plotted for each box. Field measurements that do not fit with the model predictions are enclosed in a square.....68

Figure 4.1. Depth profiles of dissolved Ag at station S4-1.5 from September 2017 to August 2018. Error bars represent one standard deviation of the analytical uncertainty.76

Figure 4.2. Depth profiles of dissolved Ag at stations located in the northern strait (NG), southern strait (S4-1.5), Haro Strait (HS), and Juan de Fuca Strait (JF2) in August 2018. Dissolved Ag concentration were also measured in four samples collected at station P4 during the September 2018 Line P cruise (samples were provided by Dr. Jay Cullen’s lab in University of Victoria). Error bars represent one standard deviation of the analytical uncertainty.....77

Figure 4.3. Depth profiles of particulate Al, P, and Ag at station S4-1.5 in December 2017 and April 2018. Error bars represent one standard deviations of analytical uncertainty.78

Figure 4.4. Time series (2011-2018) of freshwater discharge, dissolved Ag concentration, and dissolved Ag flux. Discharge is based on measurements from Fraser River at Hope and Englishman River by Water Survey of Canada. Dissolved Ag concentrations were obtained from the Fraser River Water Quality Buoy located in the Main Arm of the river (Environment and Climate Change Canada, 2018).82

Figure 4.5. Total river discharge rate (top), dissolved Ag concentrations measured in the Fraser River Main Arm (center), and dissolved Ag fluxes from rivers (bottom) all plotted against months. Black empty circles are data shown in Figure 4.4. Orange filled squares are calculated averages ± 1 SD for each time interval with relatively constant river discharge and dissolved Ag concentration.83

Figure 4.6. Dissolved Ag profile (20 – 200 m) reported for nearshore station P4 along the Line P transect during the February 2005 cruise (Kramer et al., 2011), and selective samples (25 m – 400 m) measured in the September 2018 cruise. Dissolved Ag are reported in the unit of pM by Kramer et al., and in pmol/kg for this study.84

Figure 4.7. Depth profiles of temperature at the southern SoG (station S4-1.5) in June and August 2018, and at the northern SoG (station NG) in August 2018.....91

Figure 4.8. Depth profiles of dissolved Ag at the southern SoG (station S4-1.5) in June and August 2018, and at the northern SoG (station NG) in August 2018.....92

Figure 4.9. Modelled vs measured dissolved Ag concentrations in the Strait of Georgia upper (SoGu), Strait of Georgia lower (SoGl), Haro Strait upper (HSu), Haro Strait lower (HSl), Juan de Fuca Strait upper (JFu), and Juan de Fuca Strait lower (JFl) boxes. Upper boxes represent water column from the surface to 50 m, and lower boxes are 50 m to the bottom. Model results are based on a Pacific input of 5 pM (A) and 10 pM (B). Filled and empty circles are field measurements for dissolved Ag in the upper (average concentrations between 0 and 50 m) and lower (average concentrations below 50 m) boxes, respectively. Field measurements that match with the model predictions for JFl and SoGl boxes are enclosed in a square.94

Figure 4.10. Depth profile of particulate Ag: particulate Al ratios at station S4-1.5 in December 2017 and April 2018. The red vertical line indicates the average Ag: Al crustal ratio (Taylor and McLennan, 1995). Error bars represent one standard deviation of the analytical uncertainty.....96

Figure 4.11. Correlation between particulate organic matter (POM) estimated from biogenic P, and lithogenic content estimated from Al in particulate samples collected in December 2017 and April 2018 at station S4-1.5 in the SoG.....98

Figure 4.12. A) Correlation between measured pAg concentrations and the lithogenic fraction estimated from pAl. B) Correlation between excess pAg concentrations (difference between measured and predicted from lithogenics) and the particulate organic matter (POM) content estimated from biogenic P in particulate samples collected in December 2017 and April 2018 at station S4-1.5 in the SoG..... 100

List of Symbols

Al	Aluminum
Ag	Silver
Ag ₂ S	Silver sulfide
Cd	Cadmium
CdS	Cadmium sulfide
Cd*	Cd star
HCl	Hydrochloric acid
HNO ₃	Nitric acid
HClO ₄	Perchloric acid
H ₂ O ₂	Hydrogen peroxide
H ₂ SO ₄	Sulfuric acid
M	Molar
NO ₃ ⁻	Nitrate
N*	N star
P	Phosphorous
PO ₄ ³⁻	Phosphate
SO ₄ ²⁻	Sulfate
Si(OH) ₄	Silicic acid
Zn	Zinc
ZnS	Zinc sulfide
μmol/kg	Micromole/kilogram

List of Abbreviations

AOU	Apparent oxygen utilization
BC	British Columbia
CA	Carbonic anhydrase
CTD	Conductivity-temperature-depth instrument
dCd	Dissolved cadmium
dAg	Dissolved silver
HEPA-filters	High efficiency particulate air filters
ICP-MS	Inductively coupled plasma mass spectrometry
OSP	Ocean Station Papa
pAl	Particulate aluminum
pAg	Particulate Ag
pCd	Particulate Cd
pP	Particulate phosphorous
SD	Standard deviation
SoG	Strait of Georgia
WWTP	Wastewater treatment plant

Acknowledgements

First and foremost, I would like to thank Dr. Roger Francois and Dr. Maria T. Maldonado for being the best supervisors any students could ever ask for. Thank you, Roger for being my mentor since I was an undergraduate student seeking Co-op opportunities in your lab. You've introduced me to the world of oceanography and gave me a memorable experience to work in the Arctic Ocean as a science fellow. I could not thank you enough for your relentless support and guidance throughout my academic journey. Your easy-going spirit, creative thinking, pursuit for academic excellence, and passion for wonderful creations in life such as beer, snowboarding, and mountains all make you a great role model in life.

Maite, thank you for always believing in me, especially during times when nothing seemed to be working. Your positive spirit and kind words have encouraged me to never give up, no matter how frustrating life can get sometimes. You are resourceful and are constantly seeking great opportunities for your students. Thank you for introducing me to the IsoSiM program, which helped me with establishing a career path after graduate school.

I would like to thank Maureen Soon for sharing your expertise in laboratory work and for being there for me since day one. You are the warmest and kindest person I have truly bonded with outside of my family. Thank you for trusting me, listening to my frustrations, and witnessing many significant milestones in my life.

I also thank my teammates, Iselle Flores Ruiz, Yuanji Sun, and Samuel Stevens for being on the same boat with me for this project. Many thanks to Iselle for sharing so much laughter and tears while working in the lab. Thank you, Sam for your time and help with the Box Model. A special thank you to Dr. Rich Pawlowicz for sharing your wisdom on the physical circulation of the Salish Sea.

I am also grateful to captains and crew members of the CCGS Siyay, Moytel, and Vector who made this work possible at sea. A big thank you to Chris Payne for your hard work and tremendous help in cruises, whether on calm or rough days. I am thankful for being able to analyze many of

my samples in the Pacific Centre for Isotopic and Geochemical Research. A special thank you to Vivian for always giving great suggestions and making sure my ICP-MS runs go smoothly.

I thank Metro Vancouver and the IsoSiM program for funding this research. I would also like to acknowledge that a fundamental dataset of this thesis was analyzed in the University of Victoria under the supervision of Dr. Jay Cullen. Thank you, Jay for offering me the opportunity to use the *seaFAST* for my dissolved metals analysis. This work would not have been possible without your generous help. Thank you, Jody, for being so flexible and accommodating with running my samples on the triple Quadrupole ICP-MS.

Finally, I would like to express my appreciation to my family, especially my mom and my fiancé for their selfless love and support.

Chapter 1: General introduction

1.1 Metro Vancouver's Georgia Strait Ambient Monitoring Program

The Georgia Strait Ambient Monitoring Program was initiated by Metro Vancouver in 2004 to establish baseline environmental quality data and monitor the impact of liquid waste discharge on the receiving water bodies (Metro Vancouver, 2018). In 2013, Metro Vancouver started a collaboration with the Department of Earth, Ocean, and Atmospheric Sciences at UBC with an overarching goal of understanding the modes of addition, transport, and removal of organic pollutants and toxic trace metals in the Strait of Georgia. This work is referred to as the Metro Project in the following sections of thesis. There are multiple aspects to the Metro Project, which include 1) Characterizing the general water circulation patterns in the Strait 2) Understanding how physical circulation and mixing affect the dispersion of particles from natural and anthropogenic sources 3) Determining the fate of contaminants in discharged municipal effluent and its ecological impact on the Strait of Georgia.

1.2 Environmental setting

The Strait of Georgia (SoG) is a semi-enclosed seawater basin bounded by Vancouver Island on the west, and the mainland of British Columbia (B.C.) on the east (Figure 1.1). It is one of the three major water bodies in the Salish Sea, a network of coastal waters including Juan de Fuca Strait, Puget Sound, and all channels connecting them. The SoG basin is about 200 km long and 30 km wide (Pawlowicz et al., 2007). It is subdivided into a northern and a southern basin, separated by a 170 m sill to the southwest of Texada Island (Figure 1.1). The southern regions make up 70% and 75% of the total surface area and volume of the SoG, respectively, with a maximum depth exceeding 400 m compared to 350 m for the northern basin (Pawlowicz et al., 2007).

The SoG is connected to the Pacific Ocean via complexes of channels at the northern and southern ends of the basin where intense tidal mixing takes place. Most water exchange (> 90%) with the Pacific occurs in the southern passages via deeper and wider channels in the Haro Strait region (Figure 1.1). The water column of the SoG is subdivided into three distinct layers (Figure 1.2): the

surface layer down to 50 m, which has relatively low salinity due to freshwater input; the intermediate layer between 50 m and 200 m, which is continuously renewed by shallow Pacific intermediate water; and the deep layer below 200 m, which is periodically renewed during the summer upwelling by deeper and denser Pacific water (Pawlowicz et al., 2019; Pawlowicz et al., 2007).

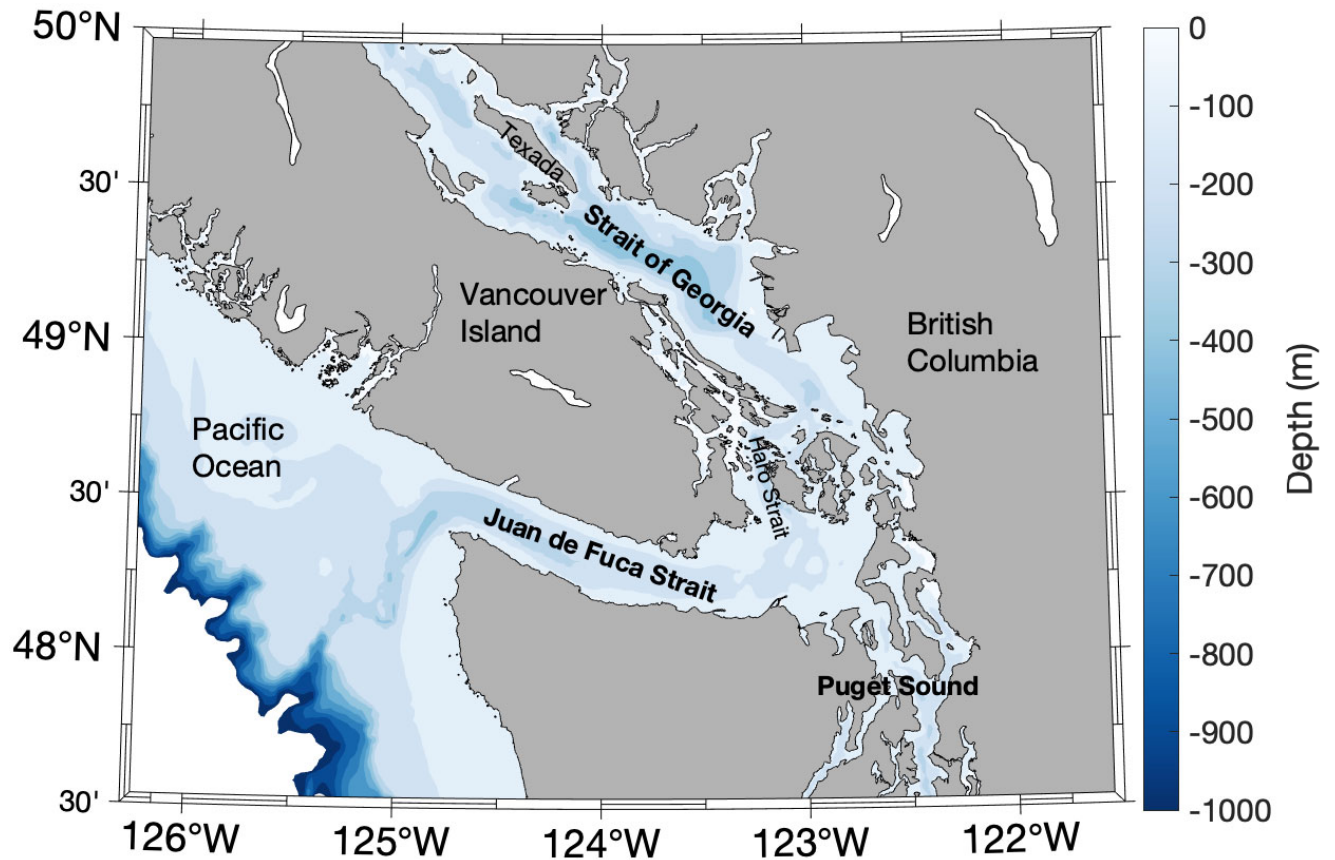


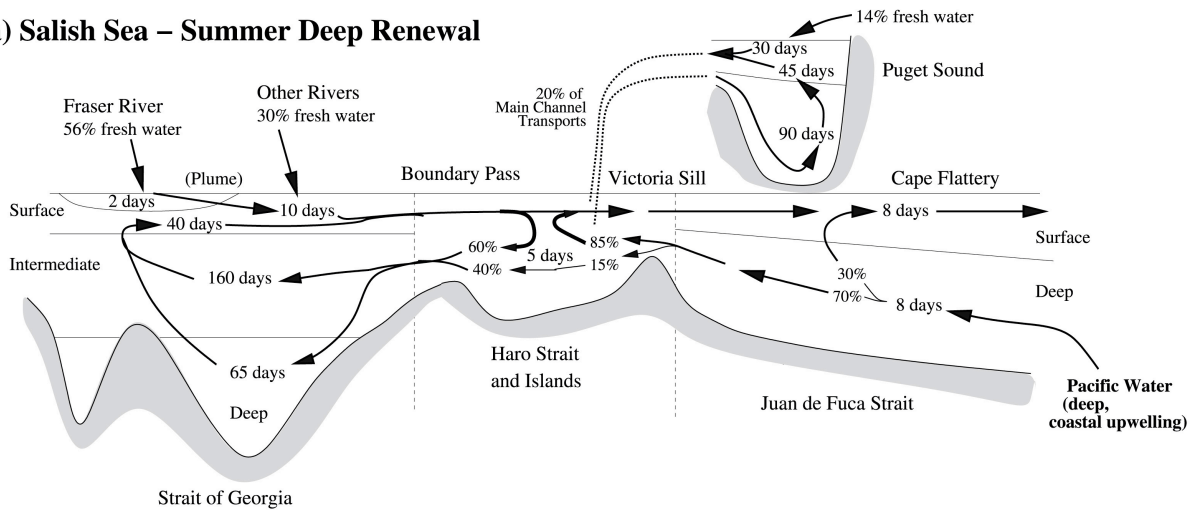
Figure 1.1. A map of the Salish Sea, which is comprised of the Strait of Georgia, Juan de Fuca Strait, and Puget Sound and all adjoining waters.

1.3 Water circulation

The water circulation in the Salish Sea is estuarine in nature, with relatively fresh surface water from the SoG flowing seaward, and saltier Pacific water entering the SoG at depth via Juan de Fuca and Haro Strait (Li et al., 2000). The main source of freshwater is the Fraser River which drains into the southern SoG, forming a thin plume of brackish water that spreads over the more

saline oceanic water (Wang et al., 2019). As a result, the surface layer of the southern SoG is strongly influenced by seasonal variations in the Fraser River discharge, which reaches its maximum in June. The large input of freshwater during peak flow season results in strong stratification in the upper water column, especially in the southern SoG given its proximity to the Fraser river mouth.

a) Salish Sea – Summer Deep Renewal



b) Salish Sea – Rest of Year

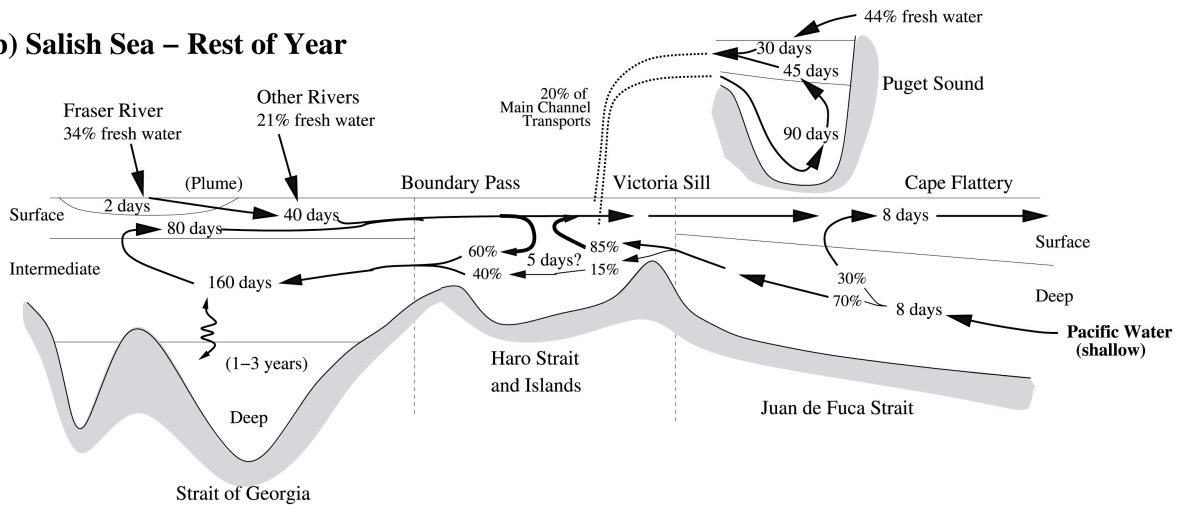


Figure 1.2. Schematic circulation in the Salish Sea taken from Pawlowicz et al., (2019). a) Summer circulation when the deep water of the SoG is being renewed. b) Circulation during the rest of the year when deep water is stagnant.

Pacific water enters the Salish Sea through the 100 km long Juan de Fuca Strait (Pawlowicz et al., 2007). During summer, the prevailing northerly winds offshore of Vancouver Island produce coastal upwelling which feeds deeper, oxygen depleted and nutrient rich water to Juan de Fuca Strait through a deep canyon dissecting the continental shelf (Figure 1.2a; Pawlowicz et al., 2019). In contrast, the prevailing offshore winds are southerly in the winter, transporting surface waters towards the coast and lowering the salinity of deeper waters via downwelling. The Pacific water entering Juan de Fuca Strait at this time of the year originates from shallower depths, thus contains higher oxygen and lower nutrient concentrations.

Inflowing Pacific water transits through the gradually shoaling Juan de Fuca Strait in about a week and it flows over the Victoria sill to reach Haro Strait (Figure 1.2). In the Haro Strait basin, the water is subject to strong tidal currents that vigorously mix the entire water column (Thomson, 1981). Incoming Pacific water and outflowing SoG surface water enter Haro Strait in a 40:60 ratio (Figure 1.2; Pawlowicz et al., 2019), and the well-mixed water subsequently flows into the intermediate layer of the SoG and gradually upwells into the surface layer as part of the estuarine circulation system (Pawlowicz et al., 2007). Intense mixing with the well-oxygenated surface water in Haro Strait elevates the concentration of dissolved oxygen relative to its Pacific source water, leading to an oxic environment throughout the water column of the SoG (Johannessen, Masson, & Macdonald, 2014).

The extent of mixing in Haro Strait varies with the fortnightly tidal cycle, and deep water renewal events occur when the density of bottom waters peaks near the sill areas, coinciding with periods of weak tidal mixing (Masson, 2002). Discrete renewal events allow pulses of relatively dense water to flow over the Victoria and Boundary Pass sills (Figure 1.2) during every second neap tides between the end of spring and early fall. The denser water intrudes the deep basin of SoG and replaces the old bottom water. The replacement water in the late summer renewal period is saltier, warmer and less oxygenated than in the spring. These successive cascading events end when the northerly offshore winds weaken in early fall. The deep water in the SoG remains stagnant through winter, and its density decreases from diffusion with the lighter water above,

allowing the relatively dense Pacific inflow to displace the old water during the next deep-water renewal season (Masson, 2002).

The temperature and dissolved oxygen concentrations of seawater in the well-mixed water column of Haro Strait varies seasonally with air temperature. Seasonal cycles of water properties propagate into the intermediate layer of the SoG with a time delay that can be used to estimate the residence time and transit time of intermediate waters in the SoG (Pawlowicz et al., 2007; Stevens and Pawlowicz, in prep). Using hydrographic datasets collected over the entire SoG, Stevens and Pawlowicz (in prep) mapped the delay in timing of the coldest temperature water observed across the SoG relative to its source water in Haro Strait. They estimated a transit time of approximately 3 months for the intermediate water to travel from Haro Strait to the northern SoG basin. A similar result was obtained when tracking water with the lowest dissolved oxygen concentration along the path. They also found that the amplitude of seasonal variations is dampened as the water flows northward into the SoG basin due to mixing with surrounding waters.

1.4 Primary productivity

Coastal upwelling brings high-nutrient Pacific water into the deep basin of Juan de Fuca Strait. Some nutrients are brought to shallow waters in Haro Strait by tidal mixing and then exported as part of the surface outflow, while the remaining flows into the SoG at intermediate and deep depths (Figure 1.2; Li et al., 2000). In the SoG water column, estuarine circulation drives the vertical entrainment of nutrients from deep waters into the surface layer for biological utilization (Yin et al., 1997). Seasonal variations of nutrients in the SoG are largest in surface waters, where significant drawdown of macronutrients (nitrate, phosphate, and silicic acid) has been observed in early April during the spring phytoplankton bloom (Pawlowicz et al., 2007). Satellite data show that the average surface chlorophyll-a concentrations in the SoG are twice as high as other regions along the coast of Northeast Pacific (Jackson et al., 2015). The high primary productivity in the SoG supports a diverse ecosystem with iconic resident species such as the Pacific herring, salmon, and killer whales (Masson & Perry, 2013).

1.5 Municipal effluent discharge into the Salish Sea

The SoG is not only home to numerous marine species, it is also located in close proximity to roughly 70% of B.C.'s population (Thomson, 1981). It is bounded by two metropolitan areas: Metro Vancouver (population 2.46 million; 2016 census) on the east, and Victoria's Capital Regional District (population 0.38 million) on the west. With a growing human population around the SoG, it is inevitably subject to anthropogenic stressors such as fishing, aquaculture, commercial shipping and wastewater discharge (Masson & Perry, 2013). There are five wastewater treatment plants (WWTPs) located in Metro Vancouver, which discharge approximately 4.5×10^{11} L of treated effluent annually (Metro Vancouver, 2018). In the Capital Regional District, wastewater from two main outfalls (Macaulay and Clover Points) is screened through a coarse mesh before being discharged into the receiving water bodies at an annual flow rate of roughly 3.2×10^{10} L (Capital Regional District, 2016).

Among the five WWTPs in Metro Vancouver, three of them (Annacis Island, Lulu Island, Northwest Langley) discharge secondary treated effluent into the lower Fraser River (Metro Vancouver, 2018). The other two (Iona Island and Lions Gate) provide primary wastewater treatment before discharging into the SoG and Burrard Inlet, respectively. The Iona Island outfall accounts for about 45% of the total wastewater discharge in Metro Vancouver (2018). Municipal wastewater can be point sources for various contaminants (e.g., pathogenic microorganisms, heavy metals, persistent organic pollutants) in aquatic systems. The potential adverse effects of wastewater discharge are dependent on both the quality of treatment effluent, and specific characteristics (e.g., hydrography, water circulation, sedimentation rate) of the receiving environment.

1.6 Contribution of thesis to the Metro Project

This thesis aims to provide the first water column measurements of two toxic trace metals, cadmium (Cd) and silver (Ag) in the SoG. Dissolved Cd concentrations in coastal waters off B.C. require attention because farmed oysters have been found to accumulate Cd from the dissolved phase to levels that exceed export limits ($> 2 \mu\text{g/g}$ wet weight), restricting access to lucrative international markets (Kruzynski, 2004). The problem arises in part from the naturally high

dissolved Cd concentration in the Pacific Ocean relative to that in the Atlantic, due to the accumulation of Cd from sinking particles along the thermohaline circulation in the global ocean (Bruland & Franks, 1983). Coastal waters of B.C. require close monitoring to ensure that anthropogenic activities do not further increase dissolved Cd concentrations in the receiving environment. Similarly, Ag is classified as an environmental hazard because it is a toxic pollutant with a strong tendency to bioaccumulate in aquatic organisms (Luoma, 2008). With the advent of nanotechnology, nanoscale particles (1-100 nm) comprised of Ag are widely used in medical applications and consumer products for their antibacterial property. With the commercialization of nanosilver, more Ag is expected to be released into the aquatic environment through wastewater discharge. Hence, monitoring is required at both point sources (WWTPs) and in the receiving aquatic environment to assess the impact of anthropogenic Ag inputs on water quality and biota.

This study has two overarching goals: 1) Determine the temporal variability and spatial distribution of dissolved Cd and Ag in the SoG, and understand how physical circulation, biological cycling and particle interactions can affect their dispersion and removal from the water column. 2) Assess whether municipal effluent from two populated urban centers are significant point sources of Cd and Ag to the SoG compared to their natural inputs. Chapter 2 gives an overview of the sampling techniques employed in the field and the analytical methods used in the laboratory. It also describes the Salish Sea box model (Wang et al., 2019), which was applied to help interpret dissolved metals data. Chapter 3 and 4 focus on the biogeochemical cycling and dispersion of Cd and Ag, respectively, in the SoG ambient waters under the influence of local wastewater discharge. Chapter 5 provides a summary of the main findings of this study and suggestions for future research.

Chapter 2: Materials and methods

2.1 Sampling locations and methods

2.1.1 Water column sampling in the Salish Sea

Time-series sampling which aims to capture the seasonal variability of trace metal concentrations in the SoG has been done at station S4-1.5, which is located outside of the Fraser River plume in the southern Strait (Figure 2.1). The station was visited five times between 2017 and 2018 to collect seawater samples for dissolved and particulate trace metal analysis. Sampling cruises were targeted to capture trace metal distributions during the fall bloom (September 2017), winter baseline conditions (December 2017), spring bloom (April 2018), peak of Fraser River freshet (June 2018), and summer conditions (August 2018). Field sampling was conducted on the CCGS hovercraft (Siyay and Moytel) for the September to June cruises. In August 2018, in addition to the time-series station S4-1.5, we also collected seawater samples at three additional stations (Figure 2.1) located in the northern SoG (NG), Haro Strait (HS), and Juan de Fuca Strait (JF2) on board the CCGS Vector. Details on the water column sampling locations and dates are listed in Table 2.1.

For each cruise, hydrographic properties of the water column including temperature, salinity, dissolved oxygen concentrations, and transmissivity were measured in-situ using a conductivity-temperature-depth instrument (CTD) supplemented with an oxygen sensor and a transmissometer. Go-Flo bottles (12 L) were deployed from a synthetic Amsteel®-Blue line and triggered with Teflon messengers at depths estimated from a Teflon-coated metered block to collect seawater samples from the surface to the bottom of the water column, capturing a 12-point depth profile. The exact sampling depths were determined post-cruise from the CTD's pressure versus time data (Appendix Table B.1).

At each depth, subsamples were taken for nutrients, dissolved and particulate trace metals. Nutrients were sampled into pre-cleaned 15 mL Falcon tubes by filtering seawater through 0.45 µm Acrodisk® syringe filters with Nylon membrane. Seawater samples for dissolved trace metal analysis were gravity-filtered through pre-cleaned 0.2 µm AcroPak™ capsule filters with

polyethersulfone membrane and collected into 250 mL acid cleaned HDPE bottles at sea. Any remaining seawater was drained directly from Go-Flo bottles into acid-cleaned LDPE cubitainers (10 L). Samples were stored double bagged inside coolers for transportation back to the laboratory. Nutrients were frozen in an upright position and stored in a -20°C freezer until analysis. Dissolved trace metal samples were acidified with 250 μL ultrapure concentrated HCl (Aristar[®] Ultra grade, VWR Chemicals BDH[®]) to reach a pH of ~ 1.8 within 24 hours of collection.

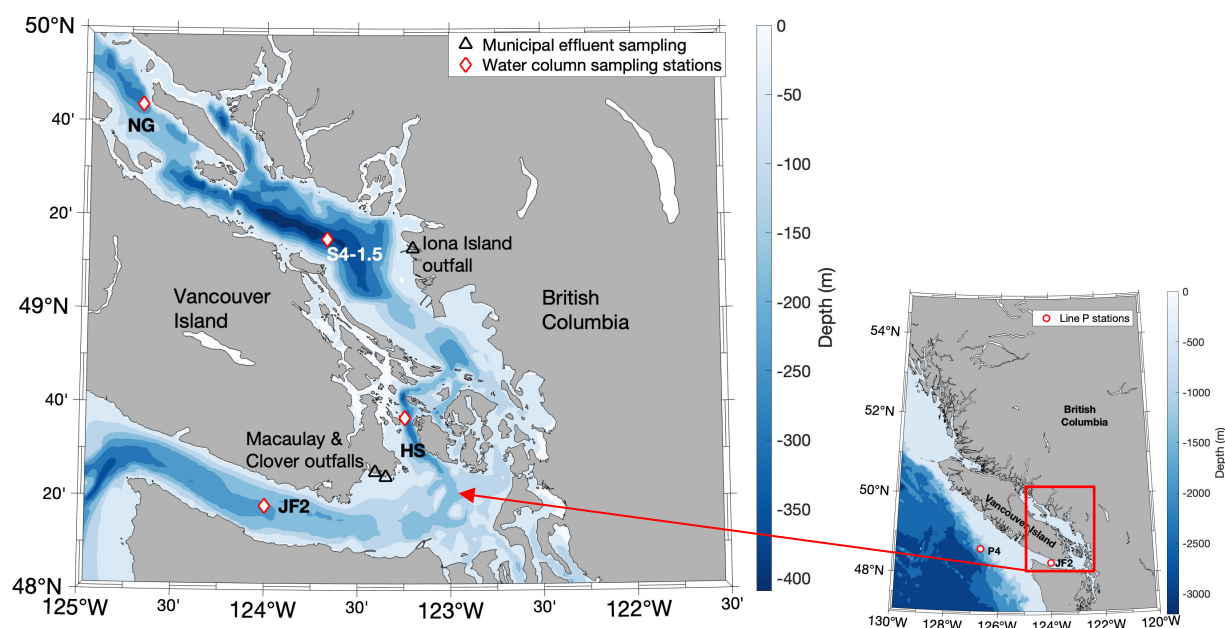


Figure 2.1. Locations of municipal sewage outfalls (black triangles) and water column sampling stations (red diamonds) in the Salish Sea. Stations P4 and JF2 (red circle) along the Line P transect sample the oceanic source water that fuels the Salish Sea.

To collect marine particles for particulate metal measurements, approximately 5 L of seawater was passed through 0.45 μm , 47 mm Supor[®] polyethersulfone membrane filters using two peristaltic pumps to simultaneously filter 4 samples at once. All samples were filtered in a class-100 cleanroom within 48 hours of collection. The filtrates were collected into respective waste containers and the exact volumes were measured using a graduate cylinder. After filtration, a gentle MQ mist was sprayed over the filters to rinse out any salt remaining on the surface. Filters were

then air-dried inside a HEPA-filtered laminar flow hood and stored in acid cleaned petri-dishes until further treatment.

Table 2.1 Seawater sampling locations, water depths, and time of sampling in the Salish Sea.

Station name	Latitude (°N)	Longitude (°W)	Water depth (m)	Time of sampling
S4-1.5	49°15.00'	123°40.00'	380	September 11 th & 12 th , 2017
S4-1.5	49°15.00'	123°40.00'	380	December 4 th , 2017
S4-1.5	49°15.00'	123°40.00'	380	April 6 th , 2018
S4-1.5	49°15.00'	123°40.00'	380	June 14 th , 2018
NG	49°43.60'	123°40.80'	357	August 24 th , 2018
S4-1.5	49°15.00'	123°40.00'	380	August 26 th , 2018
HS	48°36.91'	123°14.87'	235	August 27 th , 2018
JF2	48°18.00'	124°00.00'	180	August 27 th , 2018

2.1.2 Municipal effluent sampling

We have coordinated with Metro Vancouver and Capital Regional District to collect wastewater samples from the Iona WWTP (Vancouver), and two outfalls at Macaulay Point and Clover Point (Victoria). Locations of the three sewage outfalls are shown in Figure 2.1. Composite samples collected over 24 hours were sent to our laboratory every two months for analysis of trace metals. At the Iona WWTP, both influent and primary treated effluent (the latter passed through a settling tank) were sampled. At Macaulay and Clover Points, municipal wastewater was screened through a 6 mm mesh before being discharged into the receiving environment (Capital Regional District, 2016). Screened effluents from these two discharge points were collected within a week of sampling at the Iona WWTP to compare data within the same time frame. The three outfalls were sampled six times in total between 2017 and 2018 (November 2017, January, March, June, September, and November 2018).

Duplicates were taken from the composite samples to determine the concentrations of total and dissolved Cd and Ag in municipal wastewater. For measuring total metals, 25 mL aliquots were

subsampled into acid cleaned Teflon digestion vessels after vigorously shaking the composite bottle to ensure sample homogeneity. The weight of each aliquot was also recorded. The aliquots were acidified with 125 μL of twice distilled concentrated HNO_3 to $\text{pH} < 2$ and stored at room temperature until further treatment. For dissolved metals analysis, composite samples were vacuum filtered through 0.45 μm , 47 mm Supor[®] polyethersulfone membrane filters to collect duplicates of 25 mL filtrate. The dissolved fraction ($< 0.45 \mu\text{m}$) was weighed and then acidified with 25 μL of twice distilled concentrated HNO_3 to $\text{pH} < 2$ for storage. For the particulate fraction, digesting the chemically resistant Supor[®] filters with high particle loadings would be analytically challenging and time consuming. Hence, concentrations of particulate metals in wastewater were determined indirectly by subtracting the dissolved fractions from the total metal concentrations.

2.2 Analytical methods

2.2.1 Dissolved Cd and Ag in seawater

Seawater matrix is dominated by major ions with concentrations in the millimolar (mM) range, thus trace metal analysis requires matrix removal and preconcentration of the metals of interest in order to increase their signals, ideally well above the instrument detection limits. We used an automated seawater preconcentration system, the seaFAST-pico[™] (Elemental Scientific) at the University of Victoria for offline sample processing. The system buffers acidified seawater inline before loading into a column containing high-affinity resin for a variety of trace metals, where the bulk seawater matrix is removed, and the concentrated samples are eluted into clean collection vials. This automated method minimizes procedural blanks while providing high preconcentration factors for precise trace metal quantification by ICP-MS. Details of the seaFAST method are described in Lagerström et al., 2013.

For typical seaFAST applications, the solid phase extraction utilizes a commercially available column (Elemental Scientific) which contains the Nobias PA1 resin with ethylenediaminetriacetic acid (EDTRiA) and iminodiacetate (IDA) functional groups (Wuttig et al., 2019). Despite the resin's high affinity to a variety of transition row metals, it has shown poor recovery for Ag, which is one of the two metals of interest in our study. Hence, an alternate seaFAST resin (Elemental

Scientific) with carboxymethylated polyethylenimine (CM-PEI) as the chelating ligand was used to improve Ag recovery while maintaining quantitative chelation of other elements similar to those of the standard Nobias PA1 resin (Kagaya & Inoue, 2014). The extraction method remained unchanged, with the exception of a slight modification to the composition of the standard elution acid from 10% v/v HNO₃ to a mixture of 6% v/v HCl and 10% v/v HNO₃ to achieve quantitative recovery of Ag from the column.

A preconcentration factor of 33 was achieved by loading 20 mL of seawater sample onto the column and eluting with 600 µL of elution acid spiked with 1 ppb indium (In) to serve as an internal standard for ICP-MS analysis. Matrix-matched standards were prepared by standard additions on selected samples to cover the entire range of salinity in the water column at time of sampling. The prepared standards were loaded onto the column and extracted the same way as the samples. Post-column Ag standard curves showed a robust linear regression between concentrations of Ag added and the measured isotopic ratios of Ag-107/In-115 (Figure 2.2). However, comparison between two standard addition curves obtained with a shallow (salinity 23) and a deep (salinity 30) sample showed marked differences in the slope of the linear regression (Figure 2.2). The results indicate that Ag recovery from the resin is lower at higher salinity, likely due to the presence of stronger complexes with chloride in highly saline matrix, challenging the extraction of Ag ions.

In contrast, the slope of the Cd standard curves is constant regardless of sample salinity. In order to quantitatively measure dissolved Ag in our coastal seawater samples, measuring all samples with standard additions would minimize analytical errors associated with inconsistent recovery, but the process is very time-consuming. Instead, we derived a linear relationship between salinity and the slope of Ag standard curves by performing standard additions on samples that cover the entire range of salinity observed at our sampling stations (Figure 2.3, Appendix Table B.2 & 3). For samples without standard additions, we calculated the expected slope based on their salinity to convert measured ratios of Ag-107/In-115 to concentrations.

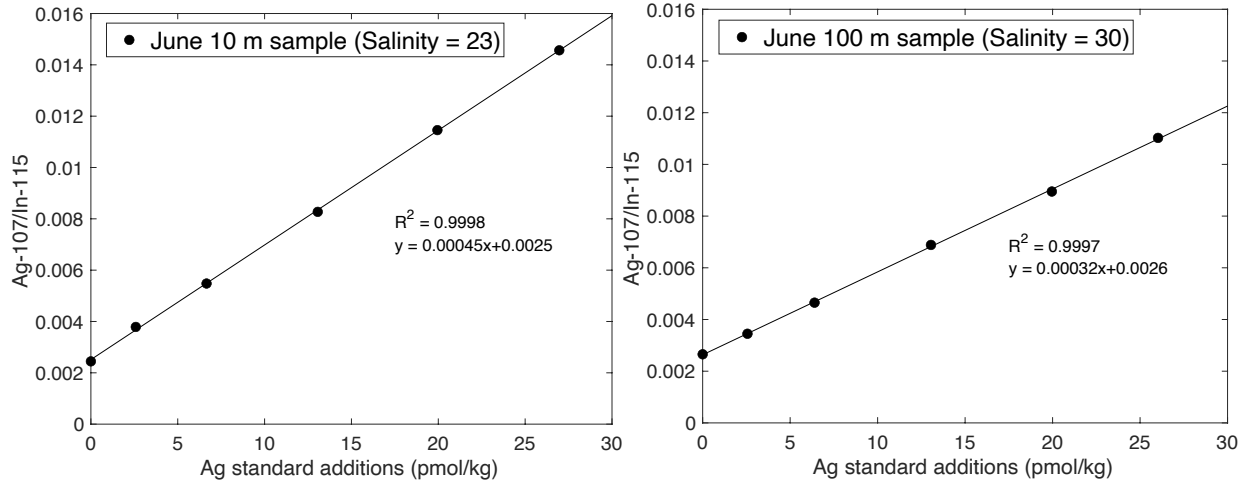


Figure 2.2. Post-column extraction standard curves for a surface sample (10 m) and a deep sample (100 m) collected in June 2018. The counts of Ag-107 are normalized by the internal standard (In-115).

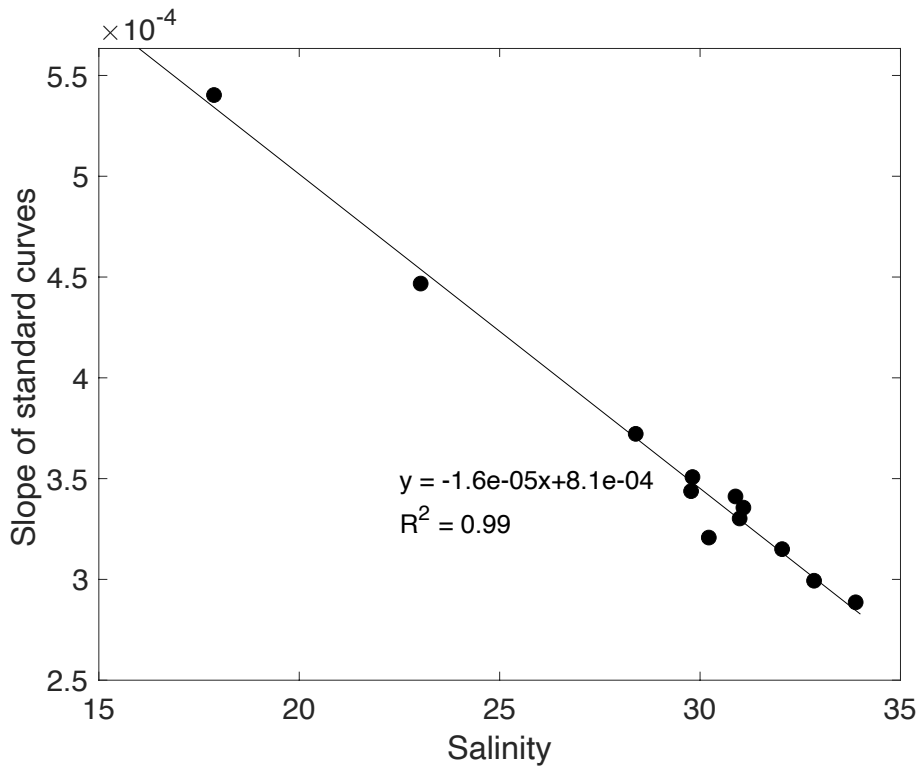


Figure 2.3. Relationship between sample salinity and the slope of post-column standard curves for Ag analysis in coastal seawater collected in the Salish Sea.

Procedural blank solution consisting of 0.1% v/v cleanly collected Ocean Station Papa surface water in 0.012 M HCl was prepared fresh for each *seaFAST* analysis (Lagerström et al., 2013). Multiple blanks were processed at the beginning and then monitored every 6 samples throughout the *seaFAST* sample extraction sequence. The average blanks and detection limits for all analytical runs are reported (Table 2.2). We suspect that the blank solution used in our 1st run was contaminated in Ag, which resulted in an overestimate of the true analytical blank. In order to confirm this hypothesis, we repeated 6 samples that were processed in this batch and compared the measured dissolved Ag concentrations without blank corrections. The results of replicates agree within the analytical error (5 – 10 %), thus the high Ag blanks in the 1st run cannot be associated with the sample extraction process (e.g., resin, elution acid, buffer solution). The most likely contamination was from the blank solution, which was prepared fresh for each run and processed independently. The average Ag blank (0.3 pmol/kg) from future runs was thus used to correct for sample concentrations measured in the 1st batch.

Table 2.2. Average procedural blanks and detection limits for three analytical runs utilizing the *seaFAST* sample preconcentration system followed by ICP-MS. Detection limits are calculated as three times the standard deviation of the procedural blank. *The Ag blank and detection limit reported for the 1st run are likely overestimates of the true values due to suspected contamination.

	Cd (pmol/kg)	Ag (pmol/kg)	Samples analyzed
1 st run			
Average (n=14)	0.40	3.94*	Sep. 2017
Detection limit	0.54	1.14*	Dec. 2017
2 nd run			
Average (n=14)	0.58	0.23	Apr. 2018
Detection limit	0.77	0.29	Jun. 2018
3 rd run			
Average (n=19)	0.90	0.36	Aug. 2018
Detection limit	0.87	0.73	Sep. & Dec. repeats

The precision and accuracy of the *seaFAST* extraction method has been reported in the scientific literature (Lagerström et al., 2013; Rapp et al., 2017; Jackson et al., 2018; Wuttig et al., 2019) and

confirmed by the analysis of nearshore seawater certified reference material CASS-6 (National Research Council Canada) in our study (Table 2.3). A 600 m water sample collected at Ocean Station Papa in August 2013 was also measured repeatedly to determine the precision of measurements between different analytical runs (Table 2.4). All of our measurements for dissolved trace metals in seawater are reported in the unit of pmol/kg instead of pM (for particulate and effluent samples) because we performed standard additions by weight for better precision.

Table 2.3. Summary of repeated measurements (± 1 SD) of certified reference material CASS-6 purchased from the National Research Council Canada in all three analytical runs.

CASS-6	Cd (n=7)	Ag (n=7)	Cu (n=7)	Zn (n=3)
	pmol/kg	pmol/kg	nmol/kg	nmol/kg
Measured	187 \pm 2	8.92 \pm 0.32	8.06 \pm 0.18	17.8 \pm 0.3
Certified	189 \pm 16	/	8.18 \pm 0.50	19.0 \pm 2.8

Table 2.4. Summary of repeated measurements (± 1 SD) of a sample collected from 600 m at Ocean Station Papa (OSP) during the August 2013 Line P cruise in all three analytical runs. Sample was provided by Dr. Kristin Orian's research group (UBC), courtesy of Nari Sim.

OSP_600 m	Cd (n=10)	Ag (n=10)	Cu (n=10)	Zn (n=2)
	pmol/kg	pmol/kg	nmol/kg	nmol/kg
Measured	958 \pm 6	22.2 \pm 1.2	2.48 \pm 0.18	10.4, 10.5

2.2.2 Particulate Cd and Ag in seawater

Particulate samples were collected on acid-cleaned, chemically resistant 0.45 μ m, 47 mm Supor[®] filters. In order to achieve complete dissolution and recovery of the filtered material, filters underwent a series of acid digestions following the Piranha digestion method (Ohnemus et al., 2014). All reagents used for digestion were of the highest grade available commercially or produced in-house by double-distilling Environmental Grade acids (VWR Chemicals BDH[®]) at sub-boiling temperatures.

Dried filters were carefully folded and placed into 15 mL PFA vials (Savillex). The Piranha solution consisting of a 3:1 v/v mixture of concentrated H₂SO₄ and H₂O₂ (1.2 mL and 0.4 mL, respectively) was added to each sample vial and heated at 110°C with lids loosely on top for 1 hour. Repeated additions (5 times on average) of concentrated H₂O₂ (0.4 mL each) followed by 2 hours of refluxing at 200°C after every addition was necessary for complete dissolution of filter pieces. Samples were gently evaporated to reduce in volume if repeated additions of H₂O₂ diluted solutions and caused reactions to cease. The solution was dried at 235°C until a solid black deposit was formed. The samples were washed and refluxed with 0.1 mL of 8 M HNO₃, and re-dried to remove any residual of H₂SO₄. Any particulate materials remaining in the sample were further digested by refluxing in a 2 mL acid mixture of HCl, HNO₃, and HF (4 M each) at 110°C for 4 hours. After refluxing, the solution was dried down, and a mixture of concentrated HNO₃ and H₂O₂ (1 mL: 1 mL) was added, refluxed, and dried down again to remove any undigested organic material. A final aliquot of 0.1 mL concentrated HNO₃ was added to the dried pellet and heated at 110°C to complete dryness. The final product, a small white pellet was re-dissolved in 2 mL of 1% HNO₃ spiked with 10 ppb In for measurement on the HR-ICPMS (ELEMENT 2, Thermo Scientific).

2.2.3 Dissolved and total Cd and Ag in municipal effluent

Municipal effluent typically has high organic loadings, thus strong oxidizing reagents are needed to break down both particulate and dissolved organic matter in the sample matrix. Acidified samples for total and dissolved metals were first evaporated to near dryness at sub-boiling temperature on a hot plate (Corning®). The dried samples were then refluxed with 1 mL of concentrated Aqua Regia (mixture of concentrated HCl and HNO₃ in a 3:1 ratio) overnight. The acid mixture was evaporated the next day, and fresh Aqua Regia was added to continue refluxing the samples. When most particles had been disintegrated, samples were refluxed in 1 mL of concentrated HNO₃ overnight, and finally fumed with 1 mL of concentrated perchloric acid (HClO₄) to ensure total dissolution of any refractory materials remaining. Sample solutions usually turned clear after 2 hours of fuming in HClO₄ at 200°C. The digested samples were dried again and re-dissolved in 5 mL of 1% HNO₃ spiked with 10 ppb In for quadrupole ICP-MS analysis of

Cd and Ag concentrations. All sample processing was done in a cleanroom environment, following trace metal clean handling techniques.

2.2.4 Salish Sea Box Model

A time-varying box model (Figure 2.4) adapted from Wang et al. (2019) was used to help interpret the spatial and temporal variations of dissolved trace metals in the Salish Sea. The model divides the Salish Sea into the Strait of Georgia (SoG), Haro Strait (HS), and Juan de Fuca Strait (JF), which are further subdivided into an upper box (representing the upper 50 m) and a lower box (representing all depths below 50 m). The model uses a suite of data from regional instrumentation and empirical estimates of estuarine circulation to simulate the volume fluxes between boxes. The salinity budget of the system is the primary forcing mechanism of the modelled estuarine circulation, which is driven by freshwater discharge into the SoG and saltwater exchange between the Pacific Ocean and Juan de Fuca strait. Details about the model setup can be found in Wang et al. (2019).

The freshwater input is calculated using a combination of river discharge measurements from Fraser River at Hope (station 08MF005) and Englishman River (station 08HB002) provided by the Water Survey of Canada (2019). The saltwater input is assessed using wind data from the west coast of Vancouver Island (which can be used as a proxy for Pacific upwelling strength). In the summer, coastal upwelling driven by northerly winds brings deep and saline Pacific water into the Juan de Fuca Strait. In the winter, wind-driven downwelling lowers the salinity of incoming Pacific water. The modelled Pacific salinity (S_p) is defined as a function of wind speed (W) along the coast, which has a baseline (S_{pw}) of 33 and an upper variation range (ΔS_p) of 1 to reflect higher salinity water in the summer upwelling season.

$$S_p = S_{pw} + \Delta S_p \times \frac{\max(0, W)}{\max(W)_{\text{annual}}}$$

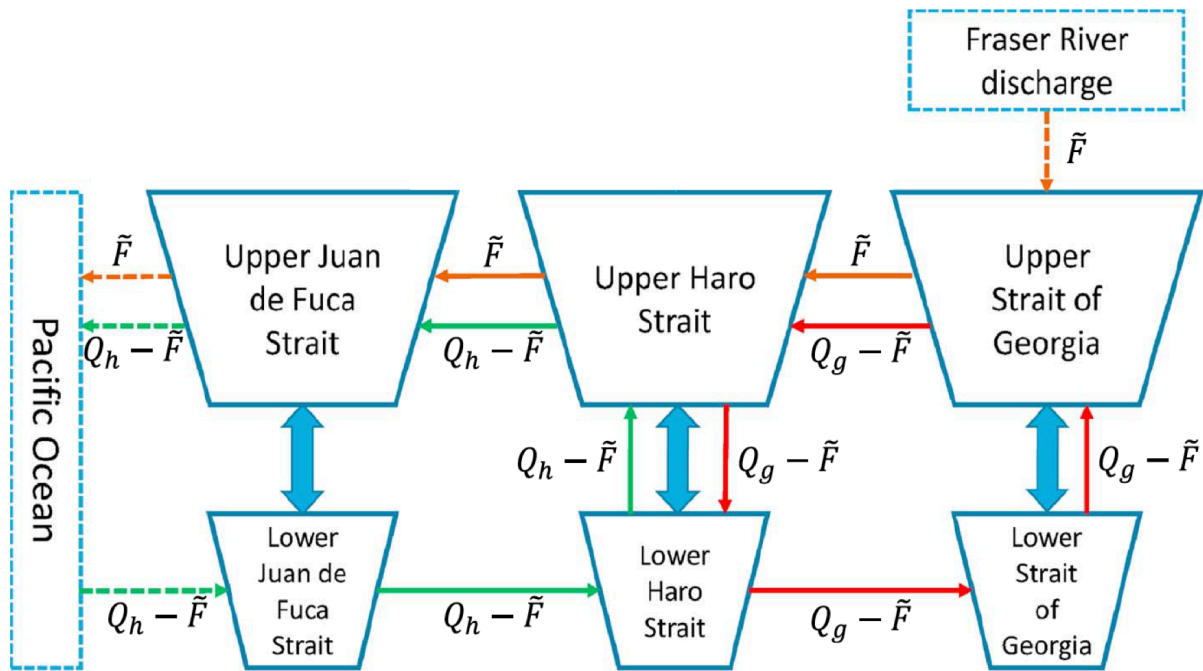


Figure 2.4. Box model schematic diagram modified from Wang et al., (2019). The system has 3 basins: Strait of Georgia (SoG), Haro Strait (HS), and Juan de Fuca Strait (JF). Each basin is divided into an upper layer (0-50m) and a lower layer (50 m to bottom). River discharge is denoted by \tilde{F} (m^3/s). Q_g and Q_h represent the volume flux (m^3/s) between the upper boxes of HS & SoG, and HS & JF, respectively. The thick arrows between upper and lower boxes in the three basins denote vertical mixings.

User-defined tracers are incorporated in the model by specifying their inputs from the Fraser River, the Pacific Ocean, and any other sources such as sewage outfalls (Iona WWTP, Macaulay and Clover Points). Users have the option of entering either a constant or a time-variable input for each source based on available data. Sources are introduced to different boxes, with the Fraser River discharging into the SoG upper box, the upwelled Pacific water flowing into the Juan de Fuca lower box, and the effluent from the Iona WWTP and the two outfalls in Victoria contributing to the lower box of SoG and HS, respectively. The model assumes conservative behavior of any given tracer, which means removal mechanisms such as biological uptake and sediment burial are not taken into account. Discrepancy between the measured and modelled data thus provide a means to gauge the influence of physical mixing on trace metal distributions and identify unknown sources or sinks.

Chapter 3: Biogeochemical cycling and anthropogenic input of cadmium in the Strait of Georgia

3.1 Introduction

3.1.1 Sources of Cd in the environment

Cadmium (Cd) is a transition metal that is easily mobilized in soils and aquatic systems, posing acute toxicity to almost all forms of life (Cullen & Maldonado, 2013). The chemical and physical properties of Cd resemble zinc (Zn), as both are Group 12 elements on the periodic table. Although it has two oxidation states (+ I and + II), Cd is found almost exclusively divalent in the environment. With an average crustal abundance of merely 98 ppb compared with other main constituents (e.g., Al, 8.04%), Cd is largely associated with metal sulfides (Taylor & McLennan, 1995). Cd can be mobilized through volcanic eruptions, weathering of rocks, and burning of terrestrial plants (Cullen & Maldonado, 2013).

Anthropogenic activities have influenced the biogeochemical cycling of Cd profoundly. Cd is primarily extracted as a by-product of mining for Zn ores. Major industrial applications of Cd include its use in nickel-cadmium (Ni-Cd) batteries, paint pigments, plastic stabilizers, and electroplating of metal surfaces (Naja & Volesky, 2009). Discharge of industrial and domestic waste into natural waters can elevate the ambient Cd concentrations (Hutton & Symon, 1986) and enhance bioaccumulation in aquatic organisms. Cd is highly toxic because it can displace Zn in many essential metallo-enzymes, causing cellular dysfunction and exacerbating health problems, mainly associated with Cd accumulation in target organs such as kidneys, liver, and bones (Maret & Moulis, 2013). Its hazardous effects on humans and the environment make it one of the three most toxic heavy metals together with mercury and lead (Naja & Volesky, 2009).

3.1.2 Biogeochemical cycling of Cd in the ocean

In the global ocean dissolved Cd (dCd) exhibits nutrient-type distributions which reflect biological uptake in surface waters and release from decomposing organic matter at deeper depths (Bruland

& Lohan, 2003). There is a positive correlation between dCd and the macronutrient phosphate (PO_4^{3-}) in the open ocean, suggesting a biological role of dCd in the marine ecosystem. Additions of dCd have been shown to enhance the growth of Zn-limited diatoms by substituting Zn in carbonic anhydrase (CA), an essential enzyme used for cellular carbon concentrating mechanism (Price & Morel, 1990). Due to the biological cycling of Cd and deep ocean circulation, as deep water travels from its origin in the north Atlantic towards the Pacific Ocean, the water ages and accumulates dCd from the remineralization of sinking particles along the path (Bruland & Franks, 1983). In the deep ocean, dCd has a relatively long residence time (~50,000 years; Bruland et al., 1994) compared with scavenging type trace metals (e.g., Fe, Mn).

Sedimentary record of Cd incorporated into foraminiferal calcite tests combined with the correlation between dCd and PO_4^{3-} have been used to infer macronutrient distributions in the paleo ocean. In order to reliably reconstruct the past nutrient conditions using foraminiferal Cd as a proxy, a deeper understanding of the biogeochemical cycling of Cd and factors controlling the dCd: PO_4^{3-} relationship in the ocean is needed. Depth profiles of dCd: PO_4^{3-} exhibit significant variations in surface waters and distinct distributions in major ocean basins (Quay et al., 2015), reflecting the influence of processes that add or remove dCd relative to PO_4^{3-} .

Uptake of dCd and phytoplankton Cd:P quota can vary with species composition and the availability of bioactive metals in seawater. Ho et al. (2013) measured the cellular elemental composition of 15 eukaryotic phytoplankton cultures which were maintained under identical culture conditions. They found that the cellular Cd quotas (normalized to P) varied by two orders of magnitude (0.007 - 0.73 mmol/mol) among major marine phyla. For example, green algae have lower Cd quotas than diatoms, which have lower Cd quotas than coccolithophores. In addition, studies found that within phyla, phytoplankton uptake of dCd was negatively influenced by the presence of other divalent metals such as Fe, Mn, and Zn due to competition for cellular uptake (Bourne et al., 2018). Therefore, both phytoplankton community composition and relative abundance of trace metals in seawater can influence the biological cycling of Cd and shape the dCd: PO_4^{3-} correlation in different oceanic environments.

Cd is known to form an insoluble complex with sulfide (CdS) under anoxic conditions in the sediment and water column where free sulfide is present. Sediment diagenesis and precipitation of CdS can reduce the concentrations of dissolved Cd in bottom waters through downward diffusion (Lekhi et al., 2008). Janssen et al. (2014) found evidence of CdS formation in oxygen deficient open ocean waters and suggested that Cd precipitation in the water column may be a significant removal mechanism of dCd. Bianchi et al. (2018) further suggested that anaerobic decomposition within particle microenvironments associated with sinking organic aggregates favors the formation of sulfide and metal precipitation. Once formed, these metal sulfide complexes are kinetically inert and stable even in oxic environments (Mullaugh & Luther, 2011; Rozan et al., 2000). The expansion of anaerobic metabolisms beyond anoxic zones in the ocean will influence the biogeochemical cycling of Cd over a larger spatial scale, potentially including oxygenated regions.

3.1.3 Previous information on Cd in the SoG

Natural and anthropogenic loadings of Cd into the coastal waters of the SoG have been assessed using sediment cores that were collected outside and within the footprint of local wastewater treatment plants (Macdonald et al., 2008). A core located with proximity to the Iona WWTP showed significant enrichment of Cd relative to the background in SoG sediment. With the available geochemical data in sediment cores and municipal effluents, Johannessen et al. (2015) assessed the influence of effluent discharge on the regional budgets of organic carbon and nitrogen, metals, and organic pollutants. They found that Cd loadings from municipal outfalls contributed less than 5% to the total sediment sink of Cd in the SoG. They argued that the elevated levels of Cd observed in sediment near the Iona outfall was not due to direct discharge of Cd from the effluent, but rather reflect precipitation of dCd with sulfides in pore water as a consequence of high organic content and anaerobic respiration on site.

In 2014, we collected a sediment core near the diffusers of the Iona outfall and analyzed for trace metal concentrations. Results show similar surface enrichment of Cd as Macdonald et al. (2008) (Appendix Figure A.1). In 2015, effluent samples from the Iona outfall were sent to our laboratory on a weekly basis to quantify the concentrations of total and dissolved Cd. The average total Cd concentration was approximately 1 nM, with 80% in the particulate fraction (Appendix, Table B.8).

Our preliminary results confirmed that the relatively low Cd input (~ 0.1 ppm) from Iona effluent cannot be directly responsible for the enhanced Cd concentrations (~ 0.4 ppm) found in surface sediments near the Iona diffusers (Appendix Figure A.1)

The SoG is a productive ecosystem which provides valuable habitats for various aquatic species. It is crucial to establish baseline conditions for Cd in the ambient environment given its high toxicity to organisms. This problem is particularly urgent in the SoG because elevated levels of Cd (> 2 $\mu\text{g/g}$ wet weight) have been detected in oysters and scallops farmed in this region (Kruzynski, 2004). Lekhi et al. (2008) found a positive correlation between dCd concentrations in seawater and Cd contents in oysters. Oysters are able to accumulate high concentrations of Cd from seawater because of their effective filtration rates. The Cd isotopic compositions of bivalves showed that the high Cd levels in B.C. oysters were primarily associated with natural sources (Shiel et al., 2012). Given the high dCd background in waters upwelled from the Pacific Ocean, monitoring efforts are required to ensure that anthropogenic activities do not further increase its concentrations in the receiving SoG waters.

3.2 Results

Following the circulation scheme proposed by Pawlowicz et al. (2007), the SoG water column can be subdivided into three distinct layers which comprise the surface (0-50 m), intermediate (50-200 m), and deep (> 200 m) waters. We begin our analysis by showing temporal variations in the physical (e.g., temperature, salinity), biological (nutrients, chlorophyll-a), and chemical properties (dCd concentrations) of the water column at station S4-1.5 located in the southern SoG. To put our SoG dCd datasets into context, we then present changes in the characteristics of the Pacific water as it upwells into the coastal basins of the Salish Sea and the resulting spatial distribution of dCd. Particulate Cd profiles collected in the water column of station S4-1.5 are also presented to investigate the partitioning of Cd between the dissolved and particulate pool in SoG waters. Lastly, anthropogenic inputs of Cd from wastewater treatment plants into the Salish Sea are reported to assess the impact of effluent discharge on the receiving environment.

3.2.1 Temporal variations of water properties in the southern SoG

3.2.1.1 Temperature, salinity, and density

Seasonal variations of temperature and salinity were measured in the water column of the southern SoG at station S4-1.5 (Figure 3.1). Surface water temperatures were relatively high in the summer, resulting in a sharp seasonal thermocline at 15 m in June, and at a slightly shallower depth (~ 10 m) in August and September (Figure 3.1A). This is in contrast with the relatively uniform temperature over the entire water column in April, and the low surface temperature observed in December. In the intermediate and deep waters, temperature was colder in the spring than in late summer/fall (Figure 3.1B).

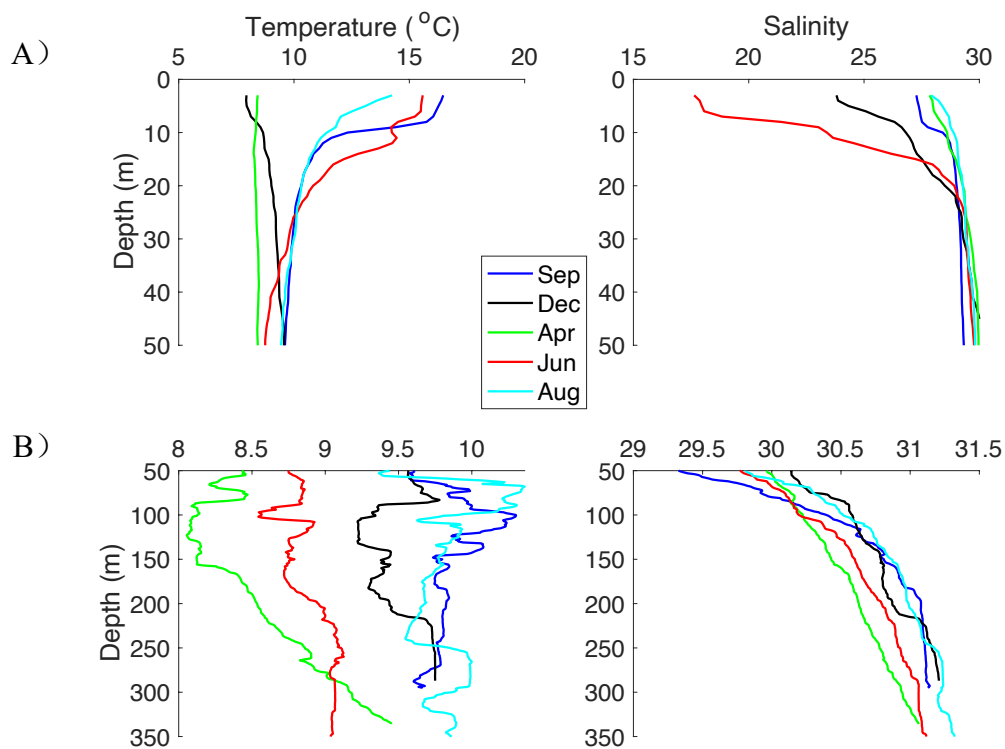


Figure 3.1. Depth profiles of temperature and salinity in the water column (A: top 50 m; B: 50 – bottom waters) of the southern Strait of Georgia at station S4-1.5 from September 2017 to August 2018.

The lowest salinity was observed in the surface waters in June, followed by December, September, April and August (Figure 3.1A). Changes in surface salinity largely reflect temporal variations of the Fraser River discharge, which peaks in June from melting of the snowpack, and gradually

decreases through late summer and fall. Periods of intense rainfall in the winter can also lead to short-lived rises in freshwater runoff from smaller rivers draining into the SoG, which could explain the relatively low surface salinity measured in December (Figure 3.1A). In the upper section of the intermediate layer (50 – 100 m), there was a relatively sharp salinity gradient in August and September (Figure 3.1B). Small but consistent seasonal variations in salinity were observed below 100 m, with the highest salinity at the end of summer (August/September), and the lowest in spring (April).

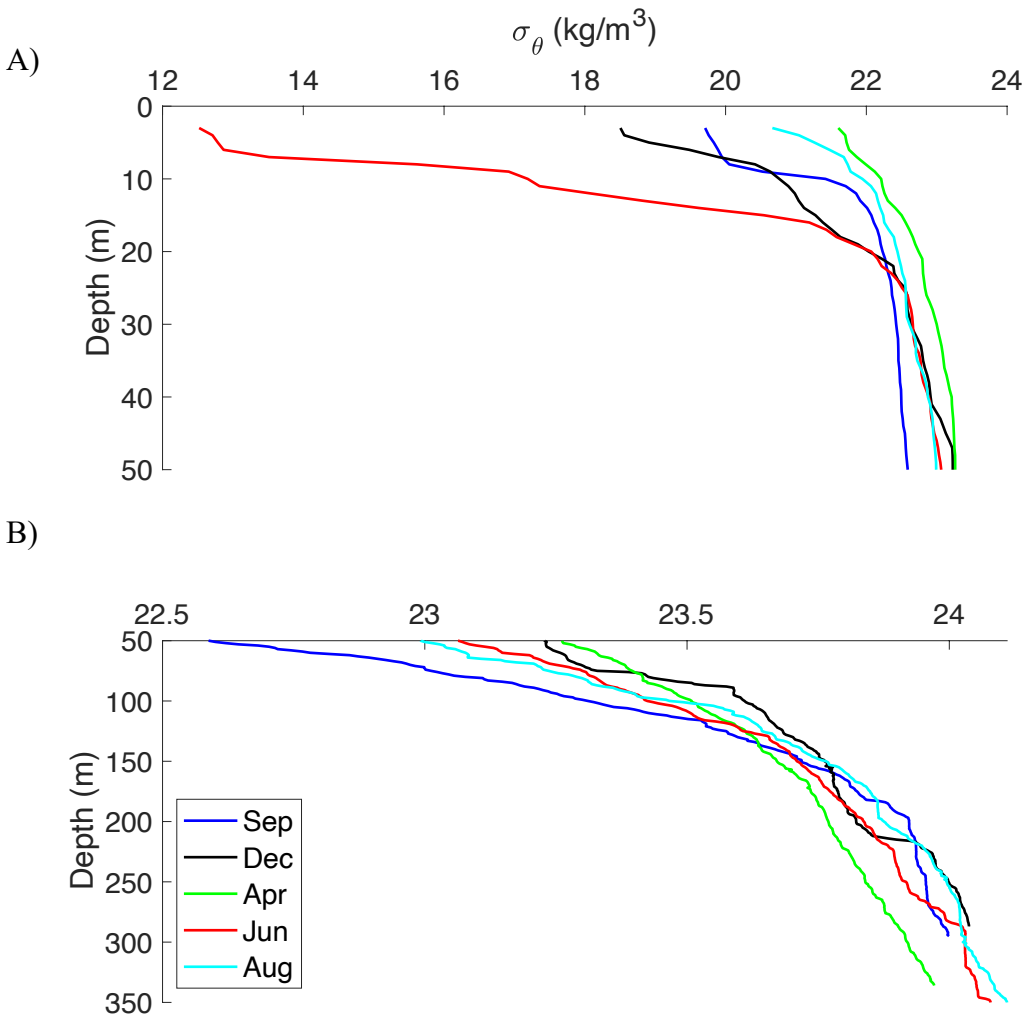


Figure 3.2. Depth profiles of density (sigma-theta) in the water column (A: top 50 m; B: 50 – bottom waters) of the southern Strait of Georgia at station S4-1.5 from September 2017 to August 2018.

The resulting density profiles showed that the upper water column was most stratified in June, with a shallow and partially mixed surface layer (ca. 6 m) over a strong pycnocline down to 20 m (Figure 3.2A). In contrast, the upper water column was least stratified and had the highest density in April, prior to the Fraser River freshet. A similarly well mixed upper water column was found in August, with a slightly lower density than in April. There was a pycnocline in the fall (September) between 8 and 10 m, and winter freshwater runoff lowered surface water density and deepened the pycnocline to 20 m in December. Water density below 50 m (Figure 3.2B) followed similar trends as salinity (Figure 3.1B) and shows marked increases with depth in the shallow section (50 – 100 m) of the intermediate layer than in deeper waters (> 100 m).

3.2.1.2 Oxygen concentration and apparent oxygen utilization

Concentrations of dissolved oxygen in the water column varied significantly with depth and season (Figure 3.3). Dissolved oxygen was highest at the surface and decreased rapidly in waters below. Surface water was near saturation in September as shown by the close to zero apparent oxygen utilization (AOU), calculated as the difference between oxygen at saturation (determined by in-situ water temperature and salinity), and measured oxygen concentrations. AOU increased rapidly along the seasonal pycnocline (Figure 3.2A and Figure 3.3), indicative of stratification in the upper water column which prevented air-sea gas exchange. At intermediate depths (50 – 200 m), there was a clear seasonal change in O₂ concentrations, with a maximum in April and a minimum in August. The lowest concentration of O₂ (~95 µM) was found in the bottom waters of December and April, which was still above the threshold of “coastal hypoxia” at 64 µM (Pawlowicz, 2017), thus the entire water column at station S4-1.5 was oxygenated at time of sampling.

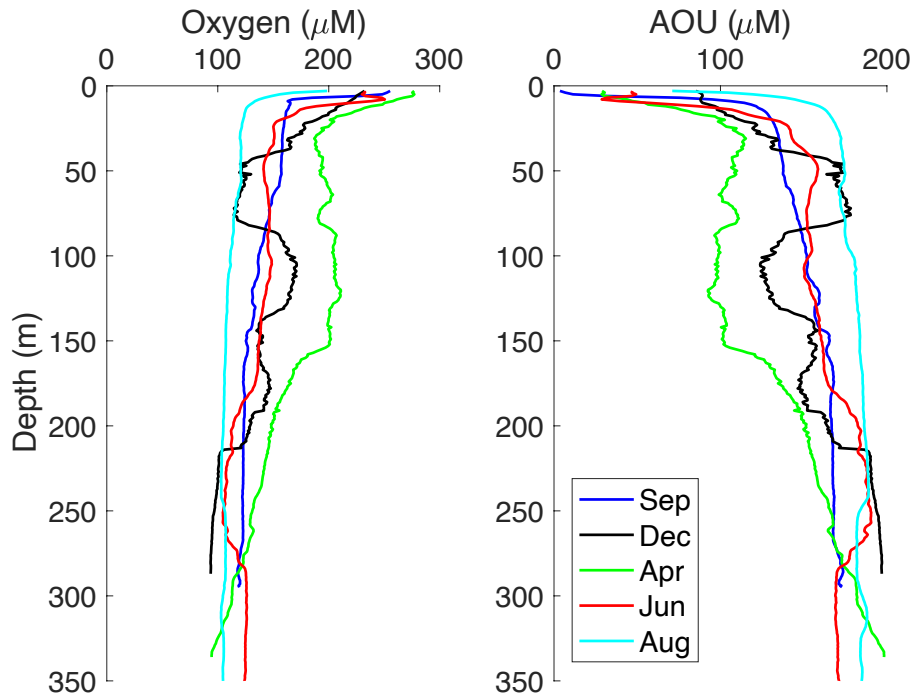


Figure 3.3. Depth profiles of dissolved oxygen and apparent oxygen utilization (AOU) in the water column of the southern Strait of Georgia at station S4-1.5 from September 2017 to August 2018. AOU is calculated as the difference between oxygen at saturation (determined by in-situ water temperature and salinity), and measured oxygen concentrations.

3.2.1.3 Macronutrients and chlorophyll-a

Vertical distributions of macronutrients all reflect surface depletions, with the largest deficits in nitrate (NO_3^-) and phosphate (PO_4^{3-}) observed in June, followed by August, April, September, and December (Figure 3.4). In contrast, the lowest concentrations of silicic acid ($\text{Si}(\text{OH})_4$, abbreviated Si onwards) were observed at the surface waters in April and August. In deeper waters, nutrient concentrations were more uniform but still showed small seasonal variations that were different for each of the three nutrients. Chlorophyll-a concentrations measured in the upper 30 m show occurrences of small-scale spring and summer/fall phytoplankton blooms in April and August/September, respectively (Figure 3.5), coinciding with the observed low concentrations of macronutrients. In June, NO_3^- and PO_4^{3-} were depleted to near zero at the surface, whereas Si concentrations have been restored to levels similar to those measured in the winter (December).

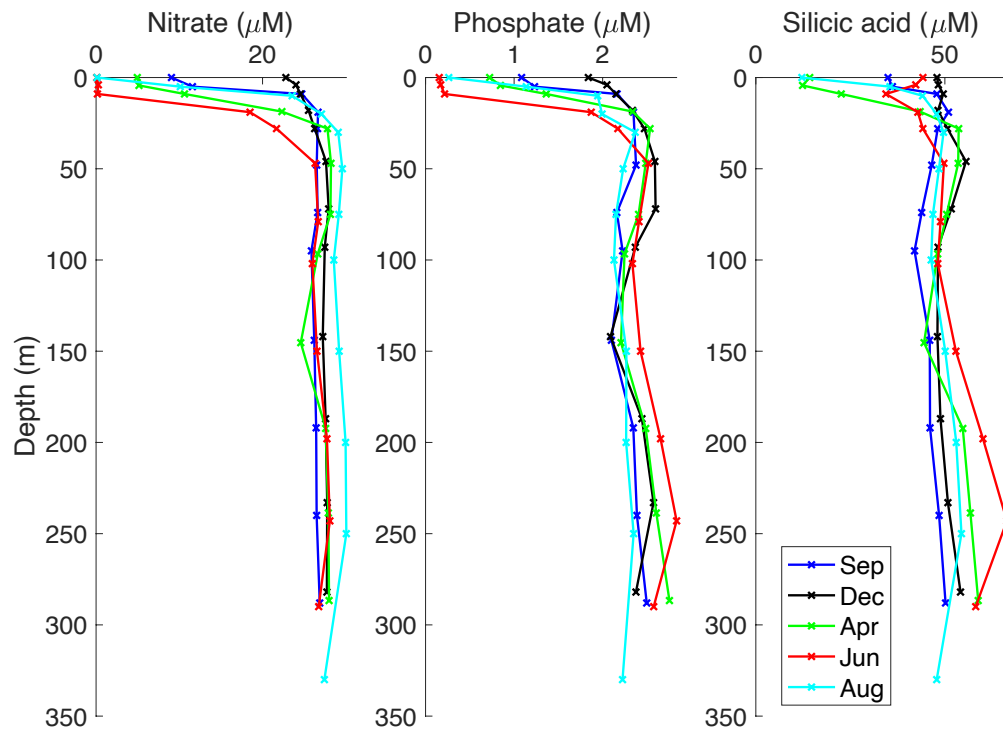


Figure 3.4. Concentrations of macronutrients (nitrate, phosphate, silicic acid) measured in the water column of the southern Strait of Georgia at station S4-1.5 from September 2017 to August 2018.

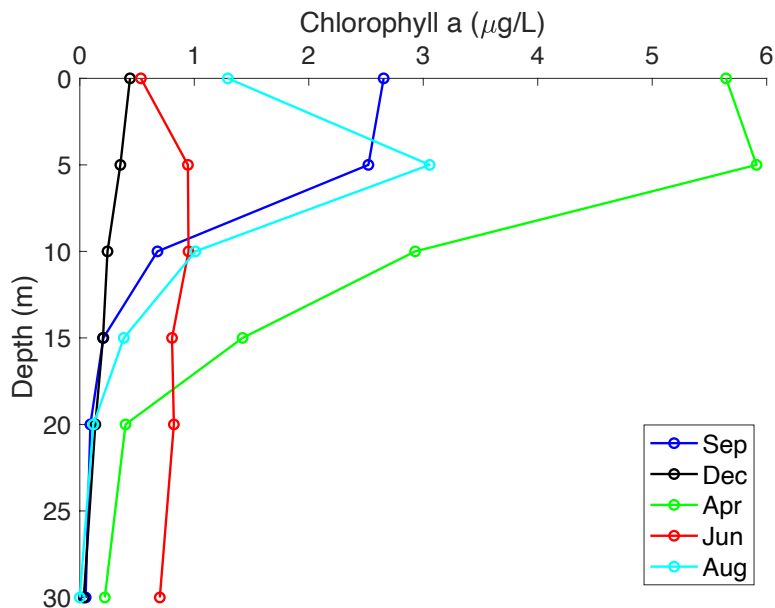


Figure 3.5. Chlorophyll-a concentrations measured in the upper 30 m at station S4-1.5 from September 2017 to August 2018.

3.2.1.4 Dissolved Cd concentrations

Similar to hydrography and macronutrients, depth profiles of dCd concentrations at station S4-1.5 were seasonally variable, with the largest variability occurring in the surface layer (Figure 3.6). A surface deficit of dCd was apparent in the euphotic zone for all months, with the lowest surface concentration of 269 pmol/kg in June, and a maximum around 550 pmol/kg in December and April. Concentrations of dCd increased gradually towards 50 m and remained relatively constant with depth in deeper waters, reflecting a typical nutrient-type distribution. At intermediate depths, dCd showed significant temporal variations, although at a smaller magnitude relative to the surface layer. Between 100 and 200 m, dCd concentrations were significantly lower in June relative to the other months (Figure 3.6). In deep waters below 200 m, higher dCd concentrations were observed in late summer (August, September) than during the springtime (April, June).

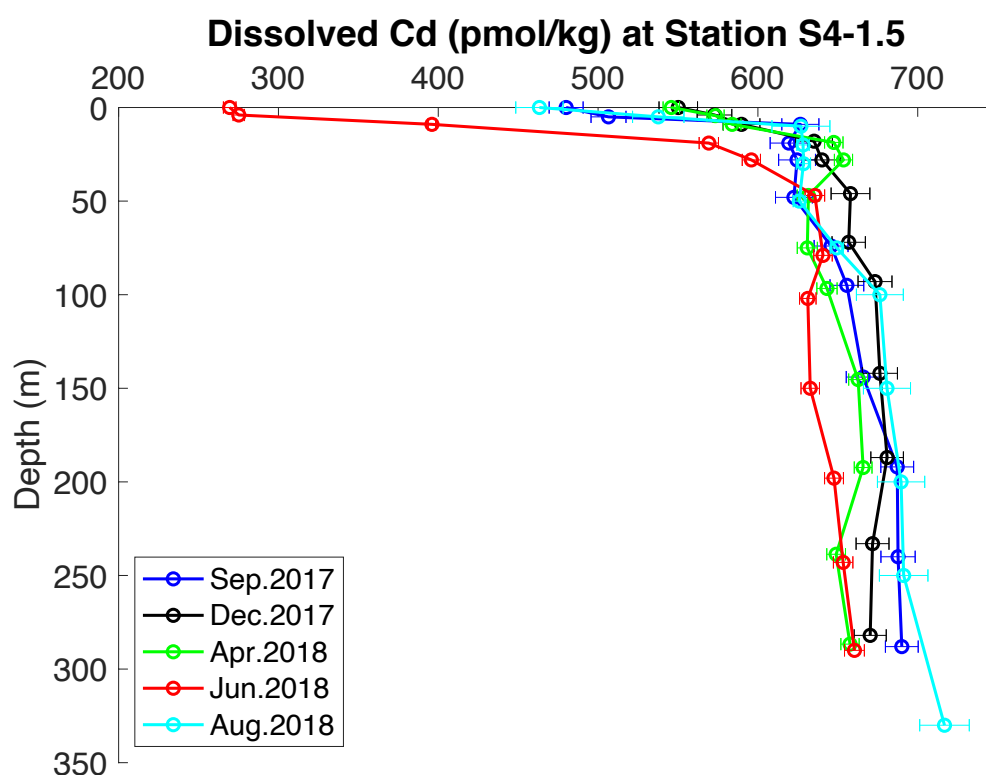


Figure 3.6. Depth profiles of dissolved Cd at station S4-1.5 from Sep. 2017 to Aug. 2018. Error bars for dissolved Cd concentrations represent one standard deviation of analytical uncertainty.

3.2.2 Spatial distributions of water properties in the Salish Sea

3.2.2.1 Temperature, salinity, and density in the Salish Sea

Hydrographic data were captured in August 2018 at 4 stations across the Salish Sea, located in Juan de Fuca Strait (JF2), Haro Strait (HS), southern SoG (S4-1.5), and northern SoG (NG). The Line P program conducts time-series sampling in the northeast Pacific, and the nearshore station P4 can represent the Pacific source water entering the deep basin of JF2 (Figure 2.1). CTD data collected by the Institute of Ocean Sciences at station P4 in September 2018 are plotted together with our Salish Sea profiles (Figure 3.7). In the SoG, temperature was the highest at the surface and decreased sharply in the upper 20 m. The thermocline was less apparent at station HS, where the entire water column showed less temperature variability with depth. At station JF2, temperature decreased gradually from the surface to 80 m and stayed constant in deeper waters. Further offshore at station P4, a sharp thermocline was extended down to 50 m and temperature continued to drop steadily below.

Similar to temperature, salinity showed the largest variations in the surface layer at all stations (Figure 3.7). A halocline was apparent in the SoG at stations S4-1.5 and NG in the upper 20 m, coinciding with the depth of the thermocline. In the intermediate and deep waters, salinity was consistently higher in the southern SoG (S4-1.5) than further north (NG). As the relatively fresh upper SoG water flows seaward into the Haro Strait region, intense tidal currents facilitate mixing with deep saline waters and weakens stratification. Nevertheless, the entire water column was not homogeneous at station HS, where a clear halocline from surface down to 100 m can be observed in the salinity depth profile. Similarly, a slightly shallower halocline (surface – 80 m) was found at station JF2, where salinity increased from 33.1 to 33.9 and stayed constant at deeper depths. The bottom waters at JF2 had the same salinity as the offshore Pacific water (station P4) below 150 m. As the summer Pacific water upwelled into JF2 and traveled northward towards station NG in the SoG, a clear decrease in salinity was shown by the depth profiles. Similar spatial trends can be observed for density since salinity exerts the primary control on water density in the Salish Sea (Figure 3.7).

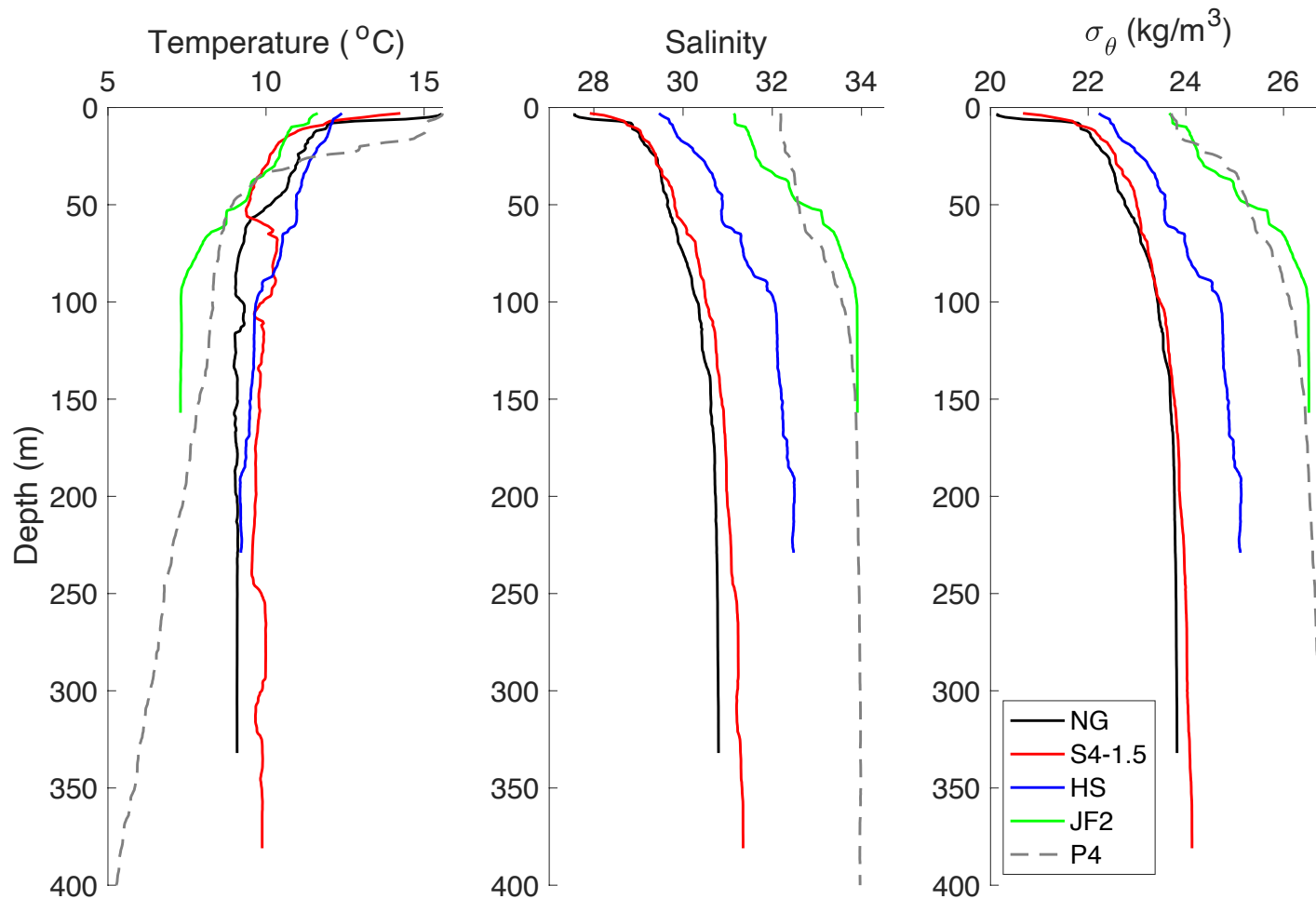


Figure 3.7. Depth profiles of temperature, salinity, and density at stations located in the northern strait (NG), southern strait (S4-1.5), Haro Strait (HS), and Juan de Fuca Strait (JF2) in August 2018. Salinity data at station P4 were obtained from the Line P program data archived for the September 2018 cruise (Institute of Ocean Sciences, 2019).

3.2.2.2 Dissolved Cd concentrations in the Salish Sea

High resolution depth profiles of dCd were collected across the Salish Sea during our August 2018 cruise (Figure 3.8). Concentrations of dCd were also measured at 25 m, 100 m, 200 m, and 400 m at station P4 from the September 2018 Line P cruise. Similar to the trends observed for salinity, clear spatial variations of dCd are illustrated in the depth profiles as the upwelled Pacific water flows landward towards the SoG. At station JF2, there was a gradual increase in dCd concentrations from the surface to 80 m, coinciding with the halocline (Figure 3.7 & Figure 3.8). There was a sharp increase of dCd from 80 to 100 m which separated the water column into two distinct layers. The deep layer from 100 m to the bottom was characterized by high salinity (33.9) water that was also rich in dCd. The dCd concentrations in the deep water of station JF2 were relatively constant with an average of 818 ± 5 pmol/kg, which resembled the Pacific water at approximately 200 m (salinity = 33.9, dCd = 774 ± 6 pmol/kg).

Water travels from the deep Juan de Fuca basin into the Haro Strait region, where it gets vigorously mixed by strong tidal currents. Similar to salinity, concentrations of dCd were not constant at station HS despite of mixing, which showed a clear increase from 629 pmol/kg in the surface to 730 pmol/kg at 100 m (Figure 3.8). Depth profiles at stations HS and JF2 illustrate a tight coupling between salinity and dCd in the water column (Figure 3.7 & Figure 3.8). As the water enters the SoG basin, no significant changes of dCd concentrations were observed between the southern and northern Strait, except for a marginal difference in the bottom water. Overall, the spatial distribution of dCd is consistent with trends observed for salinity, which both exhibits a clear gradual decrease as the oceanic water enters the coastal basins of Salish Sea (Figure 3.7 & Figure 3.8)

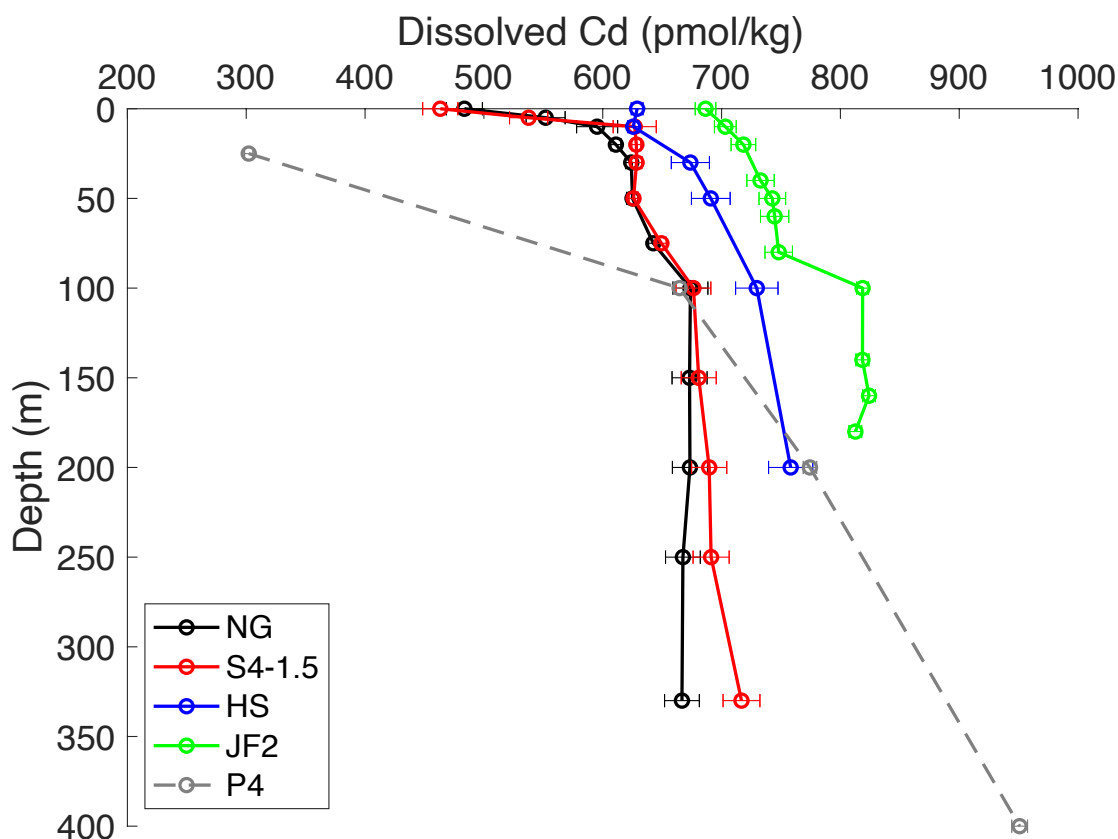


Figure 3.8. Depth profiles of dissolved Cd in the Salish Sea at stations located in the northern strait (NG), southern strait (S4-1.5), Haro Strait (HS), and Juan de Fuca Strait (JF2) in August 2018. Dissolved Cd concentration were also measured in four samples collected at station P4 during the September 2018 Line P cruise (samples were provided by Dr. Jay Cullen’s lab in University of Victoria).

3.2.3 Particulate Al, P, and Cd in the southern SoG

In addition to analysis of dissolved samples, particles suspended in the water column were collected in December 2017 and April 2018 at station S4-1.5 for determination of particulate Cd (pCd) concentrations. Particulate aluminum (pAl) and phosphorous (pP) were also measured to serve as proxies of lithogenic and biogenic materials in sinking particles, respectively. Our results showed a clear surface maximum of pAl in both months, but the concentration in December was twice as large as in April (Figure 3.9). In intermediate waters, a prominent peak of pAl with a similar concentration as the surface maximum was measured at 200 m in December. This secondary pAl maximum was also observed in April, but at a shallower depth (150 m).

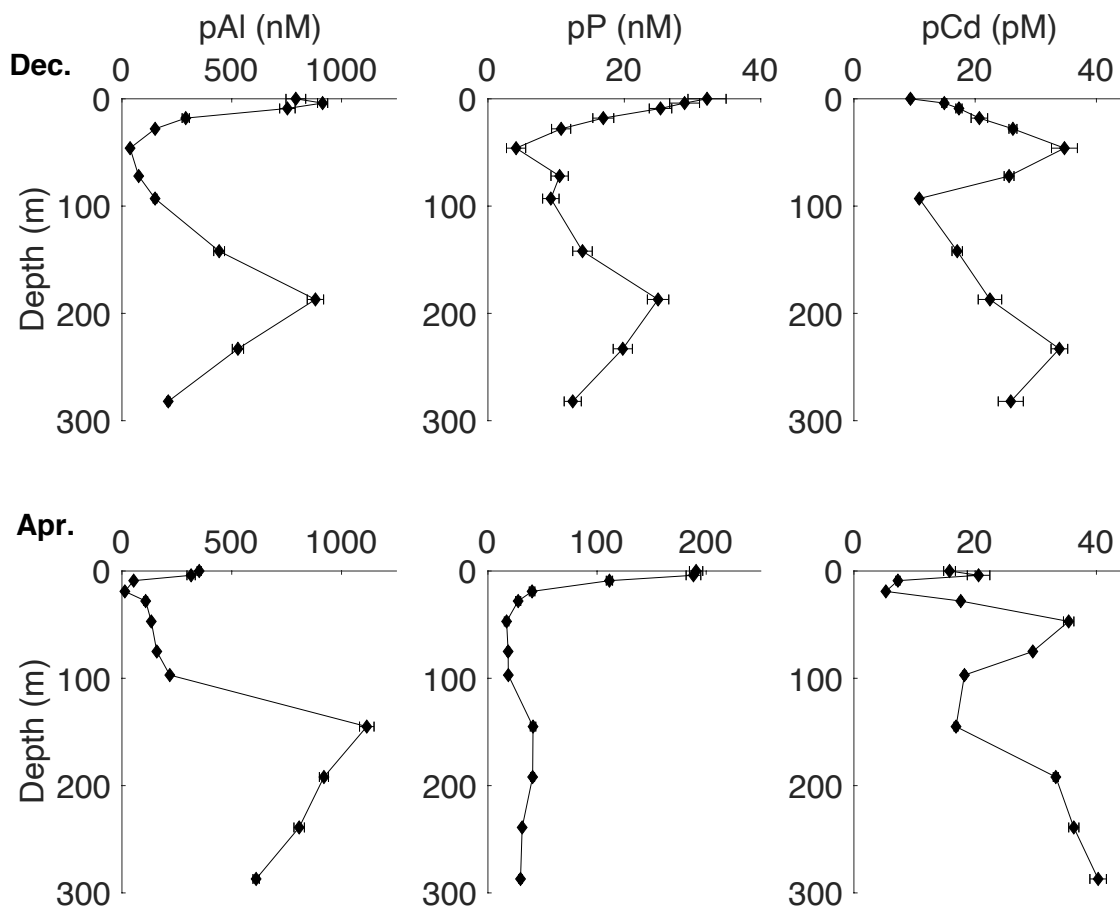


Figure 3.9. Depth profiles of particulate Al, P, and Cd at station S4-1.5 in December 2017 and April 2018. Error bars represent one standard deviations of analytical uncertainty.

Similar to pAl, concentrations of pP were highest at the surface in both months, with a deep maximum at 200 m in December and 150 m in April. In contrast to pAl, surface pP concentrations were about 5 times higher in April than in December, reflecting an increase of biogenic particles during the spring phytoplankton bloom. In intermediate waters, a secondary peak of pAl and pP was observed at the same depth in both December and April, but pAl had a more obvious local maximum than pP. The local maxima of pAl and pP coincided with the minima of transmissivity measured in-situ using a CTD (Figure 3.10). Depth profiles of transmissivity showed a clear intrusion of suspended particles between 150 – 225 m in December, and around 150 m in April.

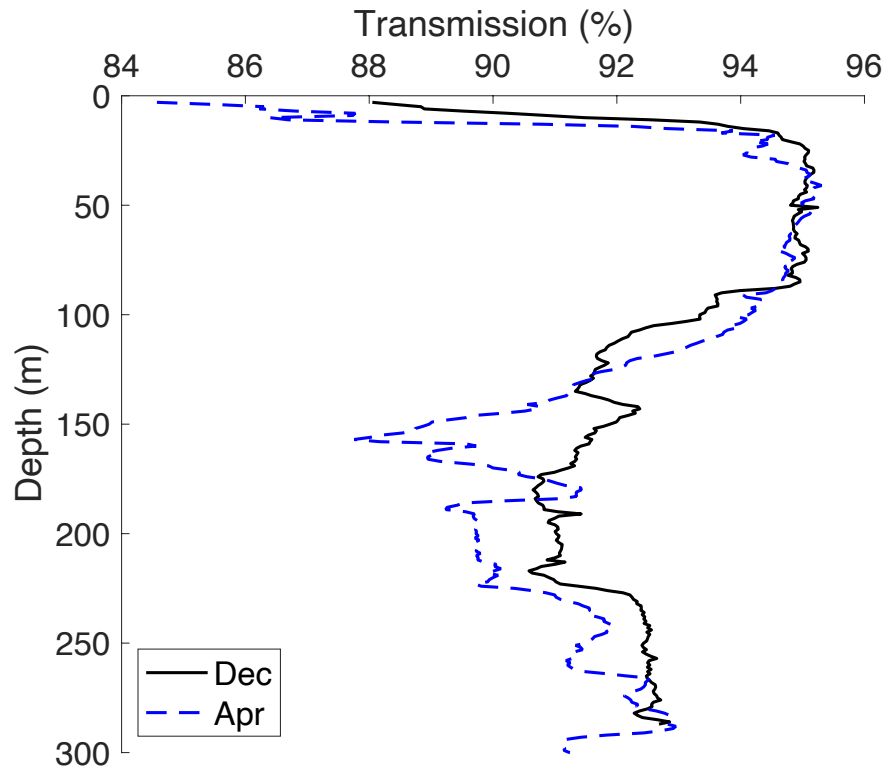


Figure 3.10. Percentage of transmission based on in-situ CTD measurements in the water column at station S4-1.5 in December 2017 and April 2018.

In contrast to the resembling vertical distributions observed for pAl and pP, the depth profiles for pCd have distinct characteristics (Figure 3.9). In both months, there was a well-defined maximum of pCd at 50 m, and a secondary peak at a depth deeper than the pAl and pP maxima in the same depth profile. In April, pCd concentrations showed a subsurface maximum at 5 m and a significant drop down to 20 m, similar to the trend observed for pP. Unlike the consistent decrease of pP with depth in April however, pCd increased again towards a maximum of the same concentration (ca. 35 pM) at 50 m as in December.

3.2.4 Concentrations and fluxes of dissolved and total Cd in municipal effluent

Total and dissolved Cd concentrations were measured in influent and effluent samples collected from the Iona WWTP, as well as in screened wastewater from Macaulay and Clover Points (Table 3.1). The average total Cd concentrations found in effluent samples (509 ± 85 pM) were

significantly lower than in the influent (840 ± 87 pM; P-value < 0.01). Average dissolved Cd concentrations measured in the influent and effluent were 81 ± 18 pM and 94 ± 25 pM, respectively, indicating little or no removal to the particulate pool during primary treatment. In contrast, concentrations of particulate Cd calculated as the difference between the total and the dissolved fraction, yield an average of 759 ± 89 pM in the influent and 415 ± 89 pM in the effluent. This indicates settling of particles in sedimentation tanks, which contributes to approximate 40% removal of particulate Cd during primary treatment.

Our results show that influent entering the Iona WWTP brings Cd mostly in the particulate form, which accounts for approximately 90% of total Cd (Table 3.1). A lower proportion of particulate Cd (~ 80% of the total) was found in the treated effluent. Similarly, Cd discharged from the Macaulay and Clover Points was dominated by the particulate fraction. (Table 3.1). On average, Cd concentrations measured in the screened samples from these two outfalls were higher than levels detected in the Iona influent. Samples collected from Macaulay Point had sporadically much higher dissolved and total Cd concentrations than wastewater discharged at Clover Point around the same time (e.g., March).

Table 3.1. Concentrations of total and dissolved Cd in wastewater samples measured in influent and effluent from the Iona WWTP, and screened samples from Macaulay Point and Clover Point outfalls. Particulate Cd* is calculated by subtracting measured concentrations of dissolved Cd from the total. Red indicates values that exceed the BC Water Quality Guidelines for total Cd in marine waters (1060 pM) without dilution.

Cd Concentrations	Nov-17	Jan	Mar	Jun	Sep	Nov-18	Max	Min	Average
Iona influent									
Dissolved Cd (pM)	65	107	68	70	75	101	107	65	81
Particulate Cd* (pM)	732	631	836	859	845	651	859	631	759
Total Cd (pM)	797	738	904	929	920	752	929	738	840
Iona effluent									
Dissolved Cd (pM)	97	124	103	61	65	113	124	61	94
Particulate Cd* (pM)	407	503	485	427	338	330	503	330	415
Total Cd (pM)	504	627	588	489	403	443	627	403	509
Macaulay Point									
Dissolved Cd (pM)	1267	319	3209	531	247	196	3209	196	961
Particulate Cd* (pM)	4743	615	8154	2162	1582	1320	8154	615	3096
Total Cd (pM)	6010	934	11363	2693	1829	1516	11363	934	4058
Clover Point									
Dissolved Cd (pM)	197	213	235	218	152	193	235	152	201
Particulate Cd* (pM)	1586	514	986	1080	1674	1648	1674	514	1248
Total Cd (pM)	1783	727	1221	1297	1826	1841	1841	727	1449

Anthropogenic Cd loadings from municipal effluent discharge are calculated by multiplying the average concentrations and annual flow rates for corresponding WWTPs (Table 3.2). The annual fluxes of Cd (both total and dissolved) are in the same order of magnitude among the three discharge points. Cd fluxes from the Iona WWTP are greater than or equal to the sum of Macaulay and Clover Points despite the relatively low concentrations measured in the Iona effluent, reflecting its higher annual discharge rate and importance as a potential point source of Cd.

Table 3.2. Average concentrations and annual fluxes of total, dissolved, and particulate Cd measured between 2017 and 2018 from three outfalls (Iona WWTP, Macaulay Point, and Clover Point). Particulate Cd* is calculated by subtracting measured concentrations of dissolved Cd from the total. Total annual flow rates are reported for 2018 (Metro Vancouver and Capital Regional District, personal communication).

Cd from effluent	Average conc.	Annual flow	Annual flux	
	pM	L/yr	mol/yr	kg/yr
Iona Island				
Dissolved Cd	94	2.08E+11	19	2.2
Particulate Cd*	415		86	9.7
Total Cd	509		106	11.9
Macaulay Point				
Dissolved Cd	961	1.63E+10	16	1.8
Particulate Cd*	3096		50	5.7
Total Cd	4058		66	7.4
Clover Point				
Dissolved Cd	201	1.64E+10	3	0.4
Particulate Cd*	1248		20	2.3
Total Cd	1449		24	2.7

3.3 Discussion

3.3.1 Natural sources of dissolved Cd to the Salish Sea

In order to understand the distributions of dCd in the Salish Sea, we first investigate the influence of conservative mixing in shaping the spatial variations of dCd in this estuarine system. A simple approach is to plot water column concentrations of dCd versus a conservative tracer (i.e., salinity)

against the mixing line between freshwater and oceanic end members (i.e., Fraser River and Pacific Ocean, respectively). If most of the dCd data collected in the Salish Sea fall on the mixing line, it would suggest that dCd concentrations are primarily governed by physical circulation and mixing. However, it is challenging to apply this approach for our data because the dCd and salinity of the Pacific end member, as well as the dCd of the freshwater end member vary seasonally. The following subsections will discuss these variations and show how the Salish Sea box model can be used to address this problem.

3.3.1.1 Freshwater end member

Concentrations of dCd have been measured in the Fraser River at the Water Quality Buoy located in the Main Arm of the river since 2011 by Environment and Climate Change Canada. Unfortunately, there are no continuous measurements of water discharge at this location. Fraser River flow is continuously monitored at Hope (150 km upstream of the river mouth, Pawlowicz et al., 2007) by the Water Survey of Canada. However, the flow rate measured at Hope does not completely represent the total Fraser River discharge into the SoG because there are a number of rivers flowing into the Fraser downstream of Hope. In addition, intense rainfall events in the fall and winter can contribute significantly to the total freshwater inflow into the SoG through smaller rivers. In this study, we used flow rates measured at two stations, Fraser River at Hope (station 08MF005) and Englishman River near Parksville (station 08HB002) to represent snowmelt and rainfall dominated rivers, respectively. A linear function employed in the Salish Sea box model is used to estimate the total freshwater inflow into the SoG (Wang et al., 2019).

$$Total\ flow\ (m^3/s) = 1.11 \times Fraser\ flow + 18.8 \times Englishman\ flow + 1651.7$$

Unlike river flow rates, time-series measurements of dissolved trace metals including dCd are only available from the Water Quality Buoy in the Fraser River. Given the lack of data in other smaller rivers, we assume that all rivers entering the SoG basin (e.g., Englishman River) have the same concentration of dCd as the Fraser River.

Our results show that concentrations and fluxes of dCd reach a maximum at the beginning of the river freshet (Figure 3.11). The time lag between highest dCd concentration and maximum river discharge is confirmed by plotting all available dCd and river flow data versus calendar months (Figure 3.12). Similarly, Voss et al. (2015) found significant changes in the geochemical properties (e.g., organic matter content) of the Fraser River at the early onset of freshet. They attributed the changes to the initial melting of snowpack and mobilization of the shallow soil pool, which releases suspended particulate matter and dissolved organic matter (DOM) to the water. Desorption of dCd from soil particles and discharge of dCd bound to dissolved organic ligands are plausible explanations for the rapid increase in dCd concentrations during the early river freshet (Figure 3.12). Average dCd concentrations and river flow rates ($\pm 1SD$) can be calculated for time intervals (i.e., months) with relatively constant concentrations or discharges. Integrating dCd fluxes over these time intervals and adding them up to a full year results in an annual riverine input of 20422 ± 3097 mol/yr (2296 ± 348 kg/yr), with an average dCd concentration of 119 ± 20 pM.

To best represent the Fraser River end member, available dCd data from the Water Quality Buoy are supplied to the Salish Sea box model in combination with flow rate data from Fraser River at Hope and Englishman River. The model then makes a monthly climatology of the time-series river input and applies it for the entire run. For instance, it takes averages for all available dCd river data in January, February, March etc., and repeat this cycle for the entire model time frame (1995-2018). Model output gives a mean annual flux of 17418 ± 1539 mol/yr (1958 ± 173 kg/yr) for the river end member, which is in agreement with our estimate based on Figure 3.12.

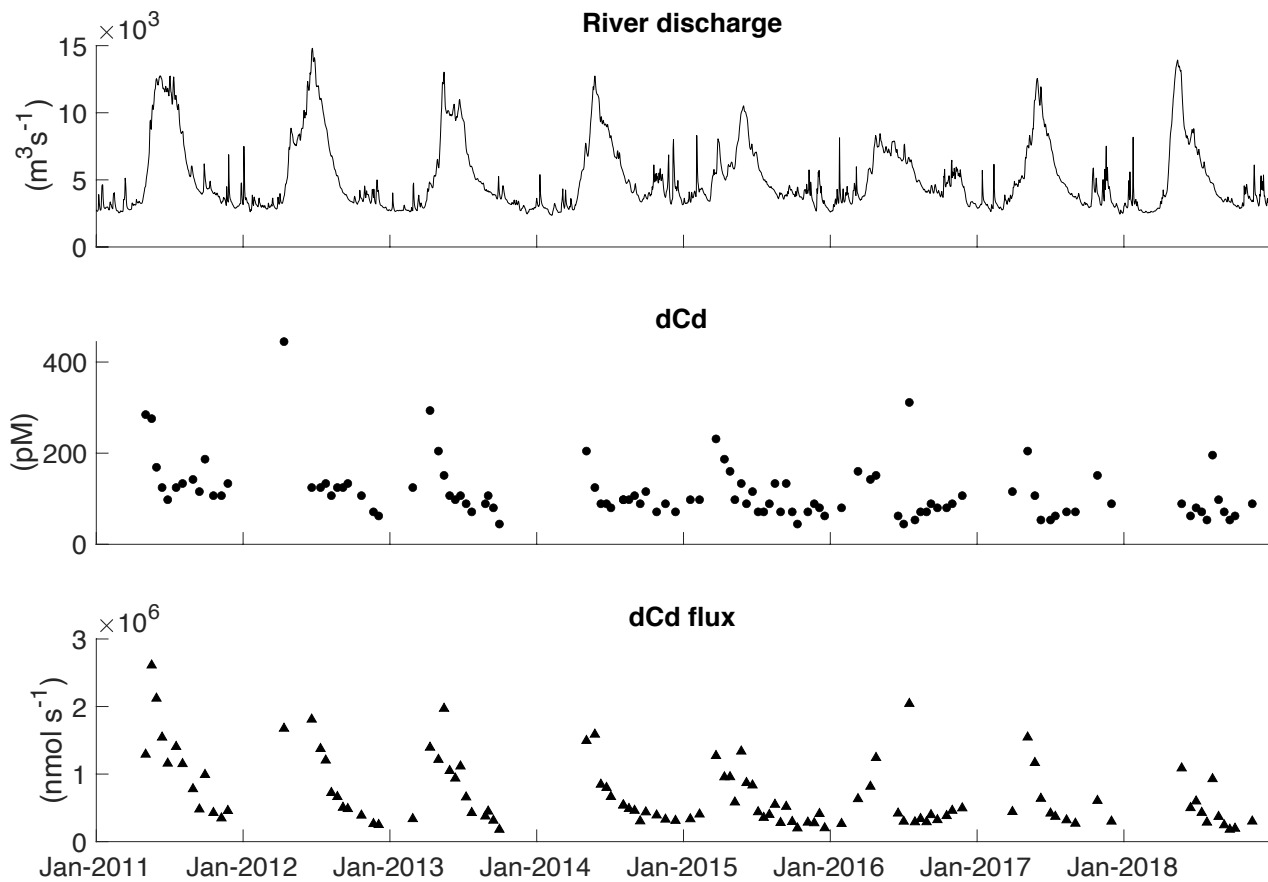


Figure 3.11. Time series (2011-2018) of freshwater discharge, dissolved Cd concentration, and dissolved Cd flux. Discharge is based on measurements from Fraser River at Hope and Englishman River by Water Survey of Canada. Dissolved Cd concentrations were obtained from the Fraser River Water Quality Buoy located in the Main Arm of the river (Environment and Climate Change Canada, 2018).

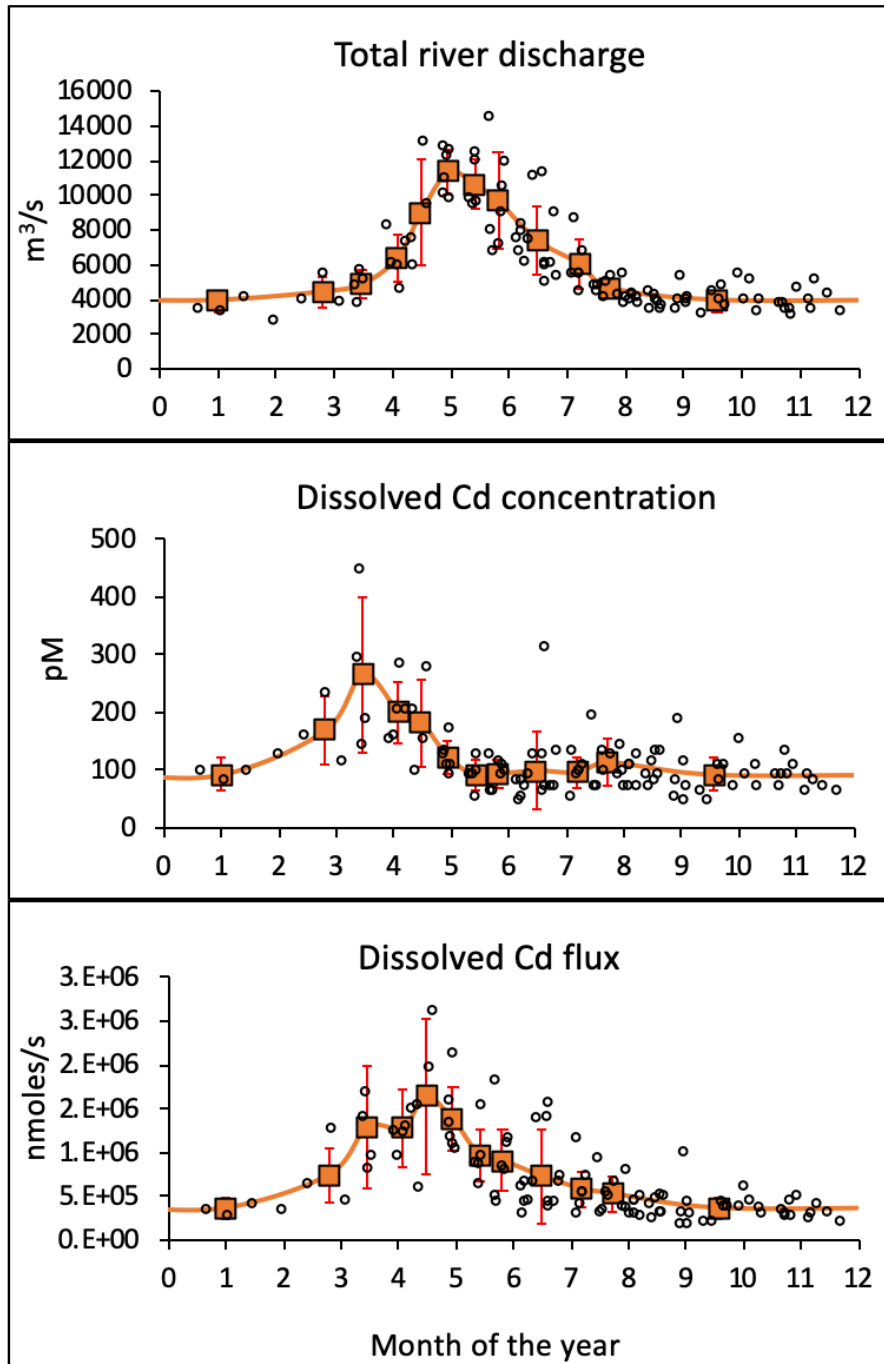


Figure 3.12. Total river discharge rate (top), dissolved Cd concentrations measured in the Fraser River Main Arm (centre), and dissolved Cd fluxes from rivers (bottom) all plotted against months. Black empty circles are data shown in Figure 3.11. Orange filled squares are calculated averages ± 1 SD for each time interval with relatively constant river discharge and dissolved Cd concentration.

3.3.1.2 Pacific end member

The properties (temperature, salinity, dissolved oxygen, nutrients) of Pacific water upwelled into the Salish Sea vary with seasons (Wang et al., 2019). From late fall to spring, prevailing offshore winds trap fresh water from continental runoff against the coast, lowering the salinity of incoming Pacific water. In the summer, wind-driven coastal upwelling brings deep and saline oceanic water into the Juan de Fuca Strait basin (Thomson, 1981). Hydrographic datasets at station JF2 located in the Juan de Fuca Strait and further offshore at station P4 in the northeast Pacific are available from the ongoing Line P program (Institute of Ocean Sciences). Historical data from these two locations can be used to understand seasonal changes in the physical (e.g., salinity) and chemical properties (e.g., dCd concentrations) of the Pacific end member.

Salinity depth profiles measured in February and September 2018 at station JF2 (Figure 3.13A) clearly show that the upwelled Pacific water is saltier, and thus denser in the summer compared to the winter. Water column observations at station P4 can be used to represent characteristics of the incoming Pacific water. Janssen et al. (2017) reported a high-resolution profile of dCd at station P4 in August 2012. Concentrations of dCd we measured in four samples between 25 m and 400 m in September 2018 are plotted against salinity and shown together with Janssen's published data (Figure 3.13B). Using salinity as a conservative tracer, we could estimate the dCd concentration in the Pacific source water based on salinity measured in the deep Juan de Fuca basin. The deep waters at Juan de Fuca Strait may be slightly less saline and lower in dCd concentration than the incoming Pacific water due to partial mixing with outflowing surface water. Salinity and dCd measured in the deep waters at station JF2 can thus be taken as minima for the Pacific end member. With a salinity of 33.9 below 100 m at station JF2 in the summer (Figure 3.13A), the estimated dCd concentration in the upwelled Pacific water is approximately 800 pmol/kg (Figure 3.13B). Assuming the Pacific water has a slightly higher salinity than deep waters at Juan de Fuca Strait, we could establish an upper boundary for dCd (950 pmol/kg at salinity of 34; Figure 3.13) in the summer upwelling season.

In February, salinity at station JF2 ranged from 33.1 at 100 m to 33.7 at 180 m (Figure 3.13A). If we assume an even flow of water over this depth range, the average salinity of winter Pacific water

would be approximately 33.4. Unfortunately, there is no winter profile of dCd available at station P4. Using the dCd profiles collected in August and September, the average dCd concentration in water with a salinity of 33.4 is roughly 650 pmol/kg (Figure 3.13B). Knowing the approximate range of dCd concentrations (650 – 950 pmol/kg) in the Pacific water, we can apply the Salish Sea box model to better quantify the varying dCd input from the Pacific end member.

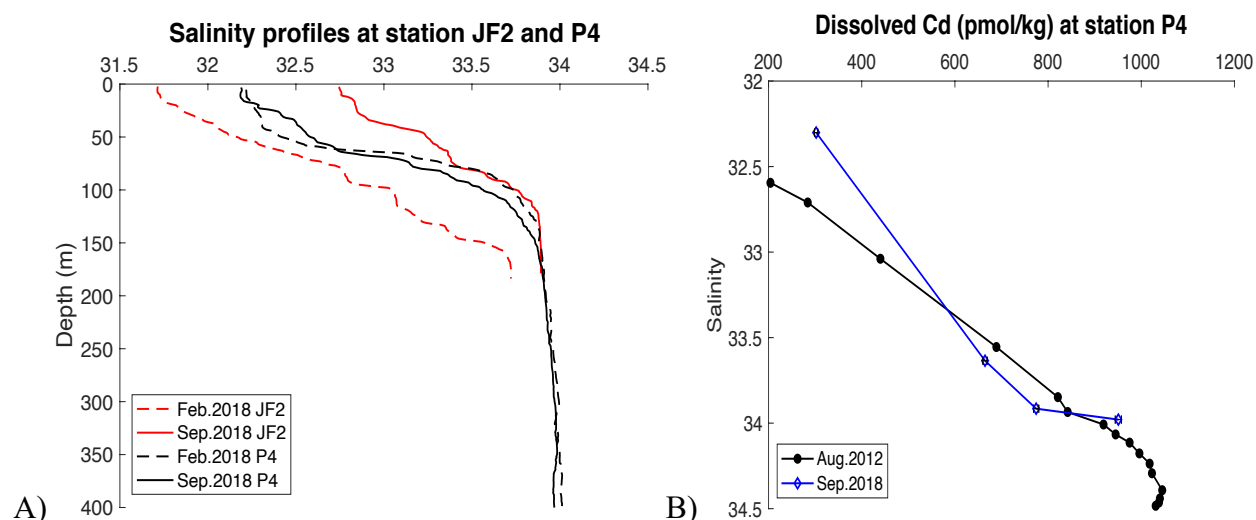


Figure 3.13. A) Salinity profiles at stations JF2 (red) and P4 (black) on the Line P cruise track in February (dash line) and September (solid line) 2018. Hydrographic data were obtained from the Line P program online data archive (Institute of Ocean Sciences). B) Dissolved Cd profiles for the entire water column at station P4 during the August 2012 cruise (Janssen et al., 2017), and selected samples (25 m – 400 m) measured from the September 2018 cruise.

3.3.1.3 Box model application for spatial distributions of dissolved Cd

The salt budget in the modelled estuarine circulation is balanced by water exchange between deep inflow of Pacific water into Juan de Fuca Strait and surface freshwater runoff from the Fraser River and other small rivers into the SoG (Wang et al., 2019). The modelled salinity is in reasonable agreement with field observations in the Salish Sea (Figure 3.14), which adds confidence in using the model to gauge the conservative behavior of any given tracer (e.g., dCd). Variable Pacific and river inputs can be supplied to the model to better constrain the two end members and then predict the spatial distributions and temporal variations of dCd in the Salish Sea due to conservative

mixing. Discrepancy between the modelled and field data thus provide a baseline to gauge the biogeochemical cycling of Cd and to identify any additional sources or sinks.

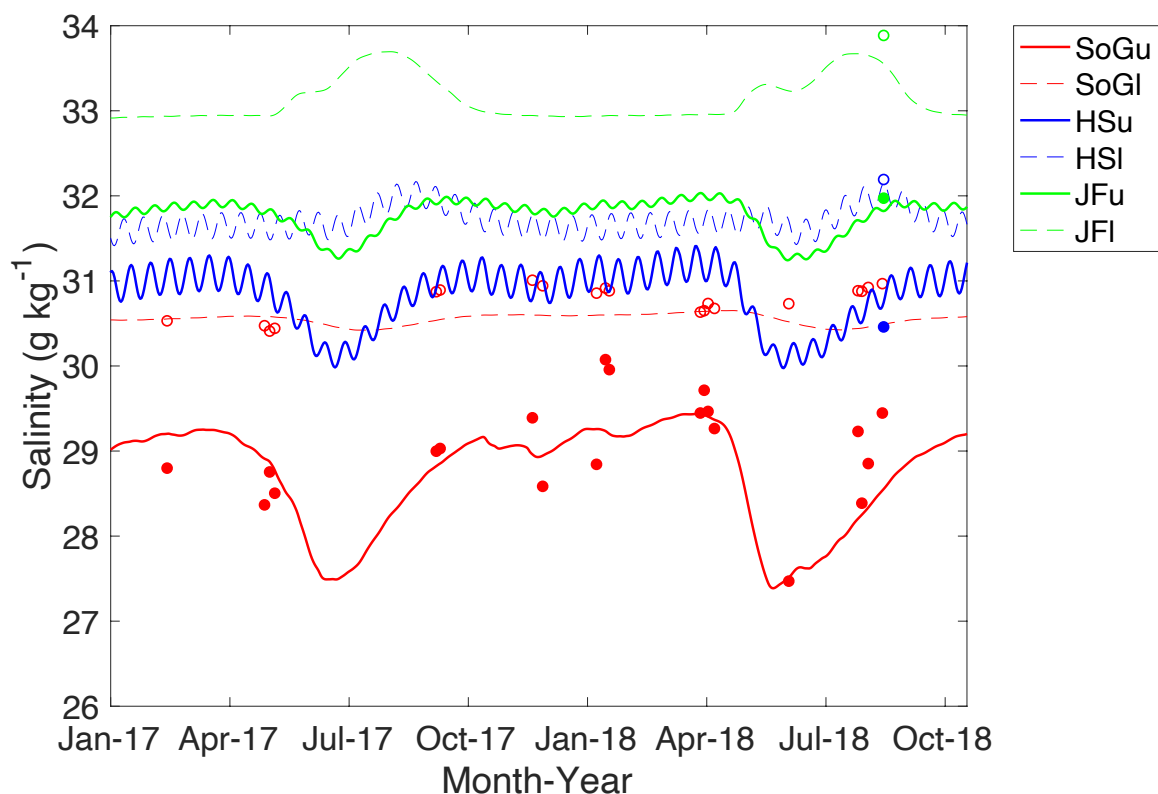


Figure 3.14. Modelled vs measured salinity in the Strait of Georgia upper (SoGu), Strait of Georgia lower (SoGl), Haro Strait upper (HSu), Haro Strait lower (HSI), Juan de Fuca Strait upper (JFu), and Juan de Fuca Strait lower (JFI) boxes. Upper boxes represent water column from the surface to 50 m, and lower boxes are 50 m to the bottom. Filled and empty circles represent the average salinity in the upper (0 – 50 m) and lower (50 m – bottom) boxes, respectively, based on CTD profiles collected at station S4-1.5 (Strait of Georgia) between February 2017 to August 2018, as well as at stations JF2 (Juan de Fuca Strait) and HS (Haro Strait) in August 2018.

In order to address the seasonal variations of dCd in the Pacific end member, we provide the model a winter baseline concentration, and a variation range that is positively correlated with the modelled Pacific salinity (i.e., higher salinity, high dCd input). Based on the available dCd profiles at station P4 (Figure 3.13), we tested plausible combinations of baseline dCd concentrations and variations for the incoming Pacific water (Table 3.3). The model inputs are considered a good fit

if the following criteria are met: 1) The modelled concentration in the Juan de Fuca lower box is similar to that observed in the deep samples at station JF2 during our August 2018 cruise. 2) Model outputs for the SoG upper box are higher than or equal to the average dCd concentrations measured in the upper 50 m. 3) Model outputs for the SoG lower box are smaller than or equal to the average dCd concentrations measured below 50 m. The second and third criteria are based on the premise of biological cycling (surface uptake followed by remineralization of dCd in deeper waters). Results show that the best fit for our dCd data is achieved with a baseline concentration of 650 pM, and a variation of 300 pM (Table 3.3).

Table 3.3. Model outputs for dissolved Cd with various Pacific input (which requires a unit in pM) . * indicates that June 2018 is an exception, where model output is greater than the average dissolved Cd concentration measured in the upper 50 m of SoG.

Pacific input (pM) baseline + variation	Juan de Fuca lower box	SoG lower box	SoG upper box	Remarks
700 + 250	model > data	model > data	model > data	Pacific input too high
650 + 325	model > data	model ≤ data	model > data	Upper threshold
650 + 300	model = data	model ≤ data	model > data	Best fit of data
625 + 300	model < data	model < data	model = data*	Lower threshold
600 + 350	model < data	model < data	model < data*	Pacific input too low

Modelled concentrations of dCd based on the best fit Pacific input are illustrated with field measurements superimposed for comparison (Figure 3.15). Both modelled and field data demonstrate the same spatial trends of dCd, which has the highest concentrations at Juan de Fuca Strait (JFu & JFl boxes), and gradually decreases as the water moves into the Haro Strait region (HSu & HSl boxes) before entering the SoG. In the SoG basin, the temporal trends of dCd concentrations observed in the field are consistent with model predictions. For example, modelled concentrations exhibit larger variability in the upper 50 m (SoGu box), with the lowest value predicted for June. The higher than measured dCd concentration in the SoGu box of June could reflect dCd sinks in surface waters that are not incorporated in the model. Plausible removal mechanisms of dCd (e.g., biological uptake, chemical precipitation) in the SoG will be discussed in more details with the mass balance calculation in section 3.3.6. Overall, results from the Salish

Sea box model confirm the significance of conservative mixing in shaping dCd distributions in the water column.

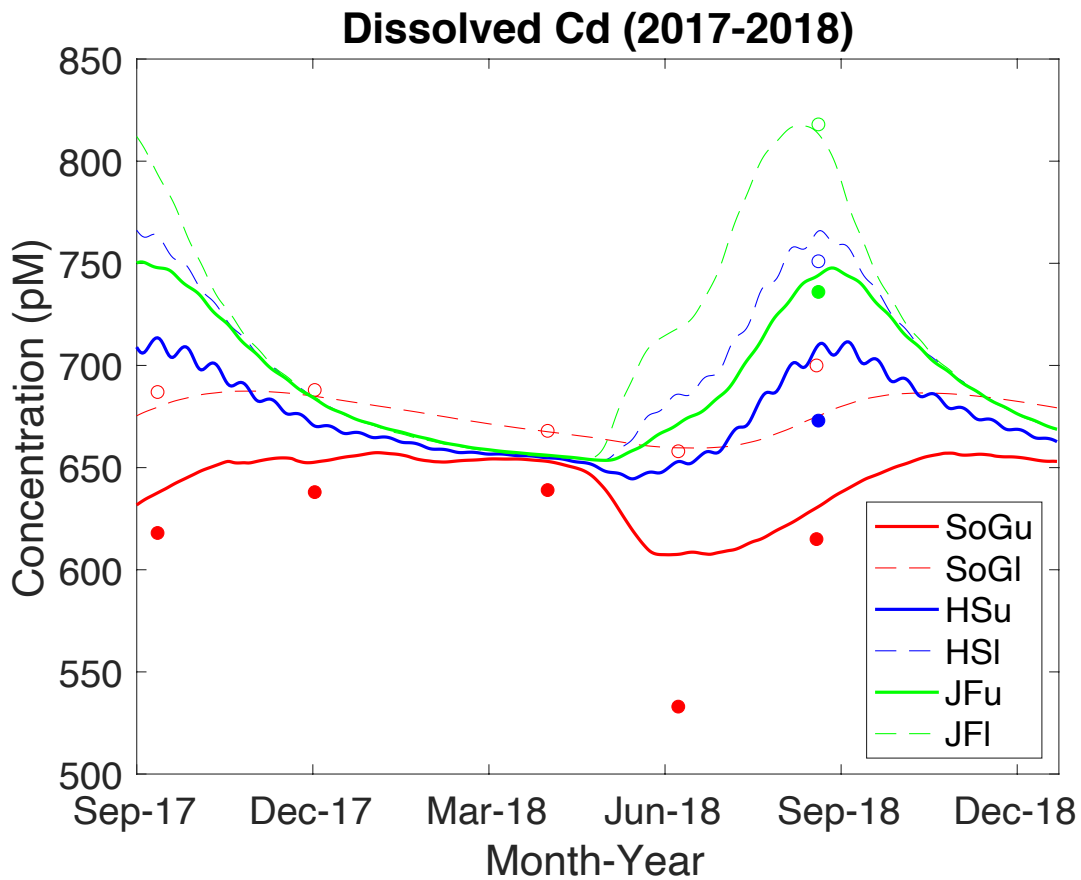


Figure 3.15. Modelled vs measured dissolved Cd concentrations in the Strait of Georgia upper (SoGu), Strait of Georgia lower (SoGl), Haro Strait upper (HSu), Haro Strait lower (HSI), Juan de Fuca Strait upper (JFu), and Juan de Fuca Strait lower (JFI) boxes. Upper boxes represent water column from the surface to 50 m, and lower boxes are 50 m to the bottom. Model results are based on the best fit Pacific input ($650 + 300$ pM; Table 3.3). Filled and empty circles are field measurements for dissolved Cd in the upper (average concentrations between 0 and 50 m) and lower (average concentrations below 50 m) boxes, respectively.

3.3.2 Anthropogenic input of Cd to the Salish Sea

Having discussed the natural sources of Cd into the Salish Sea, we then assess whether anthropogenic discharges from WWTPs could significantly elevate the ambient Cd concentrations. The British Columbia Water Quality Guideline (BC WQG) for total Cd concentration in marine

waters (Ministry of Environment British Columbia; 1060 pM) was frequently exceeded in undiluted effluents from Macaulay and Clover Points (Table 3.1). The estimated initial dilution factors for the wastewaters are 245 and 175 for Macaulay and Clover Points, respectively (Hodgins, 2006). These factors are conservative estimates of the dilution predicted to occur at the boundary of the initial dilution zone (100 m radius around the outfall). Strong currents in Juan de Fuca Strait facilitate mixing between wastewater and ambient seawater, which can effectively dilute Cd concentrations to levels below the threshold stated in the BC WQG.

Johannessen et al. (2015) constructed regional geochemical budgets for metals in the SoG and concluded that the maximum contribution of wastewater to the Cd sediment sink was 5%. Their budget was based on an annual Cd input of 230 kg/yr from the Iona WWTP, 9 kg/yr from Macaulay Point, and 6 kg/yr from Clover Point. Their estimates for Macaulay and Clover are in the same order of magnitude as our particulate Cd fluxes based on the 2017-2018 effluent data (Table 3.2). Since precise Cd concentrations in the Iona effluent were not available in the municipal annual reports, Johannessen et al. used the detection limit of Cd to estimate its annual discharge (2015). Substituting our particulate Cd flux of 9.7 kg/yr in their regional budgets suggest that the contribution of wastewater to Cd burial in SoG sediment is approximately 1%.

Inputs of dCd from municipal effluent, freshwater discharge, and the Pacific Ocean are introduced to the Salish Sea box model to predict concentrations of dCd assuming conservative mixing. A constant dCd flux of 2.2 kg/yr (Table 3.2) is added to the SoG lower box to represent the contribution from Iona effluent discharge. The combined discharges of dCd from Macaulay and Clover Points are equivalent to that from the Iona WWTP. Inputs from these two outfalls are added to the Haro Strait lower box. Anthropogenic loadings of dCd into the Salish Sea are superimposed on its natural sources. As previously discussed, concentrations of dCd from rivers and the Pacific Ocean are introduced to the model as time variables. Not only do concentrations of dCd vary with time (Figure 3.15), the flow rates of rivers and the Pacific also show seasonal trends (Figure 3.16). In the summer, stronger winds and coastal upwelling bring in a larger volume of Pacific water from deeper waters that are high in dCd. River discharge also peaks in early summer, but the volume flux is smaller relative to the Pacific inflow (Figure 3.16).

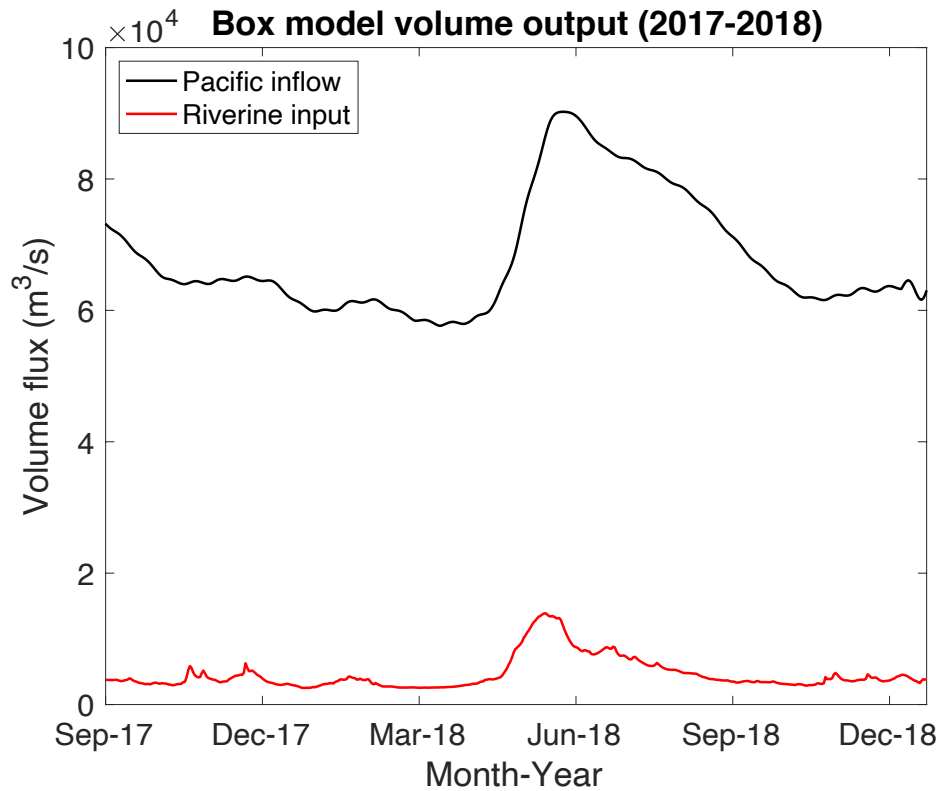


Figure 3.16. Box model outputs for the Pacific and freshwater volume fluxes into the Salish Sea.

A summary table is compiled to compare the concentrations and fluxes of dCd from three main sources into the SoG (Table 3.4). Model results confirm that the Pacific brings the largest volume of water that is also highest in dCd, making it the dominant source of dCd into the SoG. The total freshwater discharge into the SoG is relatively small compared to the Pacific volume flux (Figure 3.16). Concentrations of dCd in the Fraser River is approximately 5 – 10 times less than in the Pacific, and are similar to levels measured in the Iona effluent (Table 3.4). Given the low dCd concentrations found in municipal effluent and the relatively small volumes discharged, WWTPs add an insignificant amount of dCd into the water column. In short, the dominant source of dCd in the SoG is the Pacific Ocean, followed by continental runoff, and barely from anthropogenic effluent discharge (Table 3.4).

Table 3.4. Volume fluxes, average concentrations and loadings of dissolved Cd in effluent discharged from the Iona WWTP, from riverine input (mainly Fraser River), and from the upwelled Pacific water. Volume flux from the Iona WWTP is based on the 2018 flow data (Metro Vancouver, personal communication). Box model outputs are indicated by asterisk (*).

Sources	Volume flux (L/yr)	Dissolved Cd concentration (pM)	Dissolved Cd flux (kg/yr)
Iona Effluent	2.08×10^{11}	94 ± 25	2.2 ± 0.6
Riverine input	1.56×10^{14} *	119 ± 20	1958 ± 173 *
Pacific Ocean	2.18×10^{15} *	950 (upper threshold) 650 (winter baseline)	$186,000 \pm 5,226$ *

3.3.3 Temporal variations of dissolved Cd in the southern SoG

The vertical distribution and seasonal variability of dCd in the water column of the SoG can be influenced by various processes. Biological cycling, physical mixing, and sediment diagenesis could all play a role in determining the concentrations of dCd in the SoG water column. Hydrographic (temperature, salinity) and biological parameters (O_2 , macronutrients, chlorophyll-a) can provide the general context that is essential for understanding the dispersion and removal of Cd in the SoG. The following sections will discuss the temporal variations of dCd concentrations for the surface, intermediate, and deep layers separately, with respect to the general water circulation and biological cycling of nutrients in the SoG.

3.3.3.1 Surface layer (0 – 50 m)

A surface deficit of dCd is apparent in the euphotic zone for all months (Figure 3.6). The lowest concentration of dCd (269 pmol/kg) was observed in the surface water of June, when freshwater runoff into the southern Strait was at its annual maximum during the Fraser River freshet. The mean dCd concentration in the Fraser River water (119 ± 20 pM; Table 3.4) is much lower than that in the ambient SoG seawater (Figure 3.6). As a result of the peak riverine input, both surface salinity and dCd concentration decreased significantly in June, relative to other months of the year (Figure 3.1A & Figure 3.6). As shown by the density depth profiles recorded on station, the water column was most stratified in June, followed by December, September, August, and April (Figure

3.2A). Strong stratification in June restricted mixing with deeper waters. A combined effect of dilution by freshwater, biological uptake, and lack of supply from deep waters likely resulted in the sharp gradient of dCd observed in the upper 20 m for June. In contrast, despite the higher chlorophyll-a concentrations measured in surface waters of April, dCd was less depleted relative to June. Similar trends were observed for the macronutrients NO_3^- and PO_4^{3-} (Figure 3.4). Weaker stratification in April allowed for sufficient mixing with deeper waters to replenish macronutrients and bioactive trace metals such as dCd.

The contribution of mixing with freshwater, surface stratification, and biological uptake in creating the surface depletion of dCd can be discussed in parallel with macronutrient drawdown. To estimate the fraction of Fraser River water present in the mixed layer, we assume conservative mixing between freshwater runoff and deeper SoG waters with relatively constant salinity (below the halocline). Nutrient or dCd drawdown can then be calculated as the difference between the expected and the measured concentrations in the mixed layer.

In September 2017, the seasonal pycnocline isolated a shallow mixed layer (upper 8 m) from deeper waters (Figure 3.2A), mostly because of warm sea surface temperature. Relatively high chlorophyll-a concentrations (Figure 3.5) indicate the occurrence of a fall phytoplankton bloom. Dissolved oxygen concentration in the mixed layer was close to saturation as a result of photosynthesis and limited mixing with deeper O_2 -depleted water. Knowing the average salinity of the mixed layer (27.4) and deeper waters (20 – 50 m; 29.2), the fraction of Fraser River water and subsurface SoG waters in the mixed layer was 6.2% and 93.8%, respectively. The average nutrient concentrations in the SoG end member were 26.6 μM , 2.36 μM , and 48.5 μM for NO_3^- , PO_4^{3-} , and Si, respectively. For the Fraser River end member, we used the discharge-weighted averages (4.76 μM , 0.125 μM , and 81.2 μM , respectively) estimated by Voss et al. (2014). Biological nutrient uptake in September can be calculated as the following:

$$\text{NO}_3^- \text{ drawdown} = (6.2\% \times 4.76 \mu\text{M}) + [(93.8\% \times 26.6 \mu\text{M})] - 10.3 \mu\text{M} = 14.9 \mu\text{M}$$

$$\text{PO}_4^{3-} \text{ drawdown} = [(6.2\% \times 0.125 \mu\text{M}) + (93.8\% \times 2.36 \mu\text{M})] - 1.16 \mu\text{M} = 1.06 \mu\text{M}$$

$$\text{Si drawdown} = [(6.2\% \times 81.2 \mu\text{M}) + (93.8\% \times 48.5 \mu\text{M})] - 35.5 \mu\text{M} = 15.0 \mu\text{M}$$

Our estimates yield $\text{NO}_3^- : \text{PO}_4^{3-}$ and $\text{Si} : \text{NO}_3^-$ uptake ratios of 14 and 1, respectively during the September fall bloom, expected for diatoms growing under Fe-replete conditions. Analogously, we can estimate dCd uptake using the average concentration measured in the SoG between 20 – 50 m (622 pmol/kg) and in the Fraser River (119 pM). The difference between expected and measured dCd in the mixed layer is 98 pmol/kg, yielding a molar dCd: PO_4^{3-} uptake ratio of approximately 0.09 pmol/nmol. This uptake ratio is lower than the average phytoplankton Cd: P quota (0.21 pmol/nmol), but is in agreement with the relatively low quota measured for coastal diatom species (Ho et al., 2003).

In December 2017, there was no clearly defined mixed layer. While temperature was lowest (8 °C) at the surface, heavy precipitation and freshwater runoff resulted in relatively low surface salinity, stratifying the upper 20 m of the water column (Figure 3.1A). Surface water chlorophyll-a concentrations were the lowest measured on station, indicating very little or no primary production (Figure 3.5). This is consistent with the very small surface depletion in nutrients (Figure 3.4). The deficit of dCd in surface waters is thus attributed to dilution by freshwater.

In April 2018, the upper water column was the least stratified among all sampling months (Figure 3.2A). This is when the highest chlorophyll-a concentrations were measured in near surface waters (Figure 3.5), indicating the presence of a spring phytoplankton bloom. Notwithstanding the relatively high chlorophyll-a concentration, surface water dissolved oxygen concentration was below saturation and it decreased rapidly with depth as a result of vertical mixing with low- O_2 deep waters (Figure 3.3). Applying the same method as applied for the September 2017 data but using the 30 m sample as the SoG end member yields a 21 μM drawdown for NO_3^- , 1.6 μM for PO_4^{3-} , and 42 μM for Si in the upper 5 m of the water column. The $\text{Si} : \text{NO}_3^-$ molar uptake ratio of 2 indicate the dominance of diatoms more heavily silicified than in September 2017. Indeed, phytoplankton community composition in the upper 30 m show dominance of diatom species (97%) in April (personal communication, J. Guo, UBC). In contrast, diatoms accounted for about 30% of phytoplankton found in September, and flagellates (dinoflagellate and nanoflagellate) were more abundant in the water column at that time (personal communication, J. Guo, UBC).

The estimated uptake of dCd is 63 pmol/kg if using 119 pM as the April Fraser River end member, which results in a dCd: PO₄³⁻ uptake ratio (0.04 pmol/nmol) that is a factor of 2 lower than in September (0.09 pmol/nmol). Using a higher concentration (267 pM, Figure 3.12) for the Fraser River to represent the pulse of relatively high dCd released from the early onset of freshet gives a similar uptake ratio. The relative low uptake ratio is likely due to the dominance of diatom species in April, which have a lower cellular demand for Cd than dinoflagellates (Ho et al., 2013). In general, the low dCd: PO₄³⁻ uptake ratios during the spring and fall blooms in the SoG are consistent with the average phytoplankton Cd :P quota for coastal species (0.1 pmol/nmol; Ho et al., 2013).

The strongest surface water stratification occurred in June as a result of high summer sea temperature and low surface salinity (Figure 3.1A). A shallow mixed layer lay above a sharp pycnocline between 7 - 20 m, limiting the supply of nutrients to surface waters. This explains the trace amounts of NO₃⁻ and PO₄³⁻ detected in near surface waters, and the relatively low chlorophyll-a concentrations (Figure 3.4 & Figure 3.5). In contrast, there was no surface depletion in Si likely due to its high input from the Fraser River (81.2 μM; Voss et al., 2014). Nutrient drawdown is measurable from 5 m down to 30 m in June (calculations not shown), consistent with the uniform chlorophyll-a concentrations found over that depth range (Figure 3.5). Two months later in August 2018, a phytoplankton bloom similar in magnitude to the September 2017 fall bloom resulted in further nutrient depletion in surface waters (Figure 3.4 & Figure 3.5).

3.3.3.2 Intermediate layer (50 – 200 m)

Concentrations of dCd show significant temporal variations in the intermediate layer, although at a smaller magnitude relative to surface waters (Figure 3.6). In order to rationalize the distribution of dCd concentrations at intermediate depths, we first discuss temporal variations in the physical characteristics of this water mass to gain insight on how SoG intermediate water is formed and where it is flowing. The intermediate water mass in the SoG basin is a mixture of incoming Pacific water and outflowing SoG surface water which returns at subsurface depths after being intensely mixed in the Haro Strait region (Figure 1.2; Pawlowicz et al., 2019). The seasonal cycles of temperature and dissolved oxygen in the Haro Strait source water can propagate into the SoG with

a time delay. Using hydrographic datasets collected over the entire SoG, Stevens and Pawlowicz (in prep) estimated a transit time of approximately 2 – 3 months for the water to travel from Haro Strait to the SoG basin. They also found that the amplitude of seasonal variations is dampened as the water flows northward into the SoG basin due to mixing with surrounding waters.

Temperature shows clear seasonal changes in the intermediate layer, with the highest values observed in August/September, followed by December, June, and April (Figure 3.1B). With a transit time of 2 months between Haro Strait and the southern SoG, the cold water sampled in April at station S4-1.5 was formed in the winter (ca. February). The same delay applies for dissolved oxygen, which had the highest concentrations in April (Figure 3.3) due to higher solubility in the winter source water at Haro Strait (i.e., February). Temporal variations of temperature and dissolved oxygen at station S4-1.5 are both consistent with the hypothesis that seasonal cycles of water properties in the Haro Strait source water are advected into the SoG basin with a time delay (Stevens and Pawlowicz, in prep).

Temporal variations of salinity were also observed in the intermediate layer, but the trends were different in the shallower (50 – 100 m) and deeper (100 – 200 m) sections. While variabilities in temperature and dissolved oxygen at Haro Strait are dictated by seasonal changes in air temperature, salinity is controlled by mixing between the outflowing SoG surface water and inflowing Pacific water (Figure 1.2). Salinity in the SoG surface waters is lowest during the Fraser River freshet in June, while the incoming Pacific water has higher salinity in late summer due to stronger coastal upwelling. The marked increase in salinity between 50 – 100 m in August/September (Figure 3.1) suggests insufficient mixing of the fresh SoG surface water and saline Pacific water at the Haro Strait region in June. In other words, the shallow section of the SoG intermediate layer (towards 50 m) in late summer had a larger proportion of the outflowing surface SoG water in June, whereas the deeper section (100 – 200 m) was influenced more by the upwelled Pacific water. This is consistent with the diverging trends in salinity between 50 m and deeper depths (100 – 200 m) from April to August 2018 at station S4-1.5 (Figure 3.17). Similar to salinity, there was also a sharp increase in dCd concentrations in August/September between 50 – 100 m. This can reflect influence of the SoG return flow containing the “old” surface water from

June, which was relatively fresh and low in Cd compared with other months (Figure 3.1A & Figure 3.6).

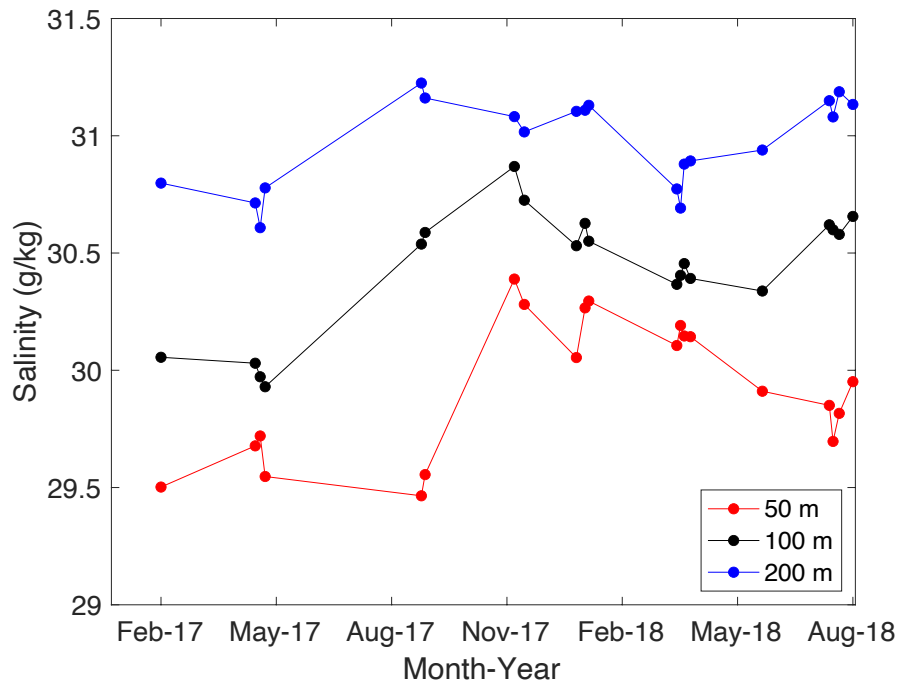


Figure 3.17. Temporal variations of salinity measured at 50 m, 100 m and 200 m from all CTD casts done at station S4-1.5.

The overall seasonal trends of salinity and dCd in the complex intermediate waters can be visualized with the Salish Sea box model. As previously mentioned, the intermediate water mass in the SoG is formed in the Hao Strait region, where incoming Pacific water and outflowing SoG surface water are mixed by tidal currents. The Pacific end member is best represented by the JF1 box, and the outflowing SoG surface water can be characterised by the SoGu box. The diverging temporal trends of salinity of the two end members result in relatively small variations of salinity in the HS boxes (Figure 3.14). Nevertheless, since river freshet precedes the maximum Pacific inflow (Figure 3.16), modelled salinity in HS shows a clear minimum in June, and a less pronounced but still observable maximum in August/September. The same temporal trend applies for modelled dCd at HS (Figure 3.15), indicative of the tight coupling between salinity and dCd. Model results for dCd (Figure 3.15) show a seasonal cycle in the lower boxes of SoG (SoG1) which

lags that in the Haro Strait (HSI). Hence, the relatively high concentrations of dCd measured at intermediate depths (50 – 200 m) at station S4-1.5 in December could be explained by propagation of high-Cd water formed at Haro Strait in the late summer.

3.3.3.3 Deep layer (> 200 m)

Similar to the intermediate water, variations of dCd concentrations in the deep layer (> 200 m) could reflect seasonal changes of dCd in the incoming Pacific water, or biogeochemical processes occurring within the SoG. The deep water of the SoG is renewed annually in the summer, when stronger coastal upwelling in the Pacific brings deeper water through Juan de Fuca Strait (Pawlowicz et al., 2007). Discrete renewal events allow pulses of relatively dense water to flow over the Victoria and Boundary Pass sills (Figure 1.2) and cascade down to the bottom of the SoG basin as a gravity current (Pawlowicz et al., 2007). Coastal upwelling weakens in fall, so the incoming Pacific water is less dense and unable to displace the bottom water of SoG. Thus, for the rest of the year, deep waters of the SoG is stagnant and only affected by mixing with water from intermediate depths. Vertical diffusion gradually lowers the density of deep water, thereby allowing their displacement by denser Pacific water in the following summer. Our water column profiles illustrated a systematic decrease of dCd concentrations in the deep water from September 2017 to April 2018 (Figure 3.6).

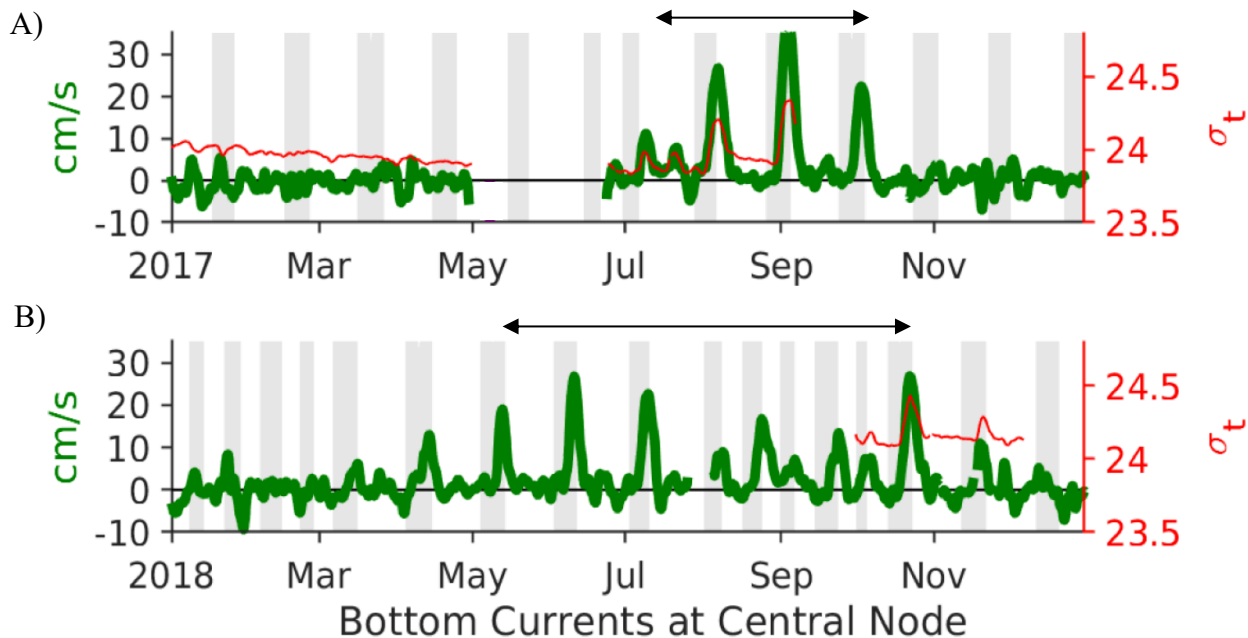


Figure 3.18. Bottom current speed (green curves) and seawater densities (red curves) at Ocean Networks Canada's Central node (49.0423°N 123.3171°W, water depth 300 m; Ocean Networks Canada) in the Strait of Georgia in 2017 (A) and 2018 (B). Grey shaded regions are periods of weak tidal mixing based on tidal predictions. Black arrows indicate deep water renewal seasons. Figure and caption are modified from the UBC-Metro 2018 report (Pawlowicz, Francois, & Maldonado, 2018).

Ocean Networks Canada's VENUS Observatory measures water properties and currents at two nodes in the SoG. The Central node (49.0423° N, 123.3171° W; water depth 300 m) located in the south-central part of the Strait can be used to monitor deep-water renewals (Appendix Figure B.3; ONC). Near-bottom currents and available density measurements at the Central node showed intrusions of denser water from the Pacific between July and October 2017, and May to November 2018 (Figure 3.18). Inflow of summer Pacific water is likely responsible for the relatively high dCd concentrations in deep samples collected at station S4-1.5 in September 2017 and August 2018 (Figure 3.6). There are no statistical differences of dCd between September and December 2017 because of their proximity to deep water pulses towards the end of 2017's renewal period. From December to April in the following year, the deep water was stagnant, and a decrease in both salinity (Figure 3.1B) and dCd below 200 m was observed during this winter period (Figure 3.6). From June to August 2018, the relatively saline and high-Cd Pacific water intruded the SoG basin

again, restoring deep-water dCd concentrations towards levels measured at the end of the 2017 summer renewal.

Since there was no deep-water renewal during the winter stagnant period (Dec. 2017 - Apr. 2018), the decrease in salinity at deep waters (Figure 3.1) could only occur as a result of vertical diffusion with the intermediate water. If the simultaneous drop in dCd is due to solely diffusion, concentrations of dCd and salinity should follow a conservative mixing line between the two end members, which are best represented by freshwater runoff and ambient SoG water in December. However, dCd concentrations measured in two deepest samples (239 m and 287 m) of April are significantly lower than predicted from salinity (Figure 3.19). Therefore, another removal process must be contributing to the gradual decrease of dCd in between deep-water renewal events.

One potential removal mechanism of dCd from bottom waters is sulfate (SO_4^{2-}) reduction in anoxic sediment and subsequent formation of the insoluble CdS complex. As Cd precipitates out as CdS, the concentration of dCd in sediment pore water decreases. This creates a strong concentration gradient in the water-sediment interface, causing dCd in the bottom SoG water to diffuse into the sediment pore water over time. Thus, dCd concentrations in the SoG deep water will keep decreasing until the water is replaced with high-Cd Pacific water during the next summer renewal event. Another possibility is chemical precipitation of Cd within particle microenvironment in the water column. This removal process is also manifested by sulfide formation, but instead of occurring in the sediment, it is mediated by anaerobic respiration of microbes (e.g., bacteria, archaea) residing within sinking particles. Data on particulate Cd in the SoG water column will be discussed in section 3.3.4 to elucidate some aspects of this hypothesis.

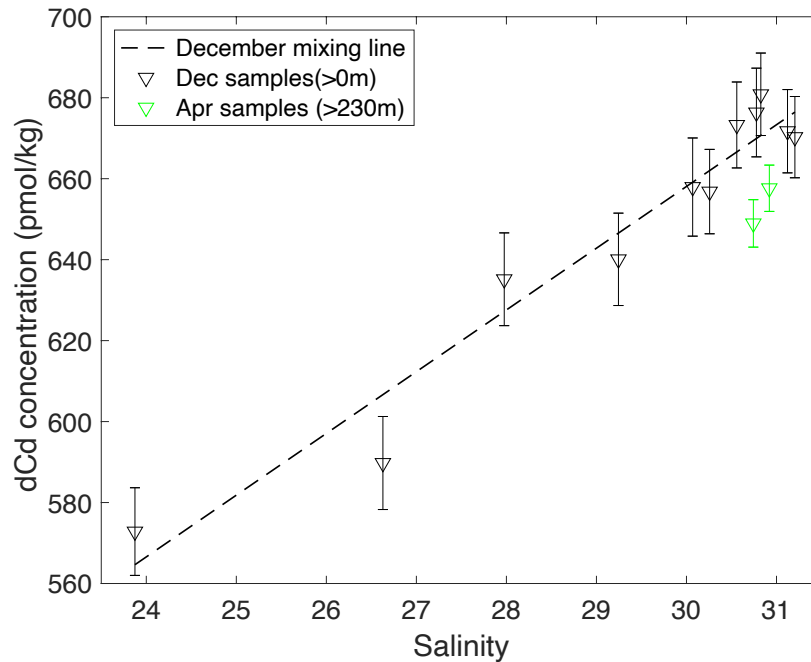


Figure 3.19. Concentrations of dissolved Cd plotted against salinity for December 2017 samples (> 0 m) and two bottom samples in April 2018 (exact depths: 239 m and 287 m). A linear fit for the December 2017 data (11 depths in total, excluding the 0 m sample) is used as the winter mixing line between SoG and riverine input.

Knowing the decrease in bottom water dCd concentrations during winter (17 ± 7 pM, Figure 3.19), and the volume of water below 230 m in the southern basin (138 km^3 , Appendix Figure A.2), we have documented a dCd removal rate of 2402 ± 989 mol over a period of 4 months. Assuming the rate of dCd diffusion into the sediment does not vary with season, we can deduce an annual removal rate of 7128 ± 2935 mol/yr (801 ± 330 kg/yr) in the southern SoG. With a surface area of 1562 km^2 below 230 m in the southern basin (Appendix, Figure A.2), the estimated dCd diffusive flux into the sediment is $0.51 \pm 0.21 \text{ kg/km}^2/\text{yr}$.

Macdonald et al. (2008) estimated a sedimentation rate of $0.64 \text{ g/cm}^2/\text{yr}$ for a core (GVRD-5) located near our station in the southern Strait. Multiplying the sedimentation rate by the average Cd concentration measured in this core (0.1 ppm), one can obtain a sediment sinking flux of $0.64 \text{ kg/km}^2/\text{yr}$. The similar fluxes based on Macdonald's sediment core data and our estimate from dCd removal in deep waters ($0.51 \pm 0.21 \text{ kg/km}^2/\text{yr}$) suggest that Cd deposited in the sediment of the southern SoG and the drop of dCd concentrations in bottom waters can be largely attributed to formation of CdS in sediments.

The surface area of the entire SoG is 6800 km², with a sediment depositional area of approximately 40% (Wilson et al., 1994). Applying our estimated dCd diffusive flux to the sediment of the entire SoG, the Cd sink associated with sulfide formation is 1387 ± 571 kg/yr. This accounts for 22% of the total Cd sediment sink estimated by Johannessen et al. (6230 kg/yr; 2015). Since our approach has not taken into account the sinking flux of particulate Cd, it is expected to be smaller than the total sediment sink based on sediment core data. The significance of sediment burial in affecting dCd concentrations in the water column of SoG will be discussed in section 3.3.6 with a mass balance calculation.

3.3.4 Particulate Cd concentrations in the southern SoG

3.3.4.1 Sources of particulate Cd

Available profiles of particulate pCd in the southern SoG water column show distinct features with depth (Figure 3.9). In both sampling times (December and April), there was a well-defined maximum of pCd at 50 m, and a secondary peak in intermediate waters at a depth deeper than the pAl and pP maxima in the same profile. Depth profiles of transmissivity shows a clear intrusion of suspended particles between 150 – 225 m in December and around 150 m in April (Figure 3.10), coinciding with the secondary peaks of pAl and pP. Johannessen et al. (2006) used CTD transmission data across the Salish Sea to track the dispersion of particles, and their results showed intrusion of particle laden Haro Strait water into the SoG at a depth between 100 m and 200 m. The vertical distributions of pAl, pP in the SoG are in agreement with the lateral transport of suspended sediments from the Haro Strait region, and trends observed in water transmissivity.

In order to determine the sources of pCd in the SoG, pAl and pP concentrations are used to assess the contribution of lithogenic and biogenic materials, respectively, to the total concentrations of pCd measured in the water column. The lithogenic fraction is estimated by multiplying the pAl concentration by the average Cd: Al ratio in Earth's crust (Taylor & McLennan, 1995). Due to Cd's low crustal abundance (3×10^{-7} mol pCd per mol of pAl), its lithogenic component is negligible in marine particles (Table 3.5 & Table 3.6). Similarly, contribution of pCd from organic matter can be determined based on the pCd: pP ratio of marine particles. We first estimate the biogenic P

concentrations by subtracting the total pP concentrations by its lithogenic fraction, which can be calculated from the molar ratio of crustal P: Al (0.0076) and the measured pAl concentrations.

$$\text{Biogenic pP (nM)} = \text{Total pP (nM)} - \text{Total pAl (nM)} \times (P/Al)_{\text{crust}} (\text{mol/mol})$$

Table 3.5. Concentrations of pCd, pAl, pP measured in the water column of station S4-1.5 in December 2017. The lithogenic fraction of P and Cd is calculated based on the molar crustal ratio of P/Al (0.008) and Cd/Al (3E-7), respectively (Taylor & McLennan, 1995). The biogenic fraction of P is calculated as the difference between the total and the lithogenic P concentrations. The ratios between pCd and biogenic P are shown to compare with the average phytoplankton Cd: P quota (0.21 pmol/nmol; Ho et al., 2013).

December Depth (m)	Total pAl (nM)	Total pP (nM)	Lithogenic pP (nM)	Biogenic pP (nM)	Total pCd (pM)	Lithogenic pCd (pM)	Non-litho pCd: biogenic P pmol/nmol
0	792	32	6	26	9.3	2.3E-04	0.36
4	914	29	7	22	14.9	2.7E-04	0.68
9	753	25	6	20	17.3	2.2E-04	0.88
18	291	17	2	15	20.7	8.5E-05	1.41
28	151	11	1	10	26.2	4.4E-05	2.74
46	37	4	0	4	34.7	1.1E-05	9.03
72	76	11	1	10	25.6	2.2E-05	2.58
93	151	9	1	8	10.8	4.4E-05	1.33
142	443	14	3	11	17.0	1.3E-04	1.62
187	881	25	7	18	22.4	2.6E-04	1.23
233	528	20	4	16	33.9	1.5E-04	2.15
282	211	12	2	11	25.9	6.2E-05	2.39

In December, the calculated pCd: biogenic P values are significantly higher than the average phytoplankton Cd :P quota of 0.21 pmol/nmol (Ho et al., 2013) except at the surface (Table 3.5). The highest ratio of pCd: biogenic P (9.03 pmol/nmol) was observed at 50 m, which could be a combined effect of the peak in pCd and the minimum in biogenic P concentrations. The high pCd signal relative to biogenic P in sinking particles cannot be attributed to Cd uptake by phytoplankton. In April, the pCd: biogenic P ratios in the upper 20 m vary between 0.07 and 0.13 pmol/nmol (Table 3.6). These ratios are in agreement with the Cd:P quotas (0.019 – 0.15 pmol/nmol) found in coastal diatom species (Ho et al., 2013). Results suggest that particles collected from the surface SoG waters in April have a biogenic signal, which is largely associated with the spring diatom

bloom. Using the previously derived dCd: PO₄³⁻ uptake ratio of 0.04 pmol/nmol in April, we could estimate the fraction of pCd that has a biogenic origin by multiplying this ratio with the concentrations of biogenic P in particles (Table 3.6, Figure 3.20). Results show a clear excess of pCd throughout the water column of April, which cannot be explained by incorporation into phytoplankton biomass or lithogenic input from weathering (Figure 3.20). Hence, additional sources of pCd such as anthropogenic discharge and authigenic formation must be contributing to the pCd pool in the SoG water column.

Table 3.6. Concentrations of pCd, pAl, pP measured in the water column of station S4-1.5 in April 2018. The lithogenic fraction of P and Cd is calculated based on the molar crustal ratio of P/Al (0.008) and Cd/Al (3E-7), respectively (Taylor & McLennan, 1995). The biogenic fraction of P is then calculated as the difference between the total and the lithogenic concentrations. The ratios between pCd and biogenic P are also shown to compare with the average phytoplankton Cd: P quota (0.21 pmol/nmol; Ho et al., 2013).

April Depth (m)	Total pAl (nM)	Total pP (nM)	Lithogenic pP (nM)	Biogenic pP (nM)	Total pCd (pM)	Lithogenic pCd (pM)	Non-litho pCd: biogenic P pmol/nmol
0	352	191	3	188	15.8	1.0E-04	0.08
4	315	188	2	186	20.6	9.2E-05	0.11
9	53	111	0	111	7.3	1.6E-05	0.07
19	13	40	0	40	5.3	3.9E-06	0.13
28	108	28	1	27	17.6	3.2E-05	0.66
47	134	17	1	16	35.4	3.9E-05	2.20
75	159	19	1	17	29.5	4.7E-05	1.70
97	218	19	2	17	18.2	6.4E-05	1.07
145	1115	41	8	33	16.8	3.3E-04	0.51
192	920	41	7	34	33.3	2.7E-04	0.98
239	807	31	6	25	36.3	2.4E-04	1.44
287	611	30	5	25	40.3	1.8E-04	1.60

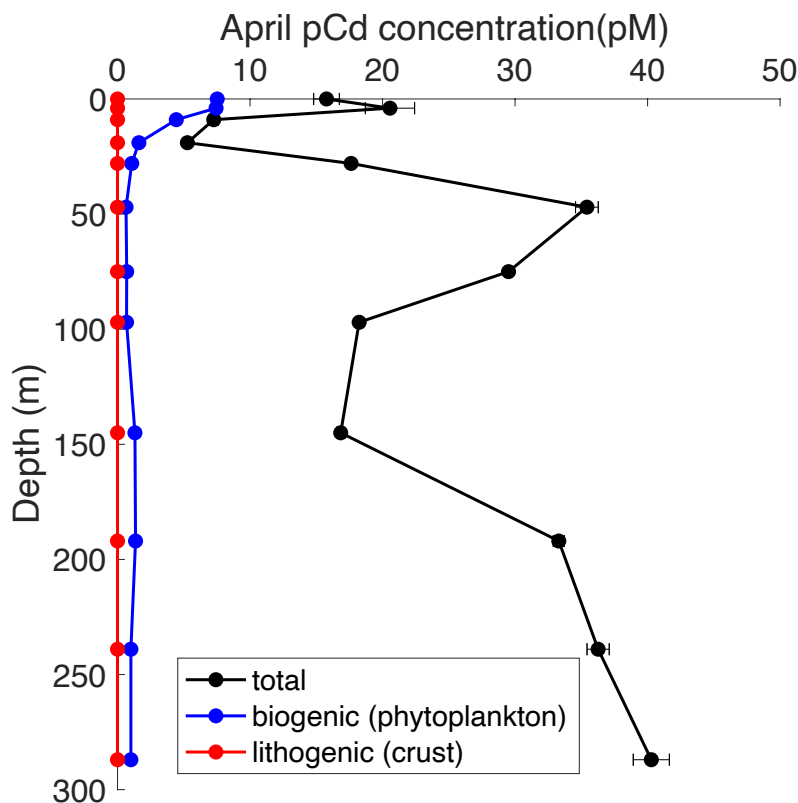


Figure 3.20. Depth profiles of total particulate Cd concentrations measured in April 2018 at station S4-1.5. The biogenic fraction of particulate Cd is estimated based on the phytoplankton $dCd: PO_4^{3-}$ uptake ratio (0.04 pmol/nmol) in April. The lithogenic fraction is calculated using the crustal abundance of Cd/Al (3×10^{-7} mol pCd per mol of pAl).

3.3.4.2 Particulate Cd enrichment in particle microenvironment

As discussed in the previous section, the contribution of biogenic particles to total pCd concentrations in the SoG water column is small except at the surface waters of April. Vertical profiles of pCd showed a clear maximum at 50 m in both December and April (Figure 3.9). Since the pCd content of marine particles cannot be explained by lithogenic or biogenic constituents, a large fraction of the pCd pool in the SoG must have a different origin. One potential anthropogenic source is the Iona WWTP, which discharges primary-treated effluent into the SoG at a depth around 100 m. Since the effluent is fresh and thus lighter than seawater, it rises as it mixes with the surrounding saltwater, bringing suspended effluent particles to its depth of neutral buoyancy at about 50 m.

In order to assess whether the peak of pCd at 50 m can be attributed to dispersion of the Iona effluent particle plume, we first compare the concentration of pCd in the Iona effluent with its ambient level at station S4-1.5. The lowest pCd concentration of 11 pM at 100 m in December (Figure 3.9) was chosen to represent its background level in the SoG. The average pCd in effluent samples collected from the Iona WWTP was 415 pM (Table 3.2), which is about 40 times higher than that in the SoG water column. A dilution factor of 250 is estimated at the initial dilution zone (100 m radius around the outfall) for the Lions Gate WWTP (Metro Vancouver, 2018). No modelled dilution factor has been reported for Iona, if we assume a similar initial dilution factor for the Iona effluent, the discharged pCd will not cause detectable changes at our sampling site (> 20 km away from the Iona WWTP). Hence, municipal sewage discharge cannot explain the three-fold increase in pCd concentration at 50 m relative to its background level (Figure 3.9).

The local maximum of pCd is defined by six depths with a gradual increase in particulate concentrations, thus it cannot be an artefact or contamination (Figure 3.9). Since the peak of pCd observed in the December and April profiles cannot be accounted for by lithogenic particles, plankton biomass, or sewage particles, the only remaining possibility is formation of an authigenic phase, which is produced by chemical reaction in the water column (Bianchi et al., 2018; Ohnemus & Lam, 2015). The contribution of authigenic particles to pCd can be visualized as the difference between the total and biogenic pCd concentrations (lithogenic pCd is negligible). Given the lack of biological uptake in December, essentially all pCd measured in particles presumably have an authigenic origin (Figure 3.21).

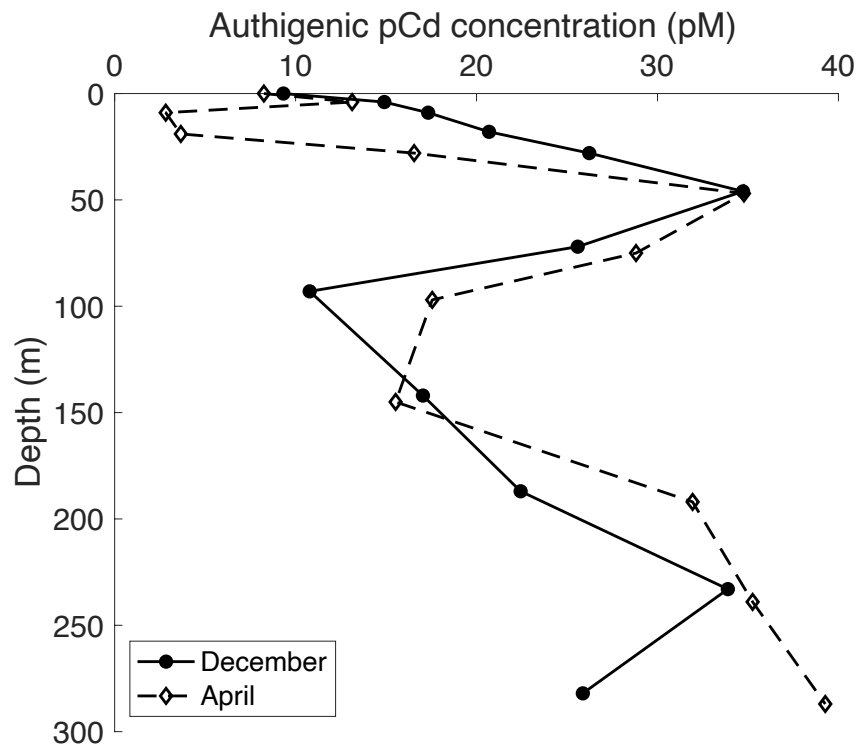


Figure 3.21. Depth profiles of the estimated authigenic pCd concentrations in marine particles collected in December 2017 and April 2018 at station S4-1.5.

Bianchi et al. (2018) proposed that the formation of sulfide ions inside microenvironments can drive the precipitation of insoluble metal sulfides. They developed a model to simulate the formation of anoxic microenvironment in the global oceans and found that SO_4^{2-} reduction can be sustained in particle aggregates over a wide range of oceanographic settings, including coastal upwelling regions of the subarctic North Pacific. The rationale is that decomposition of organic matter in sinking particles utilizes oxidants (O_2 , NO_3^- , SO_4^{2-}) diffusing from the surrounding seawater in the order of their energy yield (Bianchi et al., 2018). An anoxic microenvironment inside the particles will form when the supply of dissolved oxygen is lower than the demand by aerobic respiration. At which points, anaerobic microbes start to use NO_3^- , followed by SO_4^{2-} as the oxidant.

The model developed by Bianchi et al. (2018) successfully reproduced the observed pCd:pP ratios in the Mauritanian upwelling zone (Janssen et al., 2014) based on the hypothesis of pCd

enrichment by CdS precipitation in decaying organic particles. In the Mauritanian region, remineralization of pP and precipitation of pCd results in the decoupling between the two elements (Bianchi et al., 2018; Janssen et al., 2014). The same processes could be responsible for the opposing trends of pP and pCd in the upper 50 m of the December profile collected in the southern SoG (Figure 3.9). In April, incorporation into phytoplankton biomass can explain the increase in both pCd and pP in the upper 20 m. Between 20 m and 50 m, pP decreases due to remineralization, whereas pCd could have increased as a result of precipitation of CdS within sinking organic aggregates.

However, the limitation to this hypothesis is that the ambient oxygen concentrations in the SoG (Figure 3.3) are significantly higher than in suboxic zones in the open ocean where CdS precipitation was observed (Janssen et al., 2014). One possibility is that the Iona diffusers discharge particles which are high in organics and potentially already anoxic inside. Once in contact with the relatively high dCd concentration of SoG water, which is approximately 10 times higher than that in the Iona effluent (Figure 3.6; Table 3.4), dCd can readily diffuse into these pre-existing anaerobic particle microenvironments. In addition, SO_4^{2-} is present at much higher concentrations in the seawater matrix than in the Iona effluent (~ 24 mg/L; Metro Vancouver 2018). The diffusion of SO_4^{2-} from seawater into effluent particles, followed by SO_4^{2-} reduction in the anoxic interior could enhance authigenic precipitation of CdS as well. Hence, discharged effluent particles may act as an indirect source of pCd by providing a favorable substrate for CdS formation. The influence of CdS formation on the cycling of dCd in the SoG will be discussed in the following section together with NO_3^- , another redox-sensitive parameter. The decoupling of both dCd and NO_3^- with PO_4^{3-} can provide insight on the importance of redox-related processes on their respective distributions.

3.3.5 Seawater – particle – sediment interactions and the decoupling between dissolved Cd, NO_3^- , and PO_4^{3-} in the water column of SoG

The decoupling between dCd and PO_4^{3-} in the water column can be examined using Cd*, a variable proposed by Janssen et al. (2014):

$$Cd^* (nM) = dCd_{measured} (nM) - PO_4^{3-}_{measured} (\mu M) \times \frac{dCd_{deep} (nM)}{PO_4^{3-}_{deep} (\mu M)}$$

where $dCd:PO_4^{3-}_{deep}$ represents the average ratio in the deep waters of an ocean basin. For the northeast Pacific, they used a value of 0.35 nM/ μ M for the deep-water ratio, which is in agreement with published values (Elderfield & Rickaby, 2000; Janssen et al., 2014). We used the same ratio to calculate Cd^* for our SoG samples. Since the absolute value of Cd^* will vary depending on the value chosen for $Cd:PO_4^{3-}_{deep}$, we will only discuss trends in Cd^* within profiles. The concept of Cd^* is similar to N^* , which measures the deviations of NO_3^- and PO_4^{3-} from the Redfield ratio. Although dissolved oxygen concentrations were well above hypoxia in the SoG (Figure 3.3), prohibiting anaerobic respiration to occur in the water column, NO_3^- and SO_4^{2-} reduction could still be sustained in microenvironments within sinking particles. Based on our hypothesis of sulfide formation in particle microenvironment, we should see the same trend in N^* because NO_3^- reduction must occur prior to SO_4^{2-} reduction based on the order of preferred oxidants for decomposition.

In December, depth profiles of N^* and Cd^* exhibit similar trends in the entire water column (Figure 3.22). In the upper 50 m, both N^* and Cd^* decrease gradually towards a local minimum at 50 m as the amount of dissolved oxygen decreases from 250 μ M at the surface to 100 μ M. As oxygen concentrations increase at intermediate depths approximately between 75 and 150 m, N^* and Cd^* are restored to their surface values. Below 150 m, N^* and Cd^* decrease again and both reach a minimum at 250 m. The trends observed for these two variables correspond well to the pCd profile, which shows a major peak at 50 m and a small peak at 250 m in December (Figure 3.9). Enrichment of pCd occurs at depths where dissolved oxygen, N^* , and Cd^* are all decreasing, suggesting their distributions are redox-controlled, likely associated with anaerobic respiration within sinking particles. The December dissolved and particulate data show that precipitation of Cd as CdS within particle microenvironment in the water column is a potential removal mechanism for dCd.

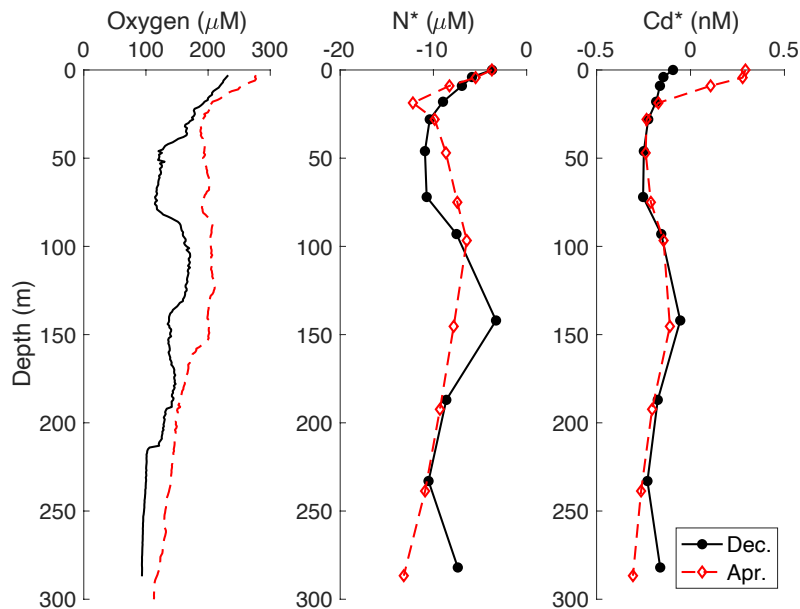


Figure 3.22. Depth profiles of dissolved oxygen (CTD), N^* , Cd^* at station S4-1.5 in December 2017 and April 2018.

In April, preferential uptake of PO_4^{3-} over dCd by diatoms could explain the positive Cd^* in near surface waters (Figure 3.22). As organic matter decomposes, PO_4^{3-} and dCd are released into the water column. Bourne et al. (2018) proposed that P is remineralized faster than Cd in shallow waters, where P is found in more labile forms associated with ATP and DNA. Hence, the gradual decrease of Cd^* in the upper 20 m could be attributed to preferential remineralization of PO_4^{3-} than dCd from sinking particles (Figure 3.22). The Cd^* minimum around 50 m is consistent with the additional removal of dCd from seawater by precipitation in microenvironments associated with effluent particles. In contrast to Cd^* , N^* does not have a local minimum around 50 m. This suggests that denitrification in particles may not be an important NO_3^- sink, as CdS is for dCd, which is consistent with the relatively large reservoir of NO_3^- in seawater.

The deep SoG water was stagnant during winter period between December 2017 and April 2018. Remineralization of organic matter in sediment can lead to the accumulation PO_4^{3-} in pore waters, which subsequently drives an upward flux across the sediment-water interface. This is supported by the increase in PO_4^{3-} concentrations from December to April in the deepest sample (Figure 3.4). In contrast, the concentration of NO_3^- in bottom water remained the same over winter. This could

be reflective of denitrification happening in the sediment, which prevented the release of NO_3^- from porewater back into the water column. When denitrifiers consume all the available NO_3^- , SO_4^{2-} reducing microbes will continue to break down any residual organic matter in the sediment. Sulfides produced through anaerobic decomposition could subsequently form insoluble complexes with dCd, hence decreasing its concentration in porewater. Downward diffusion of dCd across the water-sediment interface is likely responsible for the negative Cd* observed in the bottom water of April (Figure 3.22).

3.3.6 Cd mass balance in the SoG

We have discussed the spatial and temporal distributions of dCd in the southern SoG, assessed the contribution of dCd from natural and anthropogenic sources, and identified sinks of dCd into the sediment and suspended particles. With our current understanding of the system and available geochemical data, we can generate a mass balance of Cd for the SoG. The volume-weighted average dCd concentrations (Appendix Table B.3) in the entire water column of station S4-1.5 range between 609 pM and 687 pM, with a mean of 663 ± 31 pM. Knowing the total volume of water in the SoG (1100 km^3 , Appendix Figure A.2), we can derive a dCd reservoir of 729,300 mol (c.a. 82,000 kg) in the Strait. Johannessen et al. (2015) estimated a sediment sink of 6230 kg/yr for Cd, while our best estimate based on diffusion of dCd into sediment is 1387 ± 571 kg/y (section 3.3.3). Using the residence time of the volumetrically significant intermediate water mass (160 days; Pawlowicz et al., 2007), a removal of 2730 kg or 608 ± 250 kg is expected from the dCd pool in SoG waters, which is only 1 - 3% of the total reservoir.

As previously discussed, the Salish Sea box model can be used to gauge the biogeochemical cycling of Cd with conservative mixing as a baseline, and to identify additional sources and sinks. Uncertainties of modelled dCd concentrations for the Juan de Fuca and SoG basins are based on the variability of the Pacific end member (Table 3.3; Figure 3.23). In the SoG upper box (0 – 50 m), field data fall close to the lower boundary of model predictions except for June 2018, where the average dCd concentration is significantly lower than the modelled data. As previously discussed, the deficit in dCd is likely due to continuous biological uptake without replenishment from deeper waters due to the strong surface stratification in June.

In the SoG lower box (50 m to bottom), there is a surplus of measured dCd relative to the model prediction in August 2018 (Figure 3.23), possibly due to remineralization and release of dCd in deep waters. The rest of the dCd data plot close to the upper boundary but are still within the uncertainty of model predictions. These trends are consistent with biological cycling removing dCd from the upper 50 m and adding dCd to deeper waters. Overall, the fairly good match between modelled and measured dCd is consistent with the small sedimentary sink (1 – 3 % of the inventory) and negligible anthropogenic input of Cd (Table 3.4) identified in this study, which are too small to produce readily measurable deviations from conservative mixing. The relatively short water residence time and the small Cd sink in the SoG are largely responsible for the quasi conservative behavior of dCd.

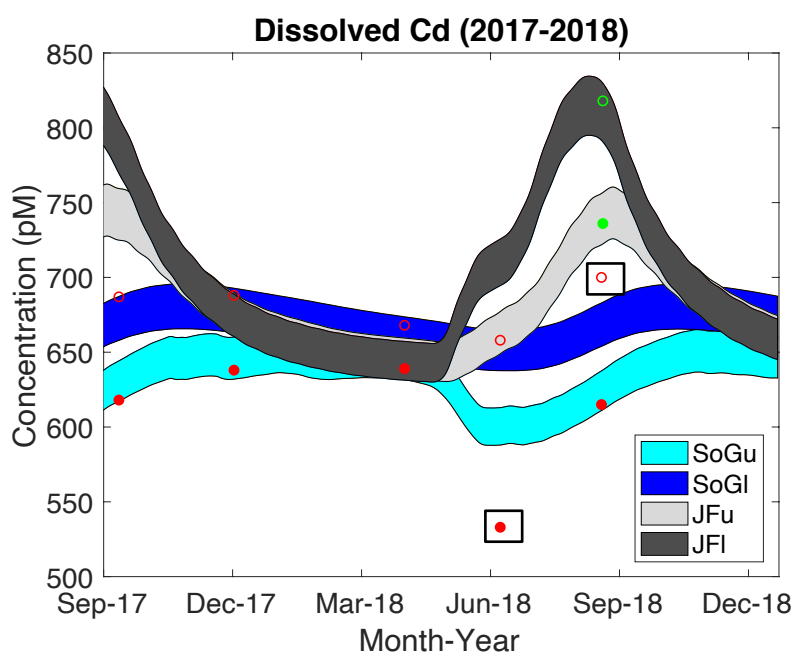


Figure 3.23. Modelled vs measured dissolved Cd concentrations in the Strait of Georgia upper (SoGu), Strait of Georgia lower (SoGl), Juan de Fuca Strait upper (JFu), and Juan de Fuca Strait lower (JFI) boxes. Filled and empty circles are field measurements for dCd in the upper and lower boxes, respectively. Red circles represent average dCd concentrations measured in the SoG, while green circles represent Juan de Fuca Strait measurements. Uncertainties in the modelled data are illustrated by the upper and lower boundaries plotted for each box. Field measurements that do not fit with the model predictions are enclosed in a square.

3.4 Conclusions for Cd

This study concludes that the dominant source of dCd in the SoG is water upwelled from the Pacific Ocean, which is naturally high in dCd due to the global ocean circulation that transports water from the North Atlantic towards the North Pacific, accumulating Cd from sinking particles along the path. Freshwater input from rivers (mainly Fraser River) flowing into the SoG is another significant source of dCd. Concentrations of dCd in the Fraser River is about 5- 10 times lower than that in the Pacific. Compared with the two natural sources of Cd, the input from municipal effluent discharge is negligible.

Conservative mixing between low-Cd freshwater and high-Cd Pacific water largely governs the spatial distribution and temporal variability of dCd in the Salish Sea. Spatially, dCd concentrations decrease as the Pacific source water travels from Juan de Fuca northward towards the SoG due to dilution by freshwater discharge. Temporally, an annual minimum of dCd in the SoG basin occurs during the Fraser River freshet in June. Comparison between our field dCd measurements and the Salish Sea box model predictions further confirms the dominating role physical circulation plays in shaping the dCd distributions in this region.

Time-series sampling (September 2017 – August 2018) in the southern SoG reveals a systematic decrease of dCd in deep waters (> 200 m) between annual deep-water renewal events. One plausible mechanism is removal of dCd from bottom waters as a result of SO_4^{2-} reduction in the sediment. Precipitation of CdS in sediment porewater can create a vertical concentration gradient driving the downward flux of dCd across the sediment-water interface. This sink of dCd is however too small to produce readily measurable deviations from conservative mixing, due to the relatively large dCd pool and short residence time of water in the Strait.

There is also evidence of CdS formation in the water column of the southern SoG, as illustrated by the distinct peak of pCd observed at 50 m of two particulate metal profiles (December 2017 and April 2018). Metal sulfides can form within anaerobic microenvironments associated with sinking particles. Although effluent discharged from the Iona WWTP is not a significant point source of Cd, it could indirectly contribute to the particulate Cd pool by releasing organic-rich

particles that can sustain sulfidic microenvironments and facilitate the formation of CdS even in oxygenated waters. In addition, particles enriched in CdS could be ingested by zooplankton and act as an entry point of Cd into the food chain. Although Iona effluent is not a direct source of particulate Cd, its potential indirect influences on the SoG aquatic environment require further investigation (section 5.2).

This study has also documented a decoupling between dCd and the macronutrient PO_4^{3-} in the SoG water column. The uptake ratio of dCd: PO_4^{3-} estimated during the spring phytoplankton bloom is consistent with the low particulate Cd: P ratio measured in marine particles collected in surface waters. Our results suggest that phytoplankton (predominantly diatoms) in the SoG have a low cellular demand for Cd. Although clearly present, the impact of biological cycling on the distribution of dCd in the SoG is obscured by the larger seasonal variations in dCd of the upwelled Pacific water. In summary, the distribution of dCd in the SoG is largely controlled by physical circulation and mixing, which mask the smaller influence of biological cycling and removal to anoxic sediments.

Chapter 4: Biogeochemical cycling and anthropogenic input of silver in the Strait of Georgia

4.1 Introduction

4.1.1 Sources of Ag in the environment

Silver (Ag) is naturally present in mineral deposits at low concentrations (50 ppb) relative to other main constituents of the earth's crust (e.g., Al, 8.04%; Taylor and McLennan, 1995). In addition to weathering of rocks containing trace amounts of Ag, the primary sources of Ag in the environment are associated with anthropogenic discharges. It is released into the atmosphere through coal burning and smelting, or into the aquatic environment via inputs of industrial, mining, and household waste (Purcell & Peters, 1998). Ag has been used as a tracer for anthropogenic pollution in marine waters and sediments due to discharge of industrial and domestic effluents (Barriada et al., 2007; Ravizza & Bothner, 1996). In the early 1990s, elevated concentrations of Ag have been found in the water column, sediment, and benthic invertebrates of San Francisco Bay mainly due to discharges of Ag-contaminated effluent from photographic processing plants (Smith & Flegal, 1993).

Once released into the aquatic environment, primary producers can bioaccumulate Ag from the dissolved phase to concentrations up to 5 orders of magnitude higher than those found in water (Fisher et al., 1984; Ratte, 1999). The toxicity of Ag is dependent on the availability of its free ions (Ag^+), which can cause negative effects on aquatic invertebrates at concentrations lower than other heavy metals (e.g., Cu, Zn, Cd) except for mercury (Luoma, 2008). With the advances of nanotechnology in the past decade, nanosilver particles (1 – 100 nm in scale) are largely incorporated into commercial products such as sportswear and bedding materials for their antibacterial properties (Luoma, 2008). There are concerns over the release of these nanosilver particles into streams, rivers, and eventually oceans through sanitary sewage discharge. Once in the aquatic environment, nanosilver particles which are engineered to release highly toxic Ag^+ ions to enhance antibacterial activity could pose a serious threat to aquatic species (Luoma, 2008).

Hence, monitoring efforts are required at Ag point sources (e.g., wastewater treatment plants) and in the receiving environment to establish baseline conditions and to develop remediation strategies if necessary.

4.1.2 Biogeochemical cycling of Ag in the ocean

Ag is present in seawater dominantly as chloro-complexes (e.g., AgCl, AgCl₂⁻, AgCl₃²⁻) with negligible complexation with organic ligands (Miller & Bruland, 1995). The dissolved fraction (dAg) typically makes up more than 90% of the total Ag concentrations in the water column (Martin et al., 1983). However, there is still a scarcity of data on dAg concentrations for oceanic waters. The knowledge gap is largely due to analytical challenges in quantifying pico-molar ranges of dAg in the complex matrix of seawater (Barriada et al., 2007). Determination of dAg in pristine oceanic waters require effective methods for matrix removal to separate and preconcentrate Ag from seawater samples.

Traditional, dAg analysis in seawater (Martin et al., 1983, Smith and Flegal, 1993) followed the organic extraction method with ammonium 1-pyrrolidine dithiocarbamate/diethylammonium diethyldithiocarbamate (APDC/DDDC), as described by Bruland and Franks (1979). Despite its effectiveness in eliminating the saline seawater matrix, the method is labour intensive and requires about 250 mL of sample for analysis (Barriada et al., 2007). In the last decade, more studies have switched to solid phase extraction systems with anion exchange resins to preconcentrate trace metals including Ag (Ndung'u et al., 2006). The advantages of solid phase extraction over the use of organic solvents are 1) easy incorporation of resin columns in automated flow-injection systems 2) small sample and reagent volumes required for analysis (Barriada et al., 2007; Fischer et al., 2018; Lagerström et al., 2013; Ndung'u et al., 2006).

With advances in trace metal analysis, profiles of dAg have been reported for major ocean basins (Gallon & Flegal, 2015). Martin et al. (1983) found extremely low surface dAg concentrations (~ 1 pmol/kg) in the open ocean of northeast Pacific, with a gradual increase with depth to reach approximately 20 pmol/kg in the deep basin (> 2000 m). In deep waters, dAg concentrations increase as the water travels from the North Atlantic to the North Pacific along the path of global

ocean circulation, suggesting that surface uptake and subsequent remineralization play an important role in the cycling of dAg (Zhang et al., 2004). Available depth profiles of dAg in the open ocean show similar distributions with the macronutrient silicic acid ($\text{Si}(\text{OH})_4$, abbreviated Si onwards), suggesting a link between their biogeochemical cycles in oceanic waters (Kramer et al., 2011; Ndung'u et al., 2001; Zhang et al., 2001; Zhang et al., 2004). Ndung'u et al. (2001) suggested that dAg is scavenged by refractory organic ligands on phytoplankton cell surfaces, and subsequently packaged into fecal pellets together with siliceous tests by grazers. The gradual dissolution of biogenic silica and remineralization of refractory organo-Ag compounds within sinking fecal pellets could explain the increase of both dAg and Si concentrations in deep waters.

However, more recent studies have shown deviations in the correlation between dAg and Si in oceanic waters, which adds more uncertainty in the nature of Ag's cycling (Zhang et al., 2001; Zhang et al., 2004; Kramer et al., 2011). Zhang et al. (2001) found that the maximum concentration of dAg occurred at deeper depths than Si in the western North Pacific, suggesting a slower rate of remineralization for dAg relative to Si. The concave shape of dAg vs Si exhibited in samples collected in the open Pacific Ocean indicates accumulation of dAg in the deep basin relative to Si (Kramer et al., 2011; Ranville and Flegal, 2005; Zhang et al., 2001). In addition, Kramer et al. (2011) suggested that formation of insoluble Ag sulfide complexes in oxygen minimum zones could be a significant sink of dAg in the water column, causing further deviations of the dAg/Si relationship.

In addition to natural processes, anthropogenic inputs could also influence the distribution of dAg in open ocean and coastal waters. Ranville and Flegal (2005) found that dAg concentrations in surface waters of the North Pacific were significantly higher (up to 12 pM) in the western than in the eastern (1 – 2 pM) basins. They speculated that the elevated concentrations of dAg found in waters near Asian mainland were from atmospheric deposition of aerosols associated with coal burning and metal refining. Under this premise, the natural biogeochemical cycling of Ag in the open ocean has already been significantly disturbed by anthropogenic inputs. Enhanced concentrations up to 250 pM of dAg were also found in European and American coastal waters under the influence of effluent discharge and acid mine drainage (Flegal et al., 2007; Ndungu,

2011; Squire et al., 2002; Tappin et al., 2010). Since Ag is highly toxic to aquatic organisms and can bioaccumulate in the food chain (Luoma, 2008), it is crucial to assess the impact of anthropogenic emissions on marine ecosystems. Monitoring and research efforts are required to understand the natural processes and anthropogenic sources that could influence the biogeochemical cycling of Ag in the ocean.

4.1.3 Previous information on Ag in the SoG

Natural and anthropogenic loadings of Ag into the coastal waters of the SoG have been assessed using sediment cores that were collected outside and within the footprint of local wastewater treatment plants (Gordon, 1994; Macdonald et al., 2008). Cores located in proximity to sewage outfalls showed significant enrichment of Ag in the top 30 cm relative to the natural SoG sediment background (Macdonald et al., 2008). Notwithstanding its use as a tracer for sewage in the SoG (Gordon, 1997), Ag loadings from wastewater treatment plants contributed less than 5% of the Ag sediment sink in the SoG based on regional geochemical budgets (Johannessen et al. 2015). Their finding is in agreement with our 2015 weekly analysis of effluent samples from the Iona WWTP, which discharged less than 40 kg/yr of total Ag into the SoG (Appendix Table B.8).

To our knowledge, there is no published data for Ag in the water column of SoG. With the extensive application of nanosilver particles in consumer products (Luoma, 2008), there is an increasing concern with Ag being discharged into ambient waters from local WWTPs. It is important to establish baseline conditions of Ag in the SoG and gain understanding of its addition, dispersion, and removal in this productive ecosystem. As part of the Metro Project, there has been ongoing efforts in analytical method development to quantitatively determine concentrations of dAg in the SoG seawater. Experiments were conducted to preconcentrate Ag from seawater samples using an anion-exchange resin, and to determine its concentrations by isotope dilution ICP-MS. Preliminary results showed that dAg concentrations in samples collected from the SoG are typically less than 10 pM. However, the precision of analysis was initially compromised by large variations in the procedural blanks, likely due to sporadic contamination during sample handling. In order to minimize the risk of contamination when processing seawater samples, we used an ultra-clean, automated seawater preconcentration system (*seaFAST*, Elemental Scientific)

for subsequent analysis. Results on the temporal variations of dAg in the southern SoG, and the spatial distributions of dAg in the Salish Sea will be discussed in this chapter.

4.2 Results

4.2.1 Temporal and spatial variations of dissolved Ag in the Salish Sea

Depth profiles of dAg in the southern SoG were captured at station S4-1.5 between September 2017 and August 2018 (Figure 4.1). In the upper 50 m, dAg concentrations exhibit large variability between different months with sporadically high values (e.g., December at 20 m, April at 5 m). At the sea surface, concentrations of dAg vary by two-fold from 5.5 to 11.9 pmol/kg. In contrast with macronutrients and dCd (Figure 3.4 and Figure 3.6), the dAg profiles do not exhibit a consistent trend of surface depletion and regeneration in deeper waters (Figure 4.1). At 100 m in the intermediate layer, the lowest and highest concentrations of dAg were observed in August/September and April, respectively (Figure 4.1). Interestingly, the seasonal variations of dAg diminished at 150 m, where an average concentration of 8.0 ± 0.4 pmol/kg was found throughout the 2017 – 2018 sampling cruises at station S4-1.5. In the deep layer (> 200 m), there was a clear increase of dAg concentrations between the fall of 2017 (September) and spring of 2018 (April). Concentrations decreased again as summer progressed (June & August).

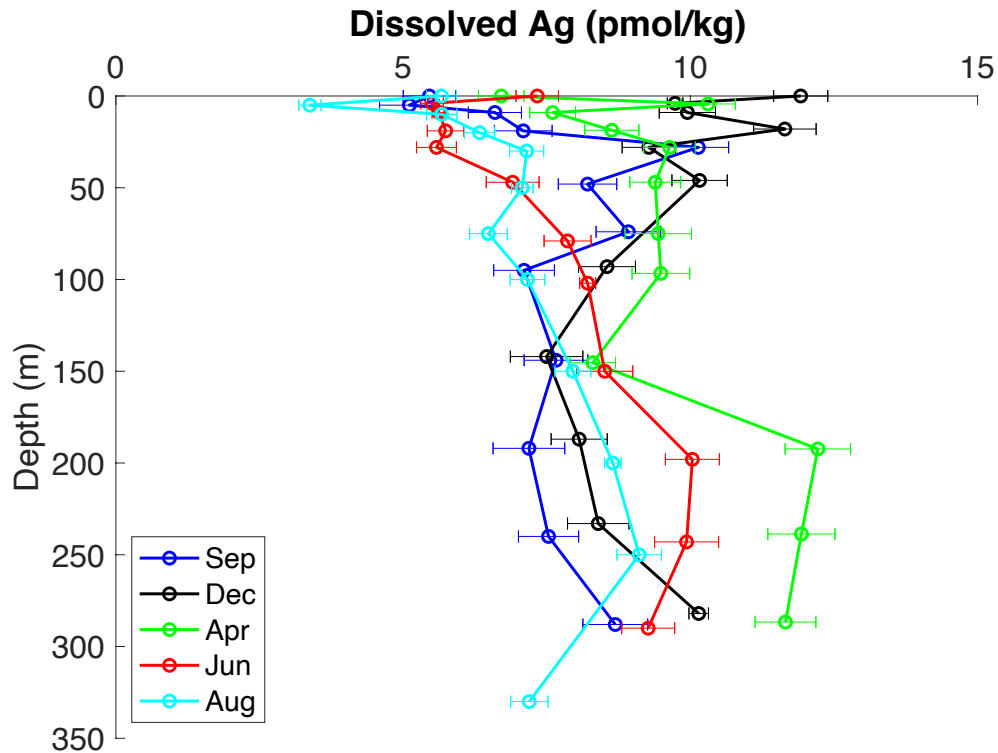


Figure 4.1. Depth profiles of dissolved Ag at station S4-1.5 from September 2017 to August 2018. Error bars represent one standard deviation of the analytical uncertainty.

Compared with the relatively noisy temporal signals of dAg in the southern SoG (Figure 4.1), vertical profiles of dAg showed clearer spatial trends across the Salish Sea in August 2018 (Figure 4.2). Concentrations of dAg measured in the upper 400 m at station P4 in the September 2018 Line P cruise were also plotted to represent the Pacific end member (Figure 4.2). Concentrations of dAg in the Pacific water increased linearly with depth, varying between 3.5 - 14.2 pmol/kg in the upper 400 m. At station JF2, concentrations of dAg in the upper 60 m were relatively constant with an average of 6.0 ± 0.1 pmol/kg. There was a slight but noticeable decrease of dAg in deeper waters (80 m to bottom), with an average of 5.3 ± 0.2 pmol/kg. The vertical distribution of dAg in August at Juan de Fuca Strait showed higher concentrations in the surface outflow than in the deep Pacific inflow (Figure 4.2). In Haro Strait (station HS), concentrations of dAg were relatively constant throughout the water column with an average of 5.7 ± 0.2 pmol/kg. Relative to Haro Strait, significantly higher dAg concentrations were found in subsurface waters in the SoG (stations S4-1.5 and NG). In addition, dAg showed spatial variations within the SoG, where concentrations

were higher in the entire water column of the northern (station NG) than in the southern (station S4-1.5) SoG.

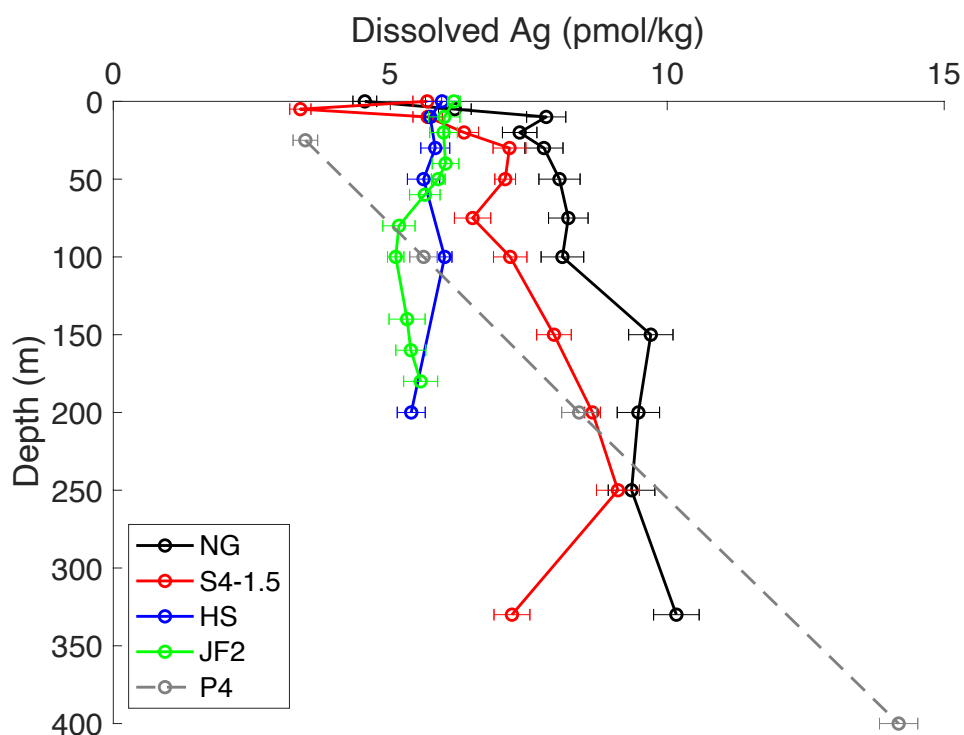


Figure 4.2. Depth profiles of dissolved Ag at stations located in the northern strait (NG), southern strait (S4-1.5), Haro Strait (HS), and Juan de Fuca Strait (JF2) in August 2018. Dissolved Ag concentration were also measured in four samples collected at station P4 during the September 2018 Line P cruise (samples were provided by Dr. Jay Cullen’s lab in University of Victoria). Error bars represent one standard deviation of the analytical uncertainty.

4.2.2 Particulate Ag concentrations in the southern SoG

Depth profiles of particulate Ag (pAg) captured in the southern SoG (station S4-1.5) in December 2017 and April 2018 exhibit trends similar to that pAl and pP (Figure 4.3). In both months, the highest pAg concentration was observed at the surface, with pAg gradually decreasing towards the bottom of the surface layer (0 – 50 m). At subsurface depths, pAg concentrations remained relatively constant with the exception of a noticeable peak of pAg occurring at 200 m and 150 m in December and April, respectively. The increase of pAg at intermediate depths corresponds well

with the local maxima of pAl and pP. The background pAg concentration in deep waters (< 1 pM; Figure 4.3) is approximately an order of magnitude lower than the dissolved fraction in SoG seawater (Figure 4.1). Our results are consistent with literature on the partitioning of Ag between the particulate (< 10%) and the dissolved fractions (> 90%) in seawater (Martin et al., 1983).

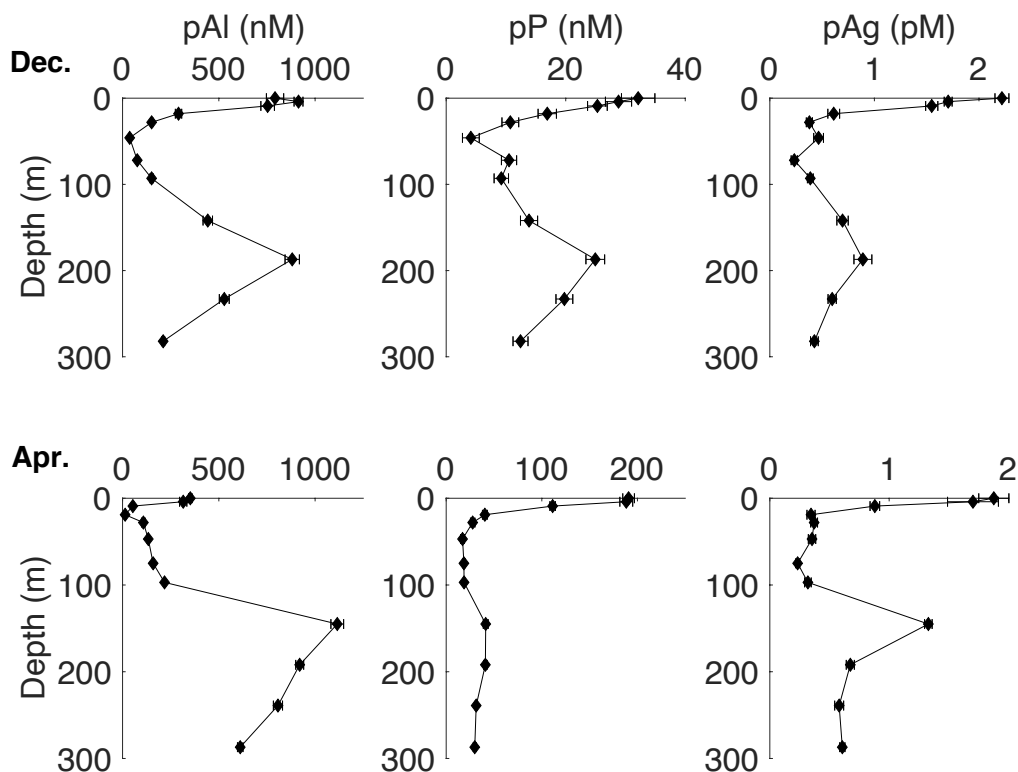


Figure 4.3. Depth profiles of particulate Al, P, and Ag at station S4-1.5 in December 2017 and April 2018. Error bars represent one standard deviations of analytical uncertainty.

4.2.3 Concentrations and fluxes of dissolved and total Ag in municipal effluents

Total and dissolved Ag concentrations were measured in influent and effluent samples collected from the Iona WWTP, as well as in screened wastewater from Macaulay and Clover Points (Table 4.1). The average total Ag concentrations in effluent samples (1284 ± 380 pM) were significantly lower than in the influent (2334 ± 1010 pM; P-value < 0.05). Dissolved Ag concentrations in the influent and effluent were 390 ± 131 pM and 377 ± 150 pM, respectively, indicating little or no removal to the particulate pool during primary treatment. In contrast, concentrations of particulate Ag calculated as the difference between the total and the dissolved fraction, yield an average of

1944 ± 1018 pM in the influent and 908 ± 409 pM in the effluent. This indicates settling of particles in sedimentation tanks, which contributes to approximate 50% removal of particulate Ag during primary treatment.

Our results show that influent entering the Iona WWTP brings Ag mostly in the particulate form, which accounts for approximately 80% of total Ag (Table 4.1). A lower proportion of particulate Ag (~ 70%) was found in the treated effluent. Similarly, Ag discharged from the Macaulay and Clover Points was dominated by the particulate fraction. Total Ag concentrations in the screened effluent were highly variable, especially at Clover Point, where sporadically high concentrations of total and dissolved Ag were detected in its effluent (i.e., January, June).

Table 4.1. Concentrations of total and dissolved Ag in wastewater samples measured in influent and effluent from the Iona WWTP, and screened samples from Macaulay Point and Clover Point outfalls. Red indicates levels that exceed the BC Water Quality Guidelines for total Ag in marine waters (27.8 nM) without dilution.

Ag Concentrations	Nov-17	Jan	Mar	Jun	Sep	Nov-18	Max	Min	Average
Iona influent									
Dissolved Ag (pM)	403	201	358	529	308	539	539	201	390
Particulate Ag* (pM)	2225	530	1923	3333	2154	1502	3333	530	1944
Total Ag (pM)	2628	731	2281	3863	2462	2041	3863	731	2334
Iona effluent									
Dissolved Ag (pM)	586	231	405	404	178	456	586	178	377
Particulate Ag* (pM)	708	433	1182	1273	854	996	1273	433	908
Total Ag (pM)	1294	664	1587	1678	1032	1452	1678	664	1284
Macaulay Point									
Dissolved Ag (pM)	314	209	603	533	281	362	603	209	384
Particulate Ag* (pM)	1930	916	6623	4650	2493	1852	6623	916	3077
Total Ag (pM)	2244	1125	7226	5183	2773	2214	7226	1125	3461
Clover Point									
Dissolved Ag (pM)	282	922	424	936	611	706	936	282	647
Particulate Ag* (pM)	2015	36496	3418	11479	6379	3710	36496	2015	10583
Total Ag (pM)	2297	37418	3842	12415	6990	4416	37418	2297	11230

Knowing the average concentrations of Ag and the 2018 annual effluent flow rate measured at Iona WWTP, Macaulay & Clover Points, the annual input fluxes of Ag from municipal effluent can be calculated (Table 4.2). Ours results show that the annual fluxes of total Ag are in the same order of magnitude for the three sewage outfalls. The total Ag flux from the Iona effluent is slightly higher than the sum of Ag loadings from Macaulay and Clover Points, despite the relatively low Ag concentrations in effluent discharged from the Iona WWTP, reflecting its higher annual discharge rate.

Table 4.2. Average concentrations and annual fluxes of total, dissolved, and particulate Ag measured between 2017 and 2018 from three outfalls (Iona WWTP, Macaulay Point, and Clover Point). Particulate Ag* is calculated by subtracting measured values of dissolved Ag from the total. Total annual flow rates reported for the year of 2018 (Metro Vancouver and Capital Regional District, personal communication).

Ag from effluent	Average conc.	Annual flow	Annual flux	
	pM	L/yr	mol/yr	kg/yr
Iona Island				
Dissolved Ag	377	2.08E+11	78	8.8
Particulate Ag*	908		189	21.2
Total Ag	1284		267	30.0
Macaulay Point				
Dissolved Ag	384	1.63E+10	6	0.7
Particulate Ag*	3077		50	5.6
Total Ag	3461		56	6.3
Clover Point				
Dissolved Ag	647	1.64E+10	11	1.2
Particulate Ag*	10583		173	19.5
Total Ag	11230		184	20.7

4.3 Discussion

4.3.1 Ag inputs from natural and anthropogenic sources

In order to determine the potential impact of wastewater discharges on the receiving environment of SoG, we need to compare Ag inputs from municipal effluents to concentrations and rates of addition from its natural sources in rivers and the Pacific Ocean.

4.3.1.1 Dissolved Ag input from continental runoff

Following the same approach as dCd, we use the publicly available time-series (2011-2018) measurements of dAg in the Main Arm of the Fraser River for quantifying the riverine input of dAg into the SoG. As discussed in Chapter 3, the total freshwater discharge into the SoG is estimated using a linear function based on the flow rates measured at two stations, Fraser River at Hope (station 08MF005) and Englishman River near Parksville (station 08HB002) to represent

snowmelt and rainfall dominated rivers, respectively. Given the lack of spatial coverage for dissolved metals in rivers, we assume that all other smaller rivers entering the SoG basin (e.g., Englishman River) have the same concentration of dAg as the Fraser River. In addition, most of the dAg concentrations in Fraser River are reported at detection limits (10 pM, Figure 4.4). However, the largely coherent peak dAg concentrations at the early onset of river freshet suggest that the observed seasonal variations are likely still valid.

Similar to the trend observed for dCd (Figure 3.11), both concentrations and fluxes of dAg peak prior to the river freshet (Figure 4.4). The time lag between highest dAg concentration and maximum river discharge is again confirmed by plotting all available dAg data and flow rate versus calendar months (Figure 4.5). Results of both dCd and dAg suggest that the early onset of freshet brings in a pulse of dissolved metals, likely associated with mobilization of the shallow soil pool and subsequent desorption/release of dissolved metals from suspended particulate matter (Voss et al., 2015). The annual riverine flux and discharge-weighted average concentration of dAg are estimated to be 2537 ± 438 mol/yr (274 ± 47 kg/yr) and 15 ± 3 pM respectively.

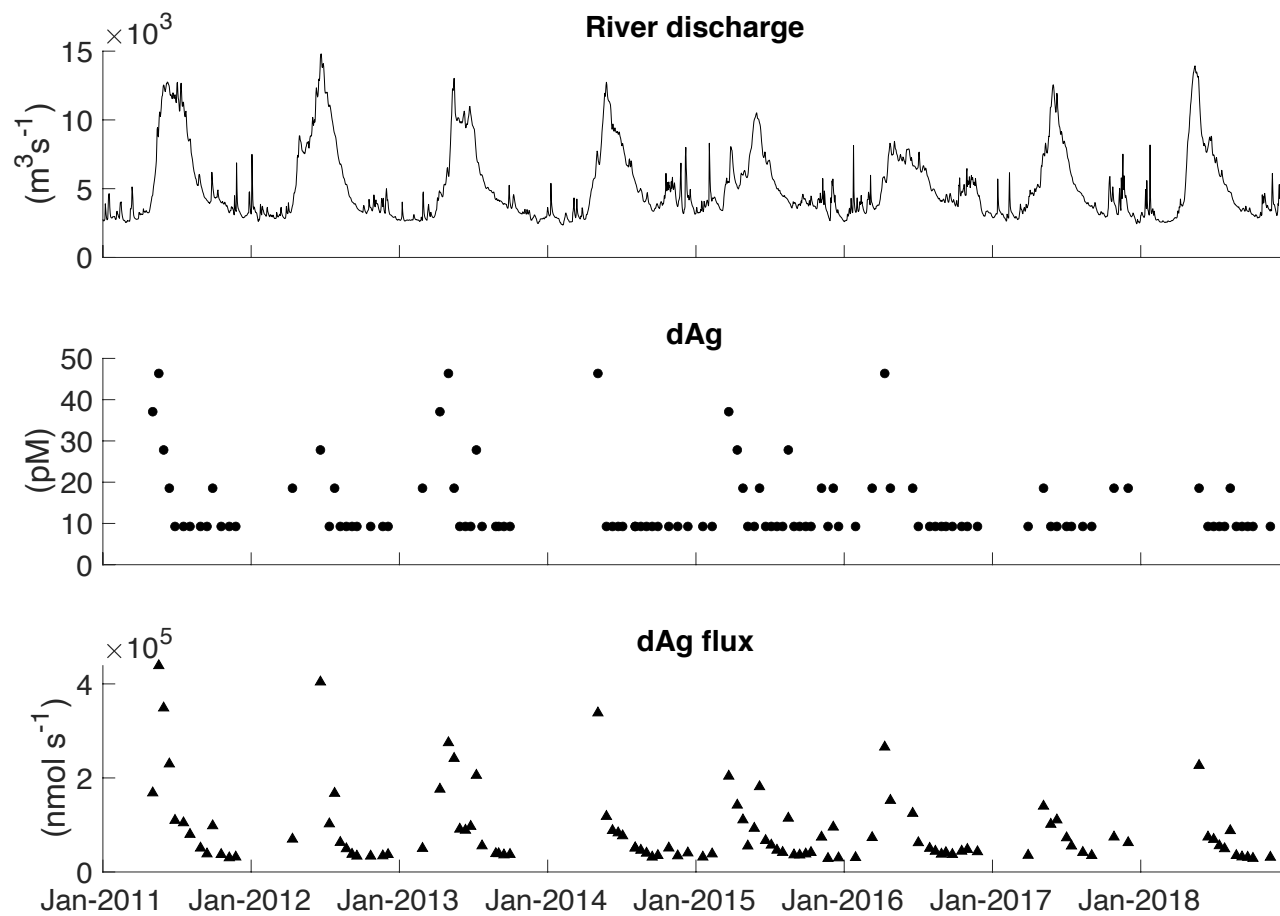


Figure 4.4. Time series (2011-2018) of freshwater discharge, dissolved Ag concentration, and dissolved Ag flux. Discharge is based on measurements from Fraser River at Hope and Englishman River by Water Survey of Canada. Dissolved Ag concentrations were obtained from the Fraser River Water Quality Buoy located in the Main Arm of the river (Environment and Climate Change Canada, 2018).

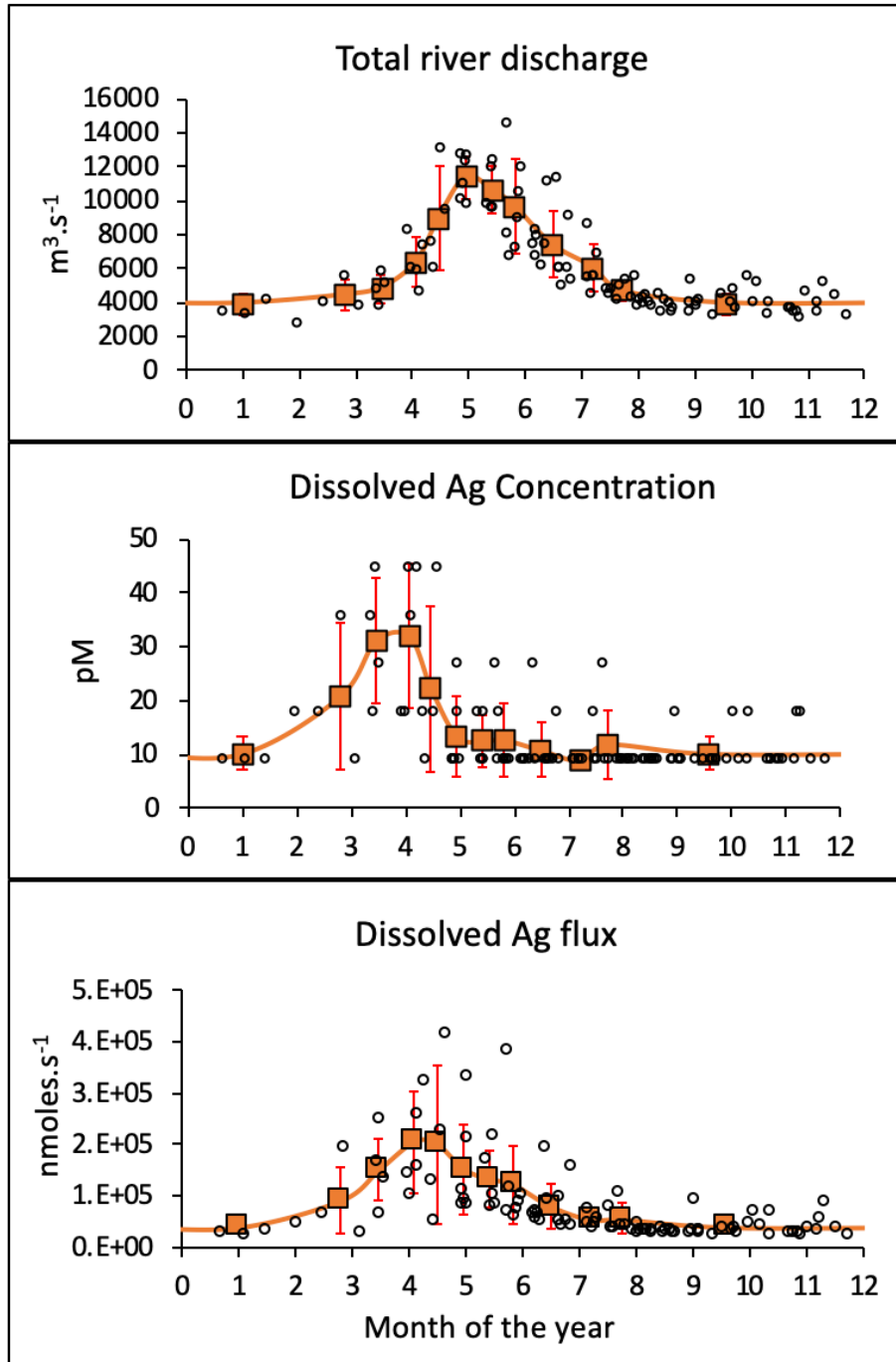


Figure 4.5. Total river discharge rate (top), dissolved Ag concentrations measured in the Fraser River Main Arm (center), and dissolved Ag fluxes from rivers (bottom) all plotted against months. Black empty circles are data shown in Figure 4.4. Orange filled squares are calculated averages ± 1 SD for each time interval with relatively constant river discharge and dissolved Ag concentration.

4.3.1.2 Dissolved Ag input from the Pacific Ocean

Water column observations made at station P4 can be used to estimate the physical and chemical properties of the source oceanic water. Kramer et al. (2011) reported depth profiles of dAg in the northeast Pacific during the February 2005 Line P cruise. We compared our measurements of dAg in 4 samples collected in September 2018 between 25 and 400 m at station P4 with Kramer's winter data (Figure 4.6). Our summer/fall data illustrate an increase of dAg with salinity, as observed for the dCd concentrations measured in the same samples. The range of dAg is between 5.6 to 14.2 pmol/kg at subsurface depths (100 – 400 m; salinity: 33.6 – 34).

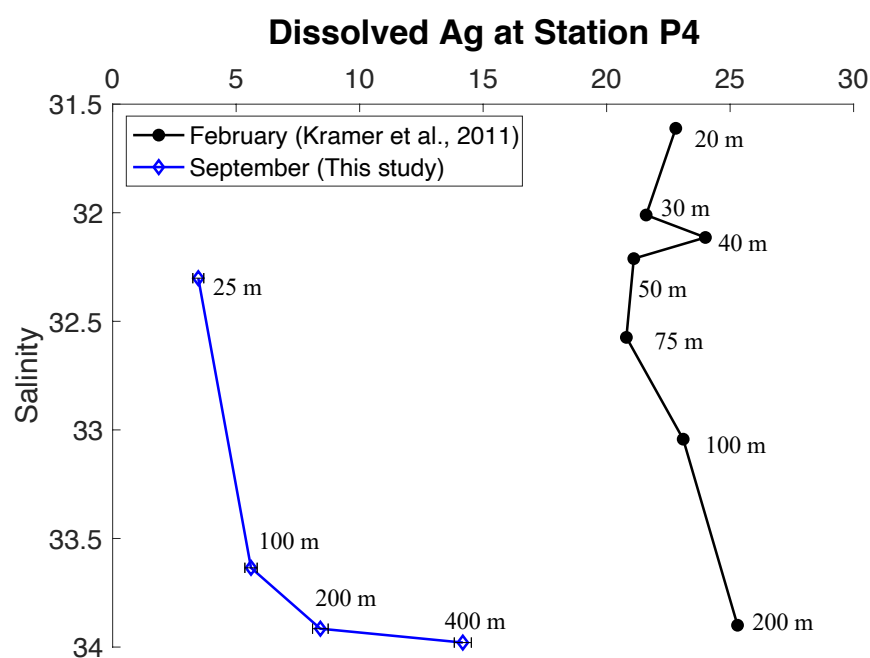


Figure 4.6. Dissolved Ag profile (20 – 200 m) reported for nearshore station P4 along the Line P transect during the February 2005 cruise (Kramer et al., 2011), and selective samples (25 m – 400 m) measured in the September 2018 cruise. Dissolved Ag are reported in the unit of pM by Kramer et al., and in pmol/kg for this study.

In contrast, Kramer's winter dAg concentrations at station P4 do not vary significantly with salinity and have an average of 23 ± 2 pM in the upper 200 m (Figure 4.6). They proposed that the high dAg signal observed at P4 was originated from the outflowing surface waters in coastal basins, which were enriched in trace metals. However, our dAg measurements in the SoG surface samples

are significantly lower (5.5 – 11.9 pmol/kg; Figure 4.1) than concentrations reported by Kramer et al. (2011, Figure 4.6), and thus contradictory to their hypothesis. Kramer's dAg data were collected in the northeast Pacific over a decade ago with no measurements available in coastal waters for comparison. The lack of historical data on dAg limits our ability to resolve the discrepancy between our measurements and Kramer's at station P4. On the other hand, results of the two studies could suggest that dAg in the offshore Pacific water have a seasonal cycle, which has significantly higher concentrations in the winter than in the summer.

Based on the two depth profiles captured at station P4, dAg concentrations in the upwelled Pacific water can vary up to five-fold from summer to winter (c.a. 5 – 25 pM; Figure 4.6). The Pacific is by far the largest source of dAg into the SoG, due to its large volume flux (Figure 3.16) and similar dAg concentrations as those found in river waters (15 ± 3 pM). Variations of dAg at the Pacific end member are expected to be reflected in the water column of the SoG. The next section (4.3.2) will focus on the temporal variations of dAg in the southern SoG (station S4-1.5), and its spatial distributions in the Salish Sea to shed light on the influence of Pacific inputs.

4.3.1.3 Anthropogenic input of Ag from municipal effluent

Having discussed the natural sources of dAg into the Salish Sea, we then assess whether anthropogenic discharges from WWTPs could significantly elevate the ambient dAg concentrations. The recommended criteria of total Ag in marine waters (27.8 nM maximum; BC WQG) was exceeded once in Clover Point's undiluted effluent (37 nM in January; Table 4.1). The estimated initial dilution factor for discharged effluent from Clover Point is 175 (Hodgins, 2006), which is a conservative estimate of the dilution predicted to occur at the boundary of the initial dilution zone (100 m radius around the outfall). After mixing with ambient seawater, the total Ag concentration resulting from effluent discharge would be well below the threshold stated in the BC WQG (Hodgins, 2006).

Johannessen et al. (2015) constructed regional geochemical budgets for metals in the SoG and concluded that the maximum contribution of wastewater to the Ag sediment sink was 4.4%. Their budget was based on an annual Ag input of 200 kg/yr from Iona WWTP, 17 kg/yr from Macaulay

Point, and 24 kg/yr from Clover Point. Their estimates for Macaulay and Clover are in the same order of magnitude as our particulate Ag fluxes based on the 2017-2018 effluent data. Since precise Ag concentrations in the Iona effluent were not available in the municipal annual reports, Johannessen et al. used the detection limit of Ag to estimate its annual discharge (2015). Substituting our particulate Ag flux of 21.2 kg/yr in their regional budgets suggest that the contribution of wastewater to Ag burial in SoG sediment is approximately 2%.

4.3.2 Temporal variations and spatial distributions of dissolved Ag

4.3.2.1 Temporal trends of dissolved Ag in the southern SoG

Analytical uncertainties for our dAg measurements are typically between 5 and 10%, with higher precision for samples processed with standard additions (section 2.2.1, Appendix Table B.2). Aside from analytical noises in the data, concentrations of dAg in surface waters could be affected by a number of factors such as riverine input, deposition of natural and anthropogenic aerosols, biological uptake, and scavenging by particles (Zhang et al., 2001). The vertical dAg profiles collected by Zhang et al. (2001) in the western North Pacific also exhibited large variations in the surface waters, which they attributed to biological uptake and particle scavenging. Surface concentrations of dAg in the SoG could be affected by the same processes, but our understanding is still poorly constrained given the available data. Unlike dCd and macronutrients, vertical profiles of dAg do not exhibit clear seasonal surface depletions (Figure 4.1). Sporadically high values measured in near surface waters (e.g., April at 5 m) further obscure any consistent trends. Higher resolution temporal profiles are needed to improve our understanding of the mechanisms that govern the distribution of dAg in surface waters of the SoG.

In the SoG intermediate layer (50 – 200 m), water is continuously renewed by a mixture of incoming Pacific water and upper SoG water formed in the turbulent Haro Strait region. As shown in Chapter 3, salinity and dCd concentrations in the intermediate layer of the SoG respond to changes in the source water leaving Haro Strait. Moreover, there is a time delay as well as an attenuation of the seasonal cycles as this water flows northward into the SoG basin. Since the transit time from Haro Strait to the southern SoG is approximately 2 months (Stevens and Pawlowicz, in prep), the relatively high dAg signal detected at 100 m on station S4-1.5 in April

could be propagated from the winter (i.e., February) Pacific water. At the same depth, the relatively low dAg concentrations during August/September could reflect lower Pacific input from the early summer (June/July). This hypothesis is in agreement with the significantly higher concentrations of dAg observed in the upper 200 m at station P4 in February than in September (Figure 4.6).

The SoG deep water (> 200 m) is renewed on an annual basis by pulses of denser summer Pacific water. The September and December sampling occurred at the end of 2017's renewal period (Figure 3.18), during which relatively low concentrations of dAg were measured in the deep basin of the SoG (Figure 4.1). From December to April in the following year, the deep water was stagnant and there was a gradual increase of dAg concentrations. From April to August 2018, the relatively dense Pacific water intruded the SoG basin again, restoring deep-water dAg concentrations towards levels measured at the end of the 2017 summer renewal (Figure 4.1). Our data suggest that the upwelled summer Pacific water is lower in dAg concentrations than the SoG deep waters overwinter. Inflow of low dAg water from the Pacific Ocean is consistent with the relatively low concentrations observed in the intermediate waters during August/September and December (Figure 4.1).

Since there was no deep-water renewal during the winter stagnant period (Dec. 2017 - Apr. 2018), the increase in dAg of deep waters could be attributed to either vertical diffusion with the intermediate water, or release from settling particles or sediments. However, mixing would have lowered the deep-water concentrations given the relatively low concentrations found at intermediate depths (Figure 4.1). Hence, the gradual increase of dAg between December and April must be attributed to another process. One possibility is remineralization of organic matter, which releases dAg into the water column. Vertical profiles of dAg in the western North Pacific suggested that concentrations of dAg are largely governed by biological uptake and particle scavenging at the surface, and regeneration in deep waters (Zhang et al., 2001). Ndung'u et al. (2001) further proposed that Ag is scavenged onto cell surfaces associated with biogenic silica (opal). The gradual dissolution of opal could be responsible for the observed increase in Si and dAg in bottom waters at station S4-1.5 between December and April (Figure 3.4).

In addition to dissolved profiles captured in the water column, Ag data in sediments and suspended particles also provide evidence for the association of Ag with biogenic materials (Martin et al., 1983; McKay & Pedersen, 2008). McKay and Pedersen (2008) measured concentrations of Ag and a group of redox-sensitive metals (i.e., Cd, Mo, Re) in surface sediments collected from productive coastal upwelling regions along the eastern margin of the Pacific Ocean. They argued that redox-controlled sedimentary processes (i.e., diagenesis) are not the primary control for Ag because its enrichment in surface sediments is not correlated with the distributions of other redox-sensitive metals. Instead, they found a positive correlation between Ag and organic carbon content in the sediment, suggesting that Ag is scavenged from the water column by sinking organic particles. Their finding is in agreement with the tight coupling between Ag and organic carbon fluxes in sinking particles collected in the open ocean of Northeast Pacific (Martin et al., 1983). Fisher et al. (1991) also found that metals such as Ag can be effectively scavenged by zooplankton fecal pellets and marine snow and transported into deep waters as particle sinking fluxes. In sum, previous studies have confirmed the importance of biogenic particles in the cycling of Ag in the ocean.

In the SoG deep basin, the marked increase in dAg concentrations between December and April (Figure 4.1), is in contrast to the trend observed for dCd (Figure 3.6). As discussed in Chapter 3, dCd concentrations decreased during the winter stagnant period likely due to precipitation of CdS in sediment porewaters and downward diffusion of dCd across the sediment-water interface. Ag and Cd both form insoluble complexes with free sulfides, and Ag_2S has a higher conditional stability constant than CdS in seawater (Al-Farawati & Van Den Berg, 1999). Hence, if there is formation of CdS in sediment porewaters, precipitation of Ag_2S should occur as well. Despite the stronger affinity of dAg to bind with sulfides than dCd, concentrations of dAg in the SoG deep waters are an order of magnitude lower than dCd. Thus, the concentration gradient of dAg across the sediment-water interface is expected to be much smaller than dCd, which consequently results in a smaller downward flux based on Fick's first law. Since the drop in dCd during the winter is merely $\sim 3\%$, the expected decrease of dAg due to Ag_2S precipitation would be even lower and within the analytical error of our measurements. Instead, the significant increase of dAg concentrations from December to April in the SoG deep basin could be explained by desorption of Ag from decomposing organic matter. Our results suggest that remineralization/desorption of

Ag from sinking particles is greater than diffusion of dAg into the sediment, leading to an increase in dAg concentrations from winter into spring, whereas the opposite applies for dCd.

4.3.2.2 Spatial distributions of dissolved Ag in the Salish Sea

The gradual increase in concentrations of dAg (Figure 4.2) as the Pacific water flows northward towards the SoG basin is the opposite of what was observed for dCd (Figure 3.8). In addition, the average dCd concentration measured in the deep samples (140 – 180 m) at station JF2 resembles that of the incoming Pacific water at approximately 200 m (Figure 3.8). However, the dAg concentration of the 200 m sample at station P4 (8.4 ± 0.3 pmol/kg) is significantly higher than the average concentration measured in the deep JF2 samples (5.4 ± 0.1 pmol/kg; Figure 4.2). Assuming the Pacific water is upwelled from that depth, our data suggest an approximate 35% removal of dAg by the time the water reaches Juan de Fuca Strait. A plausible removal mechanism for dAg is adsorption onto suspended particles as the deep water moves up the Juan de Fuca canyon onto the shelf. Alford and MacCready (2014) found that wind-driven flow through the canyon is strongly turbulent and could create intermediate nepheloid layers. Particle-laden flow in the canyon may act as a significant sink of dAg, resulting in lower concentrations in the deep basin of Juan de Fuca Strait relative to the upwelled offshore water.

As water travels from the deep Juan de Fuca basin into the Haro Strait region, it gets vigorously mixed by strong tidal currents. Concentrations of dAg are relatively constant throughout the water column at station HS, with an average of 5.5 ± 0.4 pmol/kg (Figure 4.2). This could be due to the similar dAg signals from the incoming Pacific water and outflowing SoG surface water which were then mixed in Haro Strait in August. Concentrations of dAg in surface samples collected in the SoG (station S4-1.5) and deep samples in Juan de Fuca Strait (station JF2) are consistent with this explanation (Figure 4.2). As the water leaves Haro Strait and continues to flow northward, significantly higher dAg concentrations in the SoG basin compared with the oceanic source water were observed in August (Figure 4.2). Desorption of dAg from sinking particles along the flow path could be a plausible explanation for its increase. Within the SoG, concentrations of dAg in below the surface layer were higher in the northern (station NG) compared to the southern (station S4-1.5) basins. The spatial variation within the SoG either points to an unknown source of dAg

near Texada Island (e.g., mining activities) or reflects a seasonal cycle of dAg in the incoming Pacific water being propagated into the SoG at subsurface depth. However, it is unlikely for anthropogenic inputs to contaminate the entire water column, thus the elevated dAg concentrations at station NG are more likely a result of the latter. The propagation hypothesis will be discussed in more details with the hydrographic data in the following section.

4.3.2.3 Propagation of seasonal variations of dissolved Ag

It has been demonstrated that the intermediate water mass (50 – 200 m) in the SoG travels northwards from its source in the Haro Strait, where hydrographic properties such as temperature and dissolved oxygen are determined by air-sea exchange processes in this vigorously mixed region (Stevens and Pawlowicz, in prep). In addition, seasonal variabilities of salinity and dCd in Haro Strait are shown to be propagated into the southern SoG (section 3.3.3.2). The estimated transit time for the intermediate water to travel from Haro Strait towards the SoG basin is approximately 2 – 3 months. During transit, the amplitude of the seasonal cycles of temperature and dissolved oxygen is attenuated due to mixing with ambient SoG water along the path. Hence, we would expect the seasonality of physical and possibly chemical properties to be delayed and attenuated in the northern SoG relative to the southern region. We could try to verify this hypothesis by comparing our time-series data in the southern Strait at station S4-1.5 with the August data captured in the northern Strait at station NG.

The temperature of intermediate waters (50 – 200 m) at station S4-1.5 is higher than at station NG in August. The temperature signal observed on station S4-1.5 could be reflective of the inflow of “new” summer water that was recently formed in the Haro Strait region. At station NG, due to the time delay, we could be seeing a signal of the “older” water that has been travelling across the SoG basin since it was formed in Haro Strait approximately three months prior to our August sampling (i.e., end of May). As the Haro Strait source water mixes with ambient seawater in the SoG, its seasonal cycle of water properties (e.g., temperature, dAg concentration) dampens. Between 50 – 200 m, the temperature of water at station NG in August lies between the temperature observed in June and August at station S4-1.5 (Figure 4.7), consistent with the dampening of seasonal cycle as water mixes. Interestingly, trends in dAg concentrations for the intermediate water at stations S4-

1.5 and NG are consistent with the propagation of seasonal variations in temperature (Figure 4.7 & Figure 4.8). The similar concentrations of dAg between the August water at station NG and the June water at station S4-1.5 could thus reflect the northward propagation of “older” spring water with higher dAg across the SoG basin.

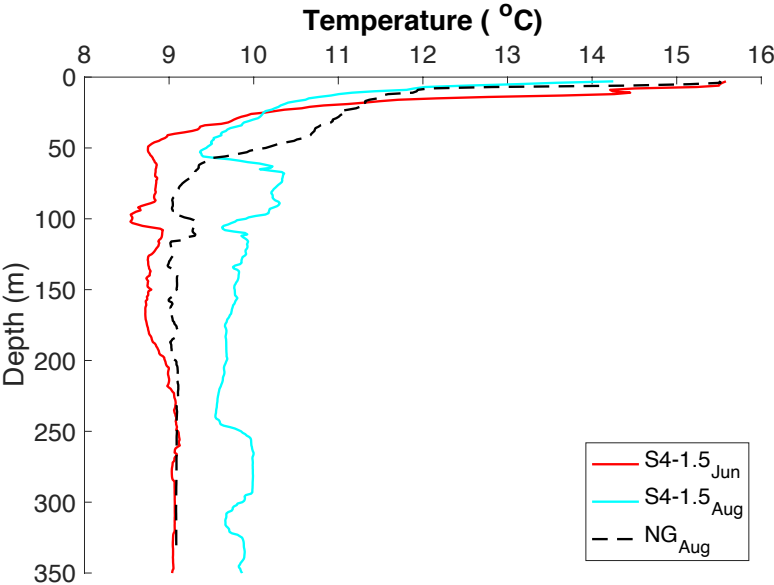


Figure 4.7. Depth profiles of temperature at the southern SoG (station S4-1.5) in June and August 2018, and at the northern SoG (station NG) in August 2018.

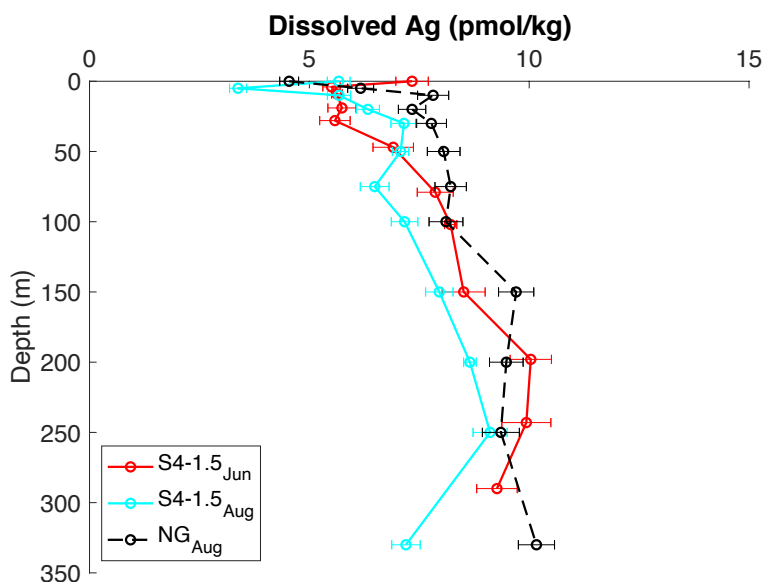


Figure 4.8. Depth profiles of dissolved Ag at the southern SoG (station S4-1.5) in June and August 2018, and at the northern SoG (station NG) in August 2018.

The Salish Sea box model can be used to provide insight on the range of dAg concentrations expected in the upwelled Pacific water in order to produce the temporal variations observed in the intermediate layer of SoG. As with dCd, time-series data of dAg from the Fraser Rivers are introduced to the model to represent the freshwater end member. A constant dAg flux of 8.8 kg/yr and 1.9 kg/yr (Table 4.2) are added to the SoG and Haro Strait basins, respectively, to represent the anthropogenic wastewater loadings from Iona WWTP and the two outfalls in Victoria. Similar to dCd, wastewater discharge is an insignificant source of dAg given the small input fluxes from sewage outfalls. For the Pacific end members, an input of 5 pM and 10 pM (Figure 4.9) are tested based on the range of dAg concentrations observed in the Salish Sea.

With a Pacific input of 5 pM, the model results match fairly well with the measured dAg concentrations in August 2018 except for the SoG lower box (SoG_l; 50 m – bottom), where the model underestimates the field observation (Figure 4.9A). The model outputs represent the average concentrations of dAg at any given time, assuming the water is homogeneous across the entire SoG. The higher than predicted dAg concentration in the SoG_l box of August could reflect the remaining signal of older SoG water (i.e., June) that is relatively enriched in dAg. This is consistent

with the temporal variations in dAg observed in the field (Figure 4.1), and the water transit time from Haro Strait into the SoG. With the exception of summer waters in the SoG upper box (SoGu; 0 – 50 m), using 5 pM as the Pacific end member significantly underestimates dAg concentrations measured in the SoGu and SoGl boxes (Figure 4.9A). This suggest that the Pacific input must be higher in other seasons. When doubling the Pacific input to 10 pM, we get a good match between the average dAg concentrations measured and modelled for the SoGl box (50 m – bottom) in April 2018 (Figure 4.9B). This is again consistent with the propagation of high-Ag winter Pacific water in February entering the southern SoG basin at intermediate depths with a time delay of approximately 2 months. Box model results confirm that a variable (high in winter, low in summer) Pacific input is needed in order to explain the temporal variations of dAg in the intermediate waters of SoG.

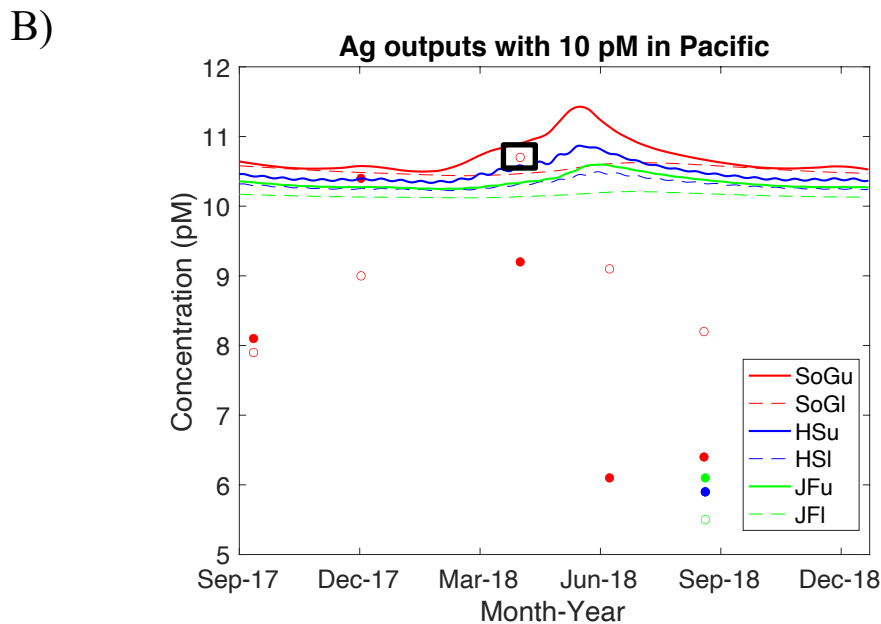
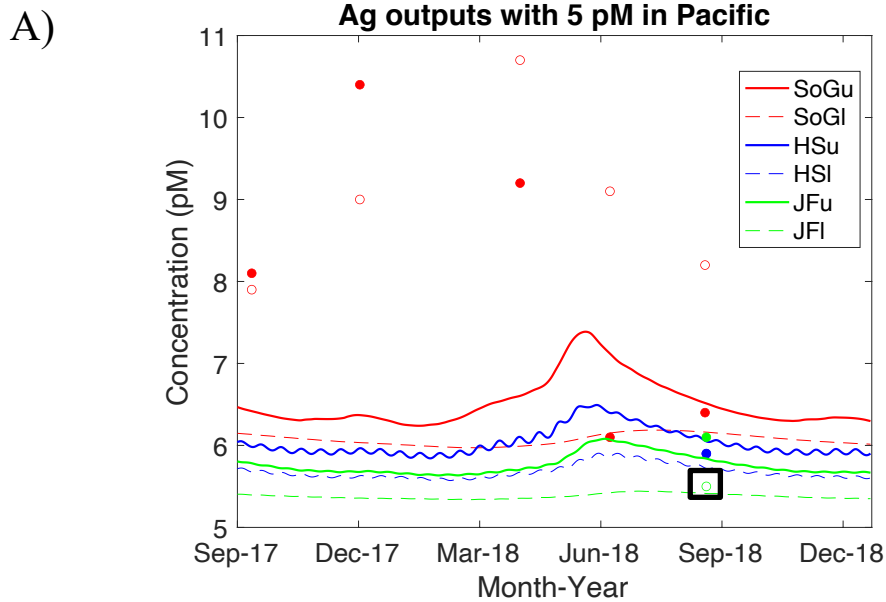


Figure 4.9. Modelled vs measured dissolved Ag concentrations in the Strait of Georgia upper (SoGu), Strait of Georgia lower (SoGl), Haro Strait upper (HSu), Haro Strait lower (HSI), Juan de Fuca Strait upper (JFu), and Juan de Fuca Strait lower (JFI) boxes. Upper boxes represent water column from the surface to 50 m, and lower boxes are 50 m to the bottom. Model results are based on a Pacific input of 5 pM (A) and 10 pM (B). Filled and empty circles are field measurements for dissolved Ag in the upper (average concentrations between 0 and 50 m) and lower (average concentrations below 50 m) boxes, respectively. Field measurements that match with the model predictions for JFI and SoGl boxes are enclosed in a square.

4.3.3 Sources of particulate Ag in the southern SoG

As previously discussed, transmissivity profiles clearly show lateral transport of suspended particles in intermediate waters between 150 and 225 m (Figure 3.10). The vertical distributions of pAg, pAl and pP in the water column of the southern SoG (Figure 4.3) are influenced by intrusions of turbid water from the Haro Strait region, where vigorous tidal mixing largely enhances suspension of particulate metals in the intermediate layer (Johannessen et al., 2006). For the study of contaminants such as Ag in the SoG, we need to distinguish its natural sources from anthropogenic inputs. Incorporation of Ag into lithogenic and biogenic particles, or adsorption onto suspended particles surfaces could all contribute to the natural abundance of pAg in seawater. Anthropogenic inputs such as particles discharge by WWTPs and deposition of contaminated aerosols can potentially disturb the natural cycling of Ag in oceanic environment.

Following the same approach for pCd, concentrations of pAl and pP are used to determine the contribution of lithogenic and biogenic materials, respectively, to the total amount of pAg present in the water column. The lithogenic fraction is estimated by multiplying the pAl concentration in sinking particles by the average Ag: Al ratio in Earth's crust (Taylor & McLennan, 1995). Due to Ag's low crustal abundance (2×10^{-7} mol pAg per mol of pAl), its lithogenic component is negligible in marine particles. This can be confirmed by plotting the pAg: pAl ratios in particles collected from December against the average crustal ratio (Figure 4.10). For the biogenic fraction of pAg, although Ag is not an essential micronutrient, studies have shown its uptake and bioaccumulation in the aquatic food chain (N. Fisher et al., 1984; Ratte, 1999; Xu & Wang, 2004). However, there is no published Ag quotas for marine phytoplankton to our knowledge, making the quantification of biogenic pAg challenging. Our data show that pAg concentrations measured at the surface waters in December 2017 (2.2 ± 0.2 pM) and April 2018 (1.9 ± 0.1 pM) are not significantly different, whereas pP concentrations have increased by six-fold as a result of the phytoplankton spring bloom (Figure 4.3). This suggests that Ag is not assimilated into biomass the same way P does.

Besides natural sources, pAg could be associated particles discharged from anthropogenic activities (e.g., domestic and industrial effluents). We thus investigate whether anthropogenic sources could contribute to the pAg pool in SoG's water column. Unlike pCd, depth profiles of pAg do not show an obvious peak (Figure 4.3). Although anthropogenic inputs did not cause significant increases in pAg concentrations, the signal from discharged effluents could be revealed by normalizing its concentration to pAl, as the pAg: pAl ratio of effluent particles is likely significantly enhanced than that of lithogenic particles. A prominent peak of pAg: pAl ratios was observed at 50 m in December, and 20 m in April (Figure 4.10). One potential anthropogenic source is the Iona WWTP, which discharges primary-treated effluent into the SoG at a depth around 100 m. Since the effluent is fresh and thus lighter than seawater, it rises as it mixes with the surrounding saltwater, bringing suspended effluent particles to its depth of neutral buoyancy at about 50 m. The potential enhancement of pAg from effluent particles was only observed in December when primary productivity was low, whereas in spring the effluent signal was overwhelmed by the abundance of biogenic particles at shallower depths (Figure 4.10).

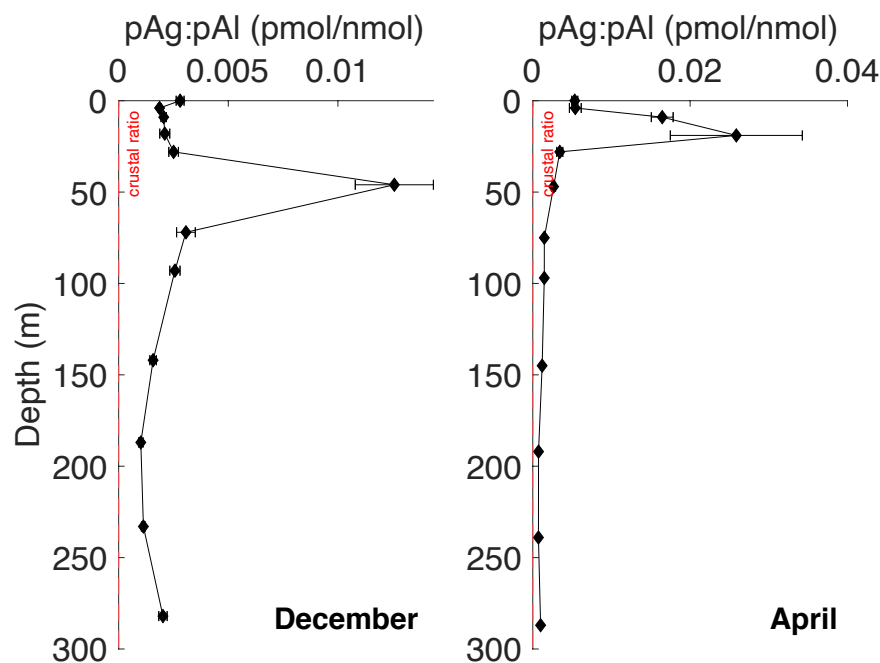


Figure 4.10. Depth profile of particulate Ag: particulate Al ratios at station S4-1.5 in December 2017 and April 2018. The red vertical line indicates the average Ag: Al crustal ratio (Taylor and McLennan, 1995). Error bars represent one standard deviation of the analytical uncertainty.

To assess whether the peak of pAg: pAl at 50 m in December (Figure 4.10) can be attributed to dispersion of effluent particles, we compared the concentration of pAg in the Iona effluent with its ambient level at station S4-1.5. We used the average pAg concentrations (0.33 ± 0.09 pM) at 30 m, 75 m, and 100 m in the December profile (Figure 4.3) to represent the background level of pAg in the SoG. For the wastewater end member, the average pAg found in the Iona effluent (908 pM; Table 4.2) was used. Assuming that pAg concentration at 50 m is governed by conservative mixing between the effluent and ambient SoG particles, the fraction of effluent needed to account for the 0.5 pM of pAg measured at 50 m is 0.02%. In other words, the plume of effluent particles would have been diluted approximately 5000 times by the time it reaches our sampling location (> 20 km from Iona WWTP). This dilution factor should be viewed as an overestimate because it assumes that pAg is not removed by sinking during transit. Given that station S4-1.5 is located outside of the initial dilution zone from the Iona outfall, the estimated dilution factor is plausible, suggesting that the small peak of pAg at 50 m could be attributed to the Iona effluent.

While the Iona effluent plume could contribute to a small fraction of pAg measured at 50 in December, the question remains as to the origin of the background pAg concentration in the SoG. The most striking aspect of the pAg depth profiles is their similarity to the vertical distributions of pAl and pP, all showing maximum concentrations at the surface and again at intermediate depths (Figure 4.3). Since pAl and pP concentrations are reflective of two of the main constituents of marine particles: lithogenic and biogenic, respectively, our results suggest that pAg concentrations could be proportional to the abundance of marine particles suspended in seawater. Ndung'u et al. (2001) proposed that Ag can be scavenged onto biogenic Si produced by algal cells (e.g., diatoms, silicoflagellates). However, the use of hydrofluoric acid in our digestion procedure limits our ability to quantify the fraction of Si in particulate samples.

We estimated the fraction of lithogenics and particulate organic matter (POM) in sinking particles of the SoG based on vertical profiles of pAl and biogenic pP measured in December and April (Table 3.5 & Table 3.6). The crustal abundance (8.04% by weight; Taylor & McLennan, 1995) and atomic weight of Al (27 g/mol) were used to convert concentrations of pAl (nM) to total mass of lithogenic particles per L ($\mu\text{g/L}$). To estimate the content of POM in particles, we assumed 1)

Redfield ratio of 106 between carbon and biogenic pP, and 2) organic matter is about 50% carbon (dry weight). Concentrations of POM can be calculated as the following:

$$POM (\mu\text{g/L}) = \text{biogenic } pP \text{ (nM)} \times 106 \text{ C/P} \times 12 \text{ g C/mol} \times 1000 \mu\text{g/ng} \times 2$$

Results show a tight linear correlation between POM and lithogenic particles, with an average slope of 0.14 for all particulate samples except in shallow waters of April (Figure 4.11), suggesting that in general, the mass of POM is 14% that of lithogenics in SoG particles. In April, there is still a good correlation ($R^2 = 0.75$) between POM and lithogenics in the upper 30 m, but there is approximately 3 times more biogenic than lithogenic particles by weight (Figure 4.11) due to the increase in planktonic biomass during the spring diatom bloom.

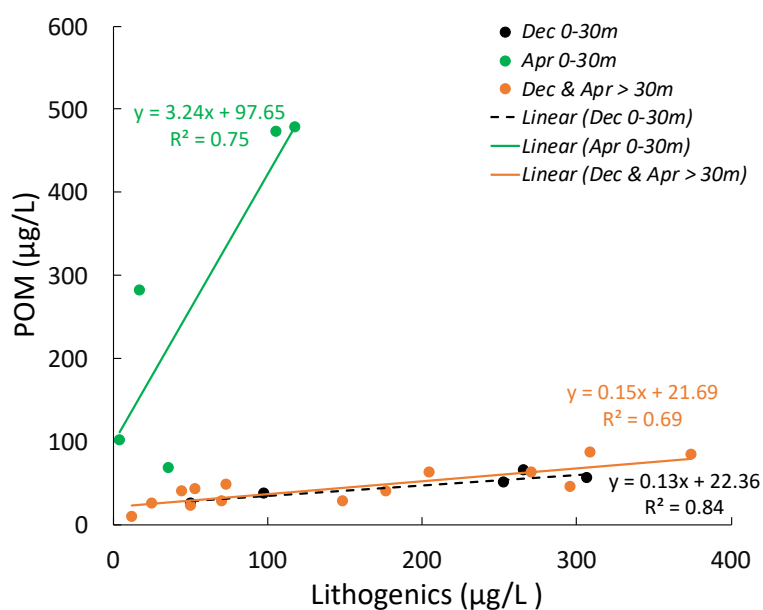


Figure 4.11. Correlation between particulate organic matter (POM) estimated from biogenic P, and lithogenic content estimated from Al in particulate samples collected in December 2017 and April 2018 at station S4-1.5 in the SoG.

Concentrations of pAg correlate with lithogenics for all samples deeper than 30 m ($R^2 = 0.74$; Figure 4.12A), indicating that Ag is scavenged onto suspended particles with an adsorption ratio of 0.002 pmol Ag per µg of lithogenics. Particles collected in the upper 30 m from December and

April have much higher pAg concentrations than expected from their lithogenic content (Figure 4.12A). The excess pAg (difference between measured and expected from lithogenics) is tightly coupled with the POM content in particles (Figure 4.12B). In December, surface particles contain 0.03 pmol Ag per μg POM ($R^2 = 0.94$). Slow growing, small phytoplankton with large surface area to volume ratios in winter could contribute to the adsorption of Ag onto cell surfaces. In April, the amount of Ag bound to POM is 10 times lower compared to that in winter (0.003 pmol/ μg ; Figure 4.12B). The rapidly growing phytoplankton cells during spring bloom might be generating particles faster than the adsorption rate of Ag. Thus, the freshly produced planktonic biomass which is high in biogenic P but low in pAg can lower the pAg/POM ratio in shallow particles. Overall, our results show a strong correlation between pAg concentrations and the abundance of marine particles, suggesting that adsorption of Ag onto particle surfaces is an important mechanism for its cycling in seawater.

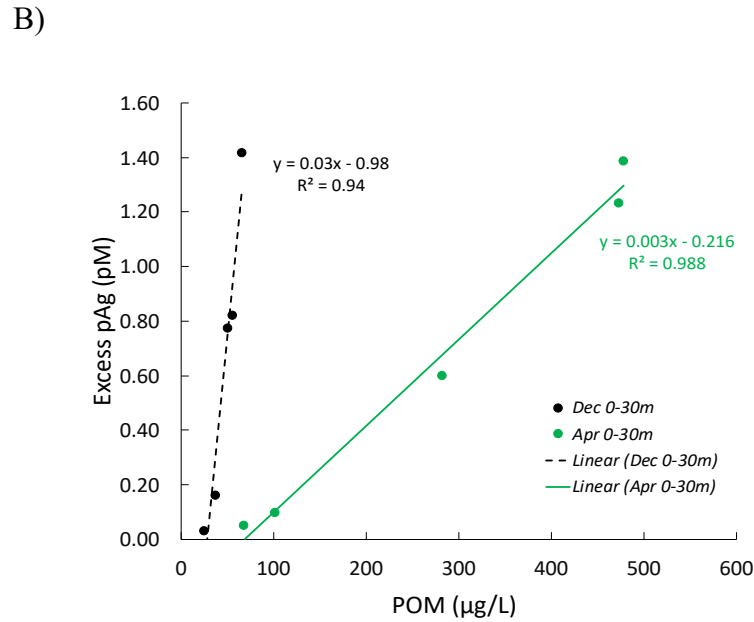
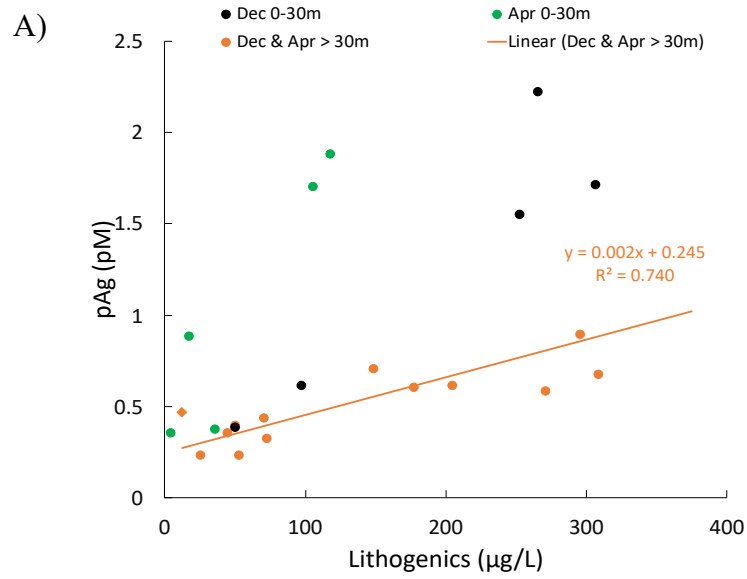


Figure 4.12. A) Correlation between measured pAg concentrations and the lithogenic fraction estimated from pAl. B) Correlation between excess pAg concentrations (difference between measured and predicted from lithogenics) and the particulate organic matter (POM) content estimated from biogenic P in particulate samples collected in December 2017 and April 2018 at station S4-1.5 in the SoG.

4.4 Conclusions for Ag

This study provides the first water column profiles of dAg in the Salish Sea, with time-series measurements conducted in the southern SoG. The overarching goals of this study are to document trends in the temporal and spatial distributions of dAg in the Salish Sea, and to assess the impact of municipal effluent discharges on the receiving SoG environment. Fluxes of dissolved and total Ag from three major outfalls located in Metro Vancouver and Capital Regional District are low compared to continental runoff from rivers (e.g., Fraser River). There are uncertainties in the dAg input from the Pacific due to lack of historical data and discrepancy in concentrations measured in the summer (this study) and in the winter (Kramer et al., 2011). Given the high volume flux of upwelled Pacific water, it is expected to be the largest source of dAg into the Salish Sea. Variations in the Pacific source water could be subsequently reflected in the water column of the SoG.

Concentrations of dAg in surface waters of the southern SoG exhibit large temporal variations with no clear seasonal depletions at surface waters. In intermediate waters, changes in dAg concentrations could reflect propagation of seasonal variations in the incoming Pacific water. Temperature and dAg signals captured in the northern and southern SoG provide some evidence for this propagation hypothesis and suggest that incoming Pacific water is enriched in dAg in the winter more than in the summer. High-resolution temporal measurements of dAg and hydrographic properties within the SoG are required in order to better constrain the propagation of seasonal cycles from the Pacific source water. In the deep basin of the southern SoG, there is a gradual increase of dAg during the winter stagnant period, which we have attributed to desorption of Ag from sinking particles during remineralization. Adsorption onto particles might be responsible for the loss of dAg as the upwelled Pacific water flows up the turbulent Juan de Fuca Canyon into the basin of Juan de Fuca Strait.

Particulate depth profiles collected in December and April in the southern SoG reveal strong correlations between pAg concentrations and abundance of marine particles. In shallow waters, scavenging of Ag by particulate organic matter and lithogenic particles both contribute to the pAg pool in the water column. In deep waters, pAg is found to be primarily associated with the lithogenic fraction of particles. Based on the dissolved and particulate Ag data presented in this

study, adsorption of dAg onto sinking particles and its subsequent release in deep waters during remineralization play an important role in the biogeochemical cycling of Ag in the SoG. Further studies are needed to understand the seasonal variations and cycling of dAg in the Pacific source water which fuels the productive SoG ecosystem.

Chapter 5: Conclusions

5.1 Major findings of study

This study investigates the modes of addition, transport, and removal of two toxic trace metals, Cd and Ag in the Salish Sea, with a focus on the southern SoG basin. Results show that anthropogenic loadings of these two metals from municipal effluent discharge are negligible compared with their input fluxes from rivers (mainly Fraser River) and the Pacific Ocean. Conservative mixing between river and Pacific water largely governs the temporal variations and spatial distributions of dCd and dAg.

5.1.1 Biogeochemical cycling of Cd in the SoG

The naturally high dCd signal in the Pacific water is diluted by mixing with low-Cd river water as it upwells into coastal basins of the Salish Sea via Juan de Fuca Strait. Field dCd observations match fairly well with predictions from the Salish Sea box model, which confirms that physical circulation shapes the temporal and spatial variations of dCd in this region. There is a tight coupling between salinity and dCd as the water travels northward from the southern passages (Haro Strait/Boundary Pass) into the SoG basin. Seasonal variations in salinity and dCd of the water at Haro Strait reflect the strength of coastal upwelling. This seasonal cycle propagates into the southern and northern SoG at intermediate depths with a time delay of approximately 2 and 3 months, respectively.

Time-series sampling in the southern SoG reveals a systematic decrease of dCd in deep waters (> 200 m) between annual deep-water renewal events. We attributed the decrease to vertical diffusion of dCd into the sediment due to CdS precipitation in anoxic sediment porewaters. This sink is however too small to produce readily measurable deviations from conservative mixing in shallower water, due to the relatively large dCd pool and short residence time of water in the SoG. There is also evidence of CdS formation in the water column of the southern Strait based on particulate Cd profiles. Although effluent discharged from the Iona WWTP is not a significant point source of Cd, it could indirectly contribute to the particulate Cd pool by releasing organic-

rich particles that can sustain sulfidic microenvironments and facilitate the formation of CdS even in oxygenated waters.

Uptake ratios of dCd: PO_4^{3-} during the spring phytoplankton bloom are in agreement with the low particulate Cd: P ratio measured in marine particles collected in the surface layer. We hypothesize that phytoplankton living in the SoG has a low cellular demand for dCd. The low uptake of dCd could also be due to competition with other metal cations for binding sites in algal cells. Although clearly present, the impact of biological cycling on the distribution of dCd in the SoG is obscured by the larger seasonal variations in dCd of the upwelled Pacific water. In summary, the distribution of Cd in the SoG is largely controlled by the physical circulation and mixing, which largely mask the smaller influence of biological cycling and removal to anoxic sediments.

5.1.2 Distribution of dissolved Ag in the SoG

This study provides the first water column profiles of dAg in coastal waters off British Columbia, with time-series measurements conducted in the southern SoG basin. Concentrations of dAg in the surface waters exhibit significant temporal variations that are difficult to explain and could be the net effect of sporadic input, biological uptake or scavenging by particles. In intermediate waters, changes in dAg concentrations appear consistent with the propagation of seasonal variations in the incoming Pacific water. Both field and modelled data for dAg suggest that the winter Pacific water is enriched in dAg relative to the upwelled summer water. Spatial and temporal water column measurements of dAg and hydrographic properties across the SoG basin and further offshore are required in order to confirm the propagation hypothesis for dAg. In the deep basin of the southern SoG, there is a gradual increase of dAg during the winter stagnant period which we have attributed to remineralization of sinking organic matter and subsequent desorption of dAg. Results from this study suggest that incorporation of dAg into sinking particles and subsequent remineralization in deep waters play an important role in the biogeochemical cycling of Ag in the SoG.

5.2 Future studies

Dissolved and particulate depth profiles of Cd collected in the southern SoG both suggest that sulfate reduction and subsequent precipitation of Cd as the insoluble complex CdS could affect Cd

cycling in the water column. In productive coastal regions, accumulation of labile organic matter on the seafloor enhances oxygen demand in sediment and can result in highly reducing conditions close to the sediment-water interface. Diffusion of dCd from bottom waters into margin sediments could thus act as a significant sink of Cd, which could have implications for the global Cd cycle. Water column profiles in regions with relatively long hydraulic residence time could provide a means of evaluating this sink. In addition, future work is needed to confirm that effluent particles could provide anoxic microenvironments for CdS precipitation in oxic seawater. If confirmed, such precipitation could provide an entry point of Cd into the pelagic food chain (e.g., via ingestion by zooplankton) that would be worth investigating.

This study documents the first temporal and spatial distributions of dAg in the coastal basins of the Salish Sea. Our results suggest a seasonal variation of dAg concentrations in the Pacific water off the coast of B.C. In order to confirm this hypothesis, dAg profiles along a transect from the northeast Pacific into the coastal basins of Salish Sea are needed for at least two seasons (winter and summer). In addition, high resolution time-series sampling is required at the southern and northern SoG to track the propagation of seasonal variations of dAg in the Pacific source water. Due to the scarcity of dAg data in global oceans, our understanding of what governs its biogeochemical cycling is still limited. Large variations of dAg are present in the surface layer of the southern SoG, yet we are unable to identify the dominant biogeochemical processes involved. In order to address this, we need to have better constraints on potential sources of Ag (e.g., continental runoff, atmospheric deposition), and sinks from scavenging by particles or biological uptake. We have done some preliminary experiments using the radiotracer ^{110m}Ag to study the uptake of dAg in calanoid copepods collected from the southern SoG, as well as in laboratory diatom cultures (Appendix C). Preliminary results show evidence of uptake even though Ag is not an essential trace metal for growth. Understanding the uptake mechanism of dAg and quantifying Ag quotas for coastal and oceanic phytoplankton species could help interpreting the surface variations of dAg.

Bibliography

- Al-Farawati, R., & Van Den Berg, C. M. G. (1999). Metal-sulfide complexation in seawater. *Marine Chemistry*, 63(3–4), 331–352.
- Alford, M. H., & Maccready, P. (2014). Flow and mixing in Juan de Fuca Canyon, Washington. *Geophysical Research Letters*, 41(5), 1608–1615.
- Barriada, J. L., Tappin, A. D., Evans, E. H., & Achterberg, E. P. (2007). Dissolved silver measurements in seawater. *Trends in Analytical Chemistry*, 26(8), 809–817.
- Bianchi et al. (2018). Global niche of marine anaerobic metabolisms expanded by particle microenvironments. *Nature Geoscience*, 11, 263–268.
- Bourne, H. L., Bishop, J. K. B., Lam, P. J., & Ohnemus, D. C. (2018). Global spatial and temporal variation of Cd:P in euphotic zone particulates. *Global Biogeochemical Cycles*, 1123–1141.
- Bruland, K. W., & Franks, R. P. (1979). Sampling and analytical methods for the determination of copper, cadmium, zinc, and nickel at the nanogram per liter level in sea water. *Analytica Chimica Acta*, 105, 233–245.
- Bruland, K. W., & Franks, R. P. (1983). Mn, Ni, Cu, Zn and Cd in the Western North Atlantic. In C. S. Wong, E. Boyle, K. W. Bruland, J. D. Burton, & E. D. Goldberg (Eds.), *Trace metals in sea water*. Springer.
- Bruland, K. W., & Lohan, M. . (2003). Controls of trace metals in seawater. In *Treatise on Geochemistry* (pp. 23–43). Elsevier Ltd.
- Bruland, K. W., Orians, K. J., & Cowen, J. P. (1994). Reactive trace metals in the stratified central North Pacific. *Geochimica et Cosmochimica Acta*, 58(15).
- Capital Regional District. (2016). *Macaulay and Clover Points Wastewater and Marine Environment Program*. Victoria.
- Cullen, J. T., & Maldonado, M. T. (2013). Biogeochemistry of cadmium and its release to the environment. In A. Sigel, H. Sigel, & R. K. . Sigel (Eds.), *Cadmium: From toxicity to essentiality* (pp. 31–56). Springer.
- Elderfield, H., & Rickaby, R. E. M. (2000). Oceanic Cd/P ratio and nutrient utilization in the glacial Southern Ocean. *Nature*, 405(6784), 305–310. <https://doi.org/10.1038/35012507>
- Environment and Climate Change Canada. (2018). Water Quality Data from Fraser River (Main Arm) at Gravesend Reach.
- Fischer, L., Smith, G., Hann, S., & Bruland, K. W. (2018). Ultra-trace analysis of silver and platinum in seawater by ICP-SFMS after off-line matrix separation and pre-concentration. *Marine Chemistry*, 199(February 2017), 44–52.
- Fisher, N., Bone, M., & Teyssie, J.-L. (1984). Accumulation and toxicity of Cd, Zn, Ag, and Hg in four marine phytoplankters. *Marine Ecology Progress Series*, 18(1977), 201–213.
- Fisher, N. S., Nolan, C. V., & Fowler, S. W. (1991). Scavenging and retention of metals by zooplankton fecal pellets and marine snow. *Deep Sea Research*, 38(10), 1261–1275.
- Flegal, A. R., Brown, C. L., Squire, S., Ross, J. R. M., Scelfo, G. M., & Hibdon, S. (2007). Spatial and temporal variations in silver contamination and toxicity in San Francisco Bay. *Environmental Research*, 105(1), 34–52.
- Gallon, C., & Flegal, A. R. (2015). Sources, fluxes, and biogeochemical cycling of silver in the oceans. In D. M. Whitacre (Ed.), *Reviews of environmental contamination and toxicology* (Vol. 235). Springer.

- Gordon, K. (1997). *Sedimentary tracers of sewage inputs to the southern Strait of Georgia*.
- Guo, J., Annett, A. L., Taylor, R. L., Lapi, S., Ruth, T. J., & Maldonado, M. T. (2010). Copper-uptake kinetics of coastal and oceanic diatoms. *Journal of Phycology*, 46(6), 1218–1228.
- Hodgins, D. O. (2006). Technical Memorandum. *Assessment of plume trapping and dilution at the Clover Point Outfall and the Macaulay Point outfall*. Report prepared for the Capital Regional district.
- Hutton, M., & Symon, C. (1986). The quantities of cadmium, lead, mercury and arsenic entering the U.K. environment from human activities. *Science of the Total Environment*, 57, 129–150.
- Institute of Ocean Sciences. (2019). Line P Program. Retrieved from <http://www.waterproperties.ca/linep/>
- Jackson, J. M., Thomson, R. E., Brown, L. N., Willis, P. G., & Borstad, G. A. (2015). Satellite chlorophyll off the British Columbia Coast, 1997-2010. *Journal of Geophysical Research : Oceans*, 5473–5489.
- Jackson, S. L., Spence, J., Janssen, D. J., Ross, A. R. S., & Cullen, J. T. (2018). Determination of Mn, Fe, Ni, Cu, Zn, Cd and Pb in seawater using offline extraction and triple quadrupole ICP-MS/MS. *Journal of Analytical Atomic Spectrometry*, 33(2), 304–313.
- Janssen, D. J., Abouchami, W., Galer, S. J. G., & Cullen, J. T. (2017). Fine-scale spatial and interannual cadmium isotope variability in the subarctic northeast Pacific. *Earth and Planetary Science Letters*, 472, 241–252.
- Janssen et al. (2014). Undocumented water column sink for cadmium in open ocean oxygen-deficient zones. *Proceedings of the National Academy of Sciences*, 111(19), 6888–6893.
- Johannessen, S. C., Masson, D., & Macdonald, R. W. (2006). Distribution and cycling of suspended particles inferred from transmissivity in the Strait of Georgia, Haro Strait and Juan de Fuca Strait. *Atmosphere - Ocean*, 44(1), 17–27.
- Johannessen, S. C., Masson, D., & Macdonald, R. W. (2014). Oxygen in the deep Strait of Georgia, 1951-2009: The roles of mixing, deep-water renewal, and remineralization of organic carbon. *Limnology and Oceanography*, 59(1), 211–222.
- Kagaya, S., & Inoue, Y. (2014). Chelating materials immobilizing carboxymethylated pentaethylenehexamine and polyethyleneimine as ligands. *Analytical Sciences*, 30(1), 35–42.
- Kramer, D., Cullen, J. T., Christian, J. R., Johnson, W. K., & Pedersen, T. F. (2011). Silver in the subarctic northeast Pacific Ocean: Explaining the basin scale distribution of silver. *Marine Chemistry*, 123(1–4), 133–142.
- Kruzynski, G. M. (2004). Cadmium in oysters and scallops : the BC experience. *Toxicology Letters*, 148, 159–169.
- Kwong, L. E. (2016). *A novel approach to estimate active carbon flux using the micronekton biomass spectra*. Retrieved from <https://open.library.ubc.ca/cIRcle/collections/ubctheses/24/items/1.0339760>
- Lagerström, M. E., Field, M. P., Séguret, M., Fischer, L., Hann, S., & Sherrell, R. M. (2013). Automated on-line flow-injection ICP-MS determination of trace metals (Mn, Fe, Co, Ni, Cu and Zn) in open ocean seawater: Application to the GEOTRACES program. *Marine Chemistry*, 155, 71–80.
- Lee, D. Y., Fortin, C., & Campbell, P. G. C. (2004). Influence of chloride on silver uptake by two green algae, *Pseudokirchneriella subcapitata* and *Chlorella pyrenoidosa*. *Environmental*

- Toxicology and Chemistry*, 23(4), 1012–1018.
- Lekhi, P., Cassis, D., Pearce, C. M., Ebell, N., Maldonado, M. T., & Orians, K. J. (2008). Role of dissolved and particulate cadmium in the accumulation of cadmium in cultured oysters (*Crassostrea gigas*). *Science of the Total Environment*, 3, 309–325.
- Li, M., Gargett, A., & Denman, K. (2000). What determines seasonal and interannual variability of phytoplankton and zooplankton in strongly estuarine systems? Application to the semi-enclosed estuary of Strait of Georgia and Juan de Fuca Strait. *Estuarine, Coastal and Shelf Science*, 50(4), 467–488.
- Luoma, S. N. (2008). *Silver nanotechnologies and the environment: Old problems or new challenges?* Woodrow Wilson International Center for Scholars. Washington. Retrieved from <https://www.nanotechproject.org/news/archive/silver/>
- Macdonald, R. W., Johannessen, S. C., Gobeil, C., Wright, C., Burd, B., Roodselaar, A. Van, & Pedersen, T. F. (2008). Sediment redox tracers in Strait of Georgia sediments – Can they inform us of the loadings of organic carbon from municipal wastewater? *Marine Environmental Research*, 66, 87–100.
- Maldonado, M. T., Allen, A. E., Chong, J. S., Lin, K., Leus, D., Limnology, S., ... Harris, S. L. (2006). Copper-Dependent Iron Transport in Coastal and Oceanic Diatoms. *Limnology and Oceanography*, 51(4), 1729–1743.
- Maldonado, M. T., & Price, N. M. (2001). Reduction and transport of organically bound iron by *Thalassiosira oceanica* (Bacillariophyceae). *Journal of Phycology*, 37(2), 298–309.
- Maret, W., & Moulis, J.-M. (2013). The bioinorganic chemistry of cadmium in the context of its toxicity. In *Cadmium: From toxicity to essentiality* (pp. 1–23). Springer.
- Martin, J. H., Knauer, G. A., & Gordon, R. . (1983). Silver distributions and fluxes in north-east Pacific waters. *Nature*, 305.
- Masson. (2002). Deep water renewal in the strait of Georgia. *Estuarine, Coastal and Shelf Science*, 54(1), 115–126.
- Masson, D., & Perry, R. I. (2013). The strait of georgia ecosystem research initiative: An overview. *Progress in Oceanography*, 115, 1–5.
- McKay, J. L., & Pedersen, T. F. (2008). The accumulation of silver in marine sediments: A link to biogenic Ba and marine productivity. *Global Biogeochemical Cycles*, 22(4), 1–17.
- Metro Vancouver. (2018). *The 2018 Greater Vancouver Sewerage and Drainage District Environmental Management and Quality Control Annual Report*. Retrieved from <http://www.metrovancouver.org/services/liquid-waste/LiquidWastePublications/2018GVSDDD-EMQCAAnnualReport.pdf>
- Miller, L. A., & Bruland, K. W. (1995). Organic Speciation of Silver in Marine Waters. *Environmental Science and Technology*, 29(10), 2616–2621.
- Ministry of Environment British Columbia. (2015). *Ambient Water Quality Guidelines for Cadmium (Technical Report)*. Retrieved from <https://www2.gov.bc.ca/assets/gov/environment/air-land-water/water/waterquality/wqgs-wqos/approved-wqgs/cadmium/cadmium.pdf>
- Mullaugh, K. M., & Luther, G. W. (2011). Growth kinetics and long-term stability of CdS nanoparticles in aqueous solution under ambient conditions. *Journal of Nanoparticle Research*, 13(1), 393–404.
- Naja, G. M., & Volesky, B. (2009). Toxicity and sources of Pb, Cd, Hg, Cr, As, and radionuclides in the environment. In L. K. Wang, J. P. Chen, Y.T. Hung, & N. K. Shammam

- (Eds.), *Heavy Metals in the Environment* (pp. 13–62). CRC Press.
- Ndung'u, K., Thomas, M. A., & Flegal, A. R. (2001). Silver in the western equatorial and South Atlantic Ocean. *Deep-Sea Research Part II: Topical Studies in Oceanography*, 48(13), 2933–2945.
- Ndung'u, Kuria, Ranville, M. A., Franks, R. P., & Flegal, A. R. (2006). On-line determination of silver in natural waters by inductively-coupled plasma mass spectrometry: Influence of organic matter. *Marine Chemistry*, 98(2–4), 109–120.
- Ndungu, K. (2011). Dissolved silver in the Baltic Sea. *Environmental Research*, 111(1), 45–49.
- Ocean Networks Canada. (2019). Strait of Georgia Observatory. Retrieved from <https://www.oceannetworks.ca/observatories/pacific/strait-georgia>
- Ohnemus, D. C., & Lam, P. J. (2015). Cycling of lithogenic marine particles in the US GEOTRACES North Atlantic transect. *Deep-Sea Research II*, 116, 283–302.
- Ohnemus et al. (2014). Laboratory intercomparison of marine particulate digestions including Piranha: a novel chemical method for dissolution of polyethersulfone filters. *Limnology and Oceanography: Methods*, 12(8), 530–547.
- Pawlowicz, R. (2017). Seasonal Cycles, Hypoxia, and Renewal in a Coastal Fjord (Barkley Sound, British Columbia). *Atmosphere - Ocean*, 55(4–5), 264–283.
- Pawlowicz, R., Francois, R., & Maldonado, M. T. (2018). *Contaminant dispersion in the Strait of Georgia*.
- Pawlowicz, R., Hannah, C., & Rosenberger, A. (2019). Lagrangian observations of estuarine residence times, dispersion, and trapping in the Salish Sea. *Estuarine, Coastal and Shelf Science*, 225, 106246.
- Pawlowicz, R., Riche, O., & Halverson, M. (2007). The circulation and residence time of the Strait of Georgia using a simple mixing-box approach. *Atmosphere - Ocean*, 45(4), 173–193.
- Price, N. ., & Morel, F. M. M. (1990). Cadmium and cobalt substitution for zinc in a marine diatom. *Nature*, 414, 11–14.
- Price, N. M., Harrison, G., Hering, J. G., Hudson, R. J., Nirel, P., Palenik, B., & Morel, F. (1989). Preparation and chemistry of the artificial algal culture medium Aquil. *Biological Oceanography*, 6, 443–461.
- Purcell, T. W., & Peters, J. J. (1998). Sources of silver in the environment. *Environmental Toxicology and Chemistry*, 17(4), 539–546.
- Quay, P., Cullen, J., Landing, W., & Morton, P. (2015). Processes controlling the distributions of Cd and PO₄ in the ocean. *Global Biogeochemical Cycles*, 29(6), 830–841.
- Rapp, I., Schlosser, C., Rusiecka, D., Gledhill, M., & Achterberg, E. P. (2017). Automated preconcentration of Fe, Zn, Cu, Ni, Cd, Pb, Co, and Mn in seawater with analysis using high-resolution sector field inductively-coupled plasma mass spectrometry. *Analytica Chimica Acta*, 976, 1–13.
- Ratte, H. T. (1999). Bioaccumulation and toxicity of silver compounds: A review. *Environmental Toxicology and Chemistry*, 18(1), 89–108.
- Ravizza, G. E., & Bothner, M. H. (1996). Osmium isotopes and silver as tracers of anthropogenic metals in sediments from Massachusetts and Cape Cod bays. *Geochimica et Cosmochimica Acta*, 60(15), 2753–2763.
- Rozan, T. F., Lassman, M. E., Ridge, D. P., & Luther, G. W. (2000). Evidence for iron, copper and zinc complexation as multinuclear sulfide clusters in oxic rivers. *Nature*, 406(August),

879–882.

- Shiel, A. E., Weis, D., & Orians, K. J. (2012). Tracing cadmium, zinc and lead sources in bivalves from the coasts of western Canada and the USA using isotopes. *Geochimica et Cosmochimica Acta*, 76, 175–190.
- Smith, G. J., & Flegal, A. R. (1993). Silver in San Francisco Bay estuarine waters. *Estuaries*, 16(3), 547–558.
- Squire, S., Scelfo, G. M., Revenaugh, J., & Flegal, A. R. (2002). Decadal trends of silver and lead contamination in San Francisco Bay surface waters. *Environmental Science and Technology*, 36(11), 2379–2386.
- Tappin, A. D., Barriada, J. L., Braungardt, C. B., Evans, E. H., Patey, M. D., & Achterberg, E. P. (2010). Dissolved silver in European estuarine and coastal waters. *Water Research*, 44(14), 4204–4216.
- Taylor, S. R., & McLennan, S. M. (1995). The geochemical evolution of the continental crust. *American Geophysical Union*, 33(2), 241–265.
- Thomson, R. E. (1981). *Oceanography of the British Columbia Coast. Canadian special publications of fisheries and aquatic sciences* (Vol. 56). <https://doi.org/DDC:551.46633>
- Voss et al. (2014). Tracing river chemistry in space and time : Dissolved inorganic constituents of the Fraser River, Canada. *ScienceDirect*, 124, 283–308.
- Voss et al. (2015). Seasonal hydrology drives rapid shifts in the flux and composition of dissolved and particulate organic carbon and major and trace ions in the Fraser River, Canada. *Biogeosciences*, 5597–5618.
- Wang, Pawlowicz, R., & Sastri, A. R. (2019). Diurnal and Seasonal Variability of Near-Surface Oxygen in the Strait of Georgia. *Journal of Geophysical Research: Oceans*, 124(4), 2418–2439.
- Wang, W. X., & Fisher, N. S. (1998). Accumulation of trace elements in a marine copepod. *Limnology and Oceanography*, 43(2), 273–283.
- Water survey of Canada. (2019). Historical hydrometric data search. Retrieved from https://wateroffice.ec.gc.ca/search/historical_e.html
- Wilson, R. C. ., Beamish, R. J., Aitkens, F., & Bell, J. (1994). Review of the marine environment and biota of Strait of Georgia, Puget Sound and Juan de Fuca Strait.
- Wuttig, K., Townsend, A. T., van der Merwe, P., Gault-Ringold, M., Holmes, T., Schallenberg, C., ... Bowie, A. R. (2019). Critical evaluation of a seaFAST system for the analysis of trace metals in marine samples. *Talanta*, 197, 653–668.
- Xu, Y., & Wang, W. X. (2004). Silver uptake by a marine diatom and its transfer to the coastal copepod *Acartia spinicauda*. *Environmental Toxicology and Chemistry*, 23(3), 682–690.
- Yin, K., Harrison, P. J., Goldblatt, R. H., St. John, M. A., & Beamish, R. J. (1997). Factors controlling the timing of the spring bloom in the Strait of Georgia estuary, British Columbia, Canada. *Canadian Journal of Fisheries and Aquatic Sciences*, 54(9), 1985–1995.
- Zhang, Y., Amakawa, H., & Nozaki, Y. (2001). Oceanic profiles of dissolved silver: Precise measurements in the basins of western North Pacific, Sea of Okhotsk, and the Japan sea. *Marine Chemistry*, 75(1–2), 151–163.
- Zhang, Y., Obata, H., & Nozaki, Y. (2004). Silver in the Pacific Ocean and the Bering Sea. *Geochemical Journal*, 38(6), 623–633.

Appendices

Appendix A. Supplementary figures

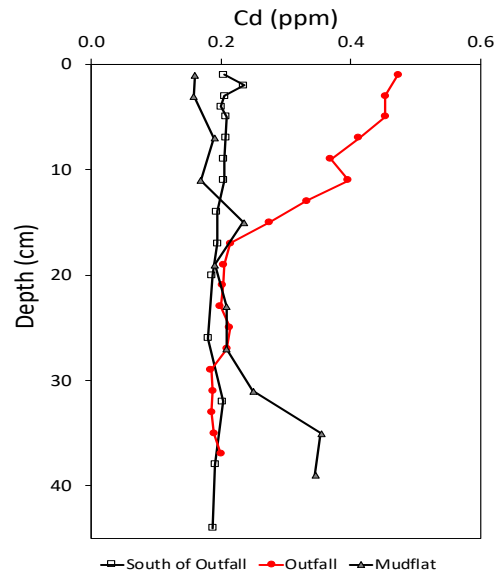


Figure A.1. Cd concentrations in sediment cores collected in 2014 from the south of the Iona outfall, near the outfall, and in a mudflat where the effluent was discharged prior to 1988.

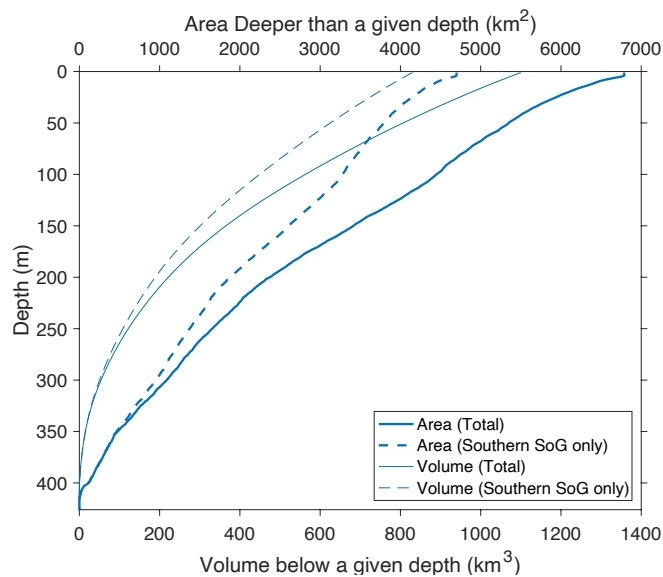


Figure A.2. Surface area and volume below a given depth in the entire SoG and the southern basin only (Rich Pawlowicz, personal communication). Hypsographic dataset used to create the plot is the same as in Pawlowicz et al., 2007.

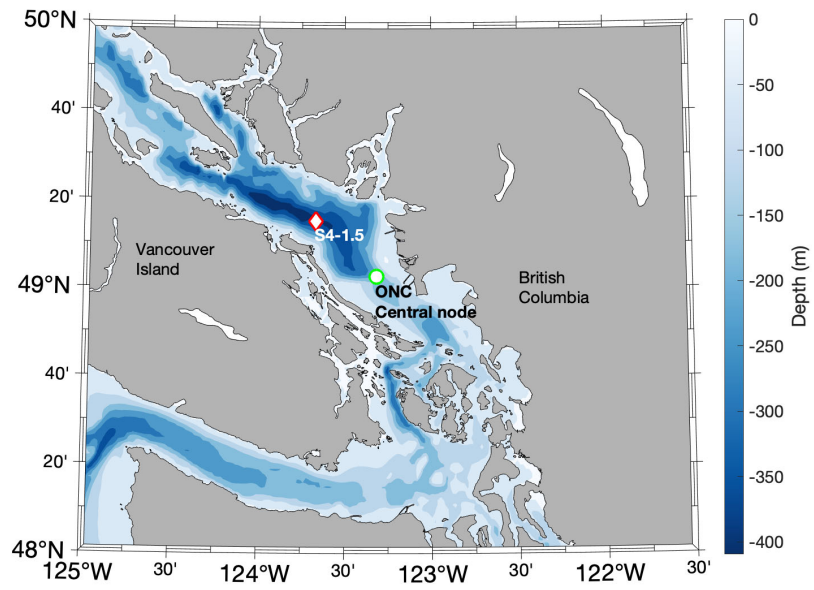


Figure A.3. Location of Ocean Network Canada’s Central node relative to our time-series station (S4-1.5) in the Strait of Georgia.

Appendix B. Supplementary tables

Table B.1. Depths and salinity of dissolved samples collected for trace metal analysis. Exact sampling depths were determined for seasonal sampling at station S4-1.5 onboard the CCGS hovercraft post-cruise using the CTD's pressure versus time data. No CTD data were available for the April 2018 trace metal bottle casts. The best estimates of April's exact sampling depths were determined by taking the average \pm 1 SD of known depths from other sampling events on station (September 2017, December 2017, June 2018). For the August 2018 spatial sampling cruise onboard the CCGS Vector, only nominal depths were reported because the CTD was not attached during trace metal bottle casts.

Station	Cruise	Depth [m]	Salinity Practical	Bottle salinity g/kg
S4-1.5	Sep.2017	0		
S4-1.5	Sep.2017	5	27.4	
S4-1.5	Sep.2017	9	27.8	
S4-1.5	Sep.2017	19	29.0	
S4-1.5	Sep.2017	28	29.2	
S4-1.5	Sep.2017	48	29.3	
S4-1.5	Sep.2017	74	29.9	
S4-1.5	Sep.2017	95	30.3	
S4-1.5	Sep.2017	144	30.8	
S4-1.5	Sep.2017	192	31.0	
S4-1.5	Sep.2017	240	31.1	
S4-1.5	Sep.2017	288	31.1	
S4-1.5	Dec.2017	0		
S4-1.5	Dec.2017	4	23.9	
S4-1.5	Dec.2017	9	26.6	
S4-1.5	Dec.2017	18	28.0	
S4-1.5	Dec.2017	28	29.2	
S4-1.5	Dec.2017	46	30.1	
S4-1.5	Dec.2017	72	30.3	
S4-1.5	Dec.2017	93	30.6	
S4-1.5	Dec.2017	142	30.8	
S4-1.5	Dec.2017	187	30.8	
S4-1.5	Dec.2017	233	31.1	
S4-1.5	Dec.2017	282	31.2	
S4-1.5	Apr.2018	0		
S4-1.5	Apr.2018	4 \pm 1	27.9	

Station	Cruise	Depth [m]	Salinity Practical	Bottle salinity g/kg
S4-1.5	Apr.2018	9 ± 0	28.5	
S4-1.5	Apr.2018	19 ± 1	29.2	
S4-1.5	Apr.2018	28 ± 0	29.5	
S4-1.5	Apr.2018	47 ± 1	29.9	
S4-1.5	Apr.2018	75 ± 4	30.1	
S4-1.5	Apr.2018	97 ± 5	30.2	
S4-1.5	Apr.2018	145 ± 4	30.4	
S4-1.5	Apr.2018	192 ± 6	30.6	
S4-1.5	Apr.2018	239 ± 5	30.7	
S4-1.5	Apr.2018	287 ± 4	30.9	
S4-1.5	Jun.2018	0		
S4-1.5	Jun.2018	4	17.9	
S4-1.5	Jun.2018	9	23.0	
S4-1.5	Jun.2018	19	28.7	
S4-1.5	Jun.2018	28	29.4	
S4-1.5	Jun.2018	47	29.7	
S4-1.5	Jun.2018	79	30.1	
S4-1.5	Jun.2018	102	30.2	
S4-1.5	Jun.2018	150	30.6	
S4-1.5	Jun.2018	198	30.8	
S4-1.5	Jun.2018	243	30.9	
S4-1.5	Jun.2018	290	31.1	
S4-1.5	Aug.2018	0		
S4-1.5	Aug.2018	5	28.4	
S4-1.5	Aug.2018	10	28.9	
S4-1.5	Aug.2018	20	29.3	
S4-1.5	Aug.2018	30	29.4	
S4-1.5	Aug.2018	50	29.8	
S4-1.5	Aug.2018	75	30.3	
S4-1.5	Aug.2018	100	30.5	
S4-1.5	Aug.2018	150	30.9	
S4-1.5	Aug.2018	200	31.0	
S4-1.5	Aug.2018	250	31.2	
S4-1.5	Aug.2018	330	31.3	
NG	Aug.2018	0		
NG	Aug.2018	5	27.7	
NG	Aug.2018	10	28.9	

Station	Cruise	Depth [m]	Salinity Practical	Bottle salinity g/kg
NG	Aug.2018	20	29.2	
NG	Aug.2018	30	29.4	
NG	Aug.2018	50	29.6	
NG	Aug.2018	75	30.0	
NG	Aug.2018	100	30.3	
NG	Aug.2018	150	30.6	
NG	Aug.2018	200	30.7	
NG	Aug.2018	250	30.8	
NG	Aug.2018	330	30.8	
HS	Aug.2018	0		
HS	Aug.2018	10	29.8	
HS	Aug.2018	30	30.6	
HS	Aug.2018	50	30.9	
HS	Aug.2018	100	32.1	
HS	Aug.2018	200	32.5	
JF2	Aug.2018	0		31.081
JF2	Aug.2018	10		31.336
JF2	Aug.2018	20		31.550
JF2	Aug.2018	40		32.327
JF2	Aug.2018	50		32.844
JF2	Aug.2018	60		33.083
JF2	Aug.2018	80		
JF2	Aug.2018	100		33.882
JF2	Aug.2018	140		33.917
JF2	Aug.2018	160		33.918
JF2	Aug.2018	180		33.918

Table B.2. Measured concentrations of dissolved Ag and Cd from September 2017 to August 2018 at station S4-1.5 located in the southern Strait of Georgia. Analytical errors reported are based on one standard deviation. Samples analyzed by standard additions are bolded.

Cruise	Depth [m]	dAg [pmol/kg]	dAg error [pmol/kg]	dCd [pmol/kg]	dCd error [pmol/kg]
Sep.2017	0	5.5	0.5	480	11
Sep.2017	5	5.1	0.5	507	11
Sep.2017	9	6.6	0.5	627	12
Sep.2017	19	7.1	0.5	619	12
Sep.2017	28	10.1	0.5	624	12
Sep.2017	48	8.2	0.5	623	12
Sep.2017	74	8.9	0.6	646	11
Sep.2017	95	7.1	0.5	656	11
Sep.2017	144	7.7	0.6	666	11
Sep.2017	192	7.2	0.6	687	10
Sep.2017	240	7.5	0.5	688	11
Sep.2017	288	8.7	0.6	690	10
Dec.2017	0	11.9	0.5	550	12
Dec.2017	4	9.7	0.1	573	11
Dec.2017	9	9.4	0.5	590	11
Dec.2017	18	11.1	0.5	635	11
Dec.2017	28	8.7	0.4	640	11
Dec.2017	46	9.6	0.5	658	12
Dec.2017	72	11.3	0.5	657	10
Dec.2017	93	8.1	0.5	673	11
Dec.2017	142	7.1	0.6	676	11
Dec.2017	187	7.7	0.5	681	10
Dec.2017	233	8.1	0.5	672	10
Dec.2017	282	10.1	0.2	670	10
Apr.2018	0	6.7	0.4	546	5
Apr.2018	4	10.3	0.5	573	5
Apr.2018	9	7.6	0.4	584	6
Apr.2018	19	8.6	0.5	647	6
Apr.2018	28	9.6	0.4	654	6
Apr.2018	47	9.4	0.4	632	7
Apr.2018	75	9.4	0.6	631	6
Apr.2018	97	9.5	0.5	643	6
Apr.2018	145	8.3	0.4	663	6

Cruise	Depth [m]	dAg [pmol/kg]	dAg error [pmol/kg]	dCd [pmol/kg]	dCd error [pmol/kg]
Apr.2018	192	11.3	0.6	666	6
Apr.2018	239	11.9	0.6	649	6
Apr.2018	287	11.7	0.5	658	6
Jun.2018	0	7.3	0.4	269	4
Jun.2018	4	5.5	0.2	275	4
Jun.2018	9	5.6	0.1	396	2
Jun.2018	19	5.7	0.3	569	6
Jun.2018	28	5.6	0.3	596	6
Jun.2018	47	6.9	0.5	636	6
Jun.2018	79	7.9	0.4	641	6
Jun.2018	102	8.2	0.1	631	5
Jun.2018	150	8.5	0.5	633	6
Jun.2018	198	10.0	0.5	648	6
Jun.2018	243	9.9	0.6	653	6
Jun.2018	290	9.3	0.5	660	6
Aug.2018	0	5.7	0.3	463	15
Aug.2018	5	3.4	0.2	538	16
Aug.2018	10	5.7	0.3	627	18
Aug.2018	20	6.3	0.3	628	4
Aug.2018	30	7.2	0.3	628	4
Aug.2018	50	7.1	0.2	626	4
Aug.2018	75	6.5	0.3	649	4
Aug.2018	100	7.2	0.3	676	15
Aug.2018	150	8.0	0.3	681	15
Aug.2018	200	8.7	0.1	690	15
Aug.2018	250	9.1	0.4	691	15
Aug.2018	330	7.2	0.3	717	16

Table B.3. Measured concentrations of dissolved Ag and Cd in the northern Strait of Georgia (NG), in Haro Strait (station HS), and in Juan de Fuca Strait (station JF2) in August 2018. Analytical errors reported are based on one standard deviation. Samples analyzed by standard additions are bolded. Depths reported are nominal.

Station	Depth [m]	dAg [pmol/kg]	dAg error [pmol/kg]	dCd [pmol/kg]	dCd error [pmol/kg]
NG	0	4.5	0.2	484	15
NG	5	6.2	0.3	552	16
NG	10	7.8	0.4	595	17
NG	20	7.3	0.3	611	4
NG	30	7.8	0.3	624	5
NG	50	8.1	0.4	625	5
NG	75	8.2	0.4	643	4
NG	100	8.1	0.4	674	15
NG	150	9.7	0.4	673	15
NG	200	9.5	0.4	673	15
NG	250	9.4	0.4	667	15
NG	330	10.2	0.4	667	15
HS	0	5.9	0.3	629	5
HS	10	5.7	0.1	626	5
HS	30	5.8	0.3	674	16
HS	50	5.6	0.3	691	16
HS	100	6.0	0.1	730	18
HS	200	5.4	0.3	758	19
JF2	0	6.1	0.1	686	9
JF2	10	6.0	0.3	703	9
JF2	20	6.0	0.2	718	10
JF2	40	6.0	0.2	733	12
JF2	50	5.9	0.1	743	11
JF2	60	5.6	0.3	745	12
JF2	80	5.2	0.3	748	12
JF2	100	5.1	0.1	819	5
JF2	140	5.3	0.3	819	5
JF2	160	5.4	0.3	824	5
JF2	180	5.5	0.3	813	5

Table B.4. Sample calculation for calculating volume-weighted average concentrations of dissolved Cd in the Strait of Georgia water column.

depth_sep (m)	cd_sep (pmol/kg)	mid depth (m)	Upper 50 m		Water column average	
0	480		0-2.5	1200	0-2.5	1200
		2.5	2.5-7	2279	2.5-7	2279
5	507		7-14	4386	7-14	4386
		7	14-23.5	5884	14-23.5	5884
9	627		23.5-38	9055	23.5-38	9055
		14	38-48	6225	38-48	6225
19	619		sum	29030	48-61	8093
		23.5	weighted pmol/kg	605	61-84.5	15176
28	624		pM	618	84.5-119.5	22949
		38			119.5-168	32297
48	623		50 m - bottom		168-216	32984
		61	48-61	8093	216-264	33009
74	646		61-84.5	15176	264-288	16561
		84.5	84.5-119.5	22949	Sum	190099
95	656		119.5-168	32297	weighted pmol/kg	660
		119.5	168-216	32984	pM	675
144	666		216-264	33009		
		168	264-288	16561		
192	687		sum	161070		
		216	weighted pmol/kg	671		
240	688		pM	687		
		264				
288	690					

Table B.5. Particulate metal concentrations in particles collected at station S4-1.5 in the southern Strait of Georgia in December 2018 and April 2018.

Analytical errors reported are based on one standard deviation.

Cruise	Depth [m]	pAg [pM]	pAg error [pM]	pCd [pM]	pCd error [pM]	pAl [nM]	pAl error [nM]	pP [nM]	pP error [nM]
Dec.2017	0	2.22	0.07	9.3	0.2	792	45	32	3
Dec.2017	4	1.71	0.04	14.9	0.4	914	23	29	2
Dec.2017	9	1.55	0.06	17.3	0.5	753	35	25	2
Dec.2017	18	0.61	0.06	20.7	1.4	291	16	17	2
Dec.2017	28	0.38	0.03	26.2	0.7	151	6	11	1
Dec.2017	46	0.47	0.05	34.7	2.1	37	4	4	1
Dec.2017	72	0.23	0.03	25.6	0.8	76	4	11	1
Dec.2017	93	0.39	0.03	10.8	0.2	151	8	9	1
Dec.2017	142	0.70	0.05	17.0	0.9	443	25	14	1
Dec.2017	187	0.89	0.09	22.4	1.9	881	37	25	2
Dec.2017	233	0.60	0.04	33.9	1.4	528	26	20	1
Dec.2017	282	0.43	0.04	25.9	2.1	211	8	12	1
Apr.2018	0	1.88	0.13	15.8	1.0	352	9	191	6
Apr.2018	4	1.70	0.21	20.6	1.9	315	19	188	7
Apr.2018	9	0.88	0.04	7.3	0.3	53	4	111	3
Apr.2018	19	0.35	0.03	5.3	0.1	13	4	40	3
Apr.2018	28	0.37	0.03	17.6	0.2	108	9	28	2
Apr.2018	47	0.35	0.03	35.4	0.9	134	5	17	2
Apr.2018	75	0.23	0.02	29.5	0.2	159	5	19	1
Apr.2018	97	0.32	0.03	18.2	0.2	218	3	19	1
Apr.2018	145	1.33	0.03	16.8	0.3	1115	33	41	2
Apr.2018	192	0.67	0.03	33.3	0.4	920	21	41	2
Apr.2018	239	0.58	0.04	36.3	0.8	807	24	31	1
Apr.2018	287	0.61	0.02	40.3	1.4	611	14	30	2

Table B.6. Concentrations of dissolved and total Cd in wastewater samples measured in influent and effluent from the Iona WWTP, and screened samples from Macaulay Point and Clover Point outfalls. 24-hr composite wastewater samples (250 mL) collected at each outfall were sent to our UBC lab every two months between November 2017 and November 2018. Duplicates (A & B) of 25 mL aliquots were taken to measure total metal concentrations and the dissolved fractions.

Dissolved Cd (pM)	Nov-17	Jan-18	Mar-18	Jun-18	Sep-18	Nov-18
Iona effluent A	97	124	104	56	70	115
Iona effluent B	97	123	102	67	60	112
Iona influent A	60	108	69	75	85	96
Iona influent B	71	107	67	65	64	106
Macaulay A	1280	312	3091	552	224	189
Macaulay B	1255	326	3326	511	269	202
Clover A	192	215	240	209	142	191
Clover B	202	210	231	226	163	194

Total Cd (pM)	Nov-17	Jan-18	Mar-18	Jun-18	Sep-18	Nov-18
Iona effluent A	481	598	601	489	401	428
Iona effluent B	526	656	575	489	404	458
Iona influent A	774	728	899	998	1020	671
Iona influent B	821	749	910	859	820	834
Macaulay A	6012	918	11576	2683	1843	1471
Macaulay B	6009	950	11149	2704	1815	1560
Clover A	1684	722	1264	1262	1795	1836
Clover B	1882	731	1178	1333	1857	1846

Table B.7. Concentrations of dissolved and total Ag in wastewater samples measured in influent and effluent from the Iona WWTP, and screened samples from Macaulay Point and Clover Point outfalls. 24-hr composite wastewater samples (250 mL) collected at each outfall were sent to our UBC lab every two months between November 2017 and November 2018. Duplicates (A & B) of 25 mL aliquots were taken to measure total metal concentrations and the dissolved fractions.

Dissolved Ag (pM)	Nov-17	Jan-18	Mar-18	Jun-18	Sep-18	Nov-18
Iona effluent A	576	231	398	373	208	359
Iona effluent B	596	231	411	436	148	553
Iona influent A	384	201	341	548	345	579
Iona influent B	422	201	375	511	271	499
Macaulay A	330	198	475	558	233	352
Macaulay B	298	221	730	508	328	372
Clover A	272	790	422	771	496	682
Clover B	292	1055	426	1100	725	730

Total Ag (pM)	Nov-17	Jan-18	Mar-18	Jun-18	Sep-18	Nov-18
Iona effluent A	1232	656	1626	1678	949	1439
Iona effluent B	1355	672	1548	1677	1115	1465
Iona influent A	2317	739	2289	3749	2590	2094
Iona influent B	2938	723	2272	3976	2335	1988
Macaulay A	2246	1146	10542	6962	2295	2114
Macaulay B	2241	1104	3910	3404	3251	2314
Clover A	2215	38096	3630	11508	5896	4204
Clover B	2378	36740	4054	13322	8084	4627

Table B.8. Average concentrations dissolved, particulate, and total Ag and Cd measured in the 2015 Iona effluent samples. Particulate Cd is calculated by subtracting measured values of dissolved Cd from the total. Total annual flow rates reported for the year of 2015 (Metro Vancouver, personal communication).

2015 Iona effluent	Average conc.	2015 Annual flow	Annual flux	Ag loading
	pM	L/yr	mole/yr	kg/yr
Dissolved Ag	767	1.85E+11	142	15.3
Particulate Ag*	983		182	19.6
Total Ag	1750		324	35.0
Dissolved Cd	415		77	8.6
Particulate Cd*	846		157	17.6
Total Cd	1261		234	26.3

Appendix C. Preliminary laboratory experiments to determine dissolved Ag uptake rates by SoG calanoid copepods (*Metridia pacifica*) and by a model diatom (*Thalassiosira oceanica*)

C.1. Uptake of dissolved Ag by calanoid copepods in the SoG

Wang and Fisher (1998) used a kinetic model to quantify the relative importance of Ag uptake in the marine copepod *Temora longicornis* from ingested food and the dissolved phase. Their results showed that more than 50% of Ag accumulated in copepods were taken up from the dissolved phase. Additionally, the Ag uptake rate increased linearly with concentrations of dissolved Ag (dAg) over a range between 0.09 and 4.6 nM (Wang & Fisher, 1998). We repeated their experiments for dAg uptake from seawater at a lower concentration range, which was 0 - 200 pM above background, in filtered seawater from the SoG. The range was chosen based on reported concentrations of dAg in the global ocean (Kramer et al., 2011; Martin et al., 1983; Ndung'u et al., 2001; Ndungu, 2011; Zhang et al., 2004) , including contaminated waters such as the San Francisco Bay (Smith & Flegal, 1993) to assess accumulation of Ag in marine zooplankton in both pristine and contaminated environments.

In September 2017, on board the Canadian Coast Guard ship Siyay, we collected live zooplankton using a whole water column vertical Bongo net (250 μm mesh) at station S4-1.5 in the southern SoG. Immediately after collection, the live zooplankton were gently size fractionated using 250, 500, 1000, 2000 and 4000 μm sieves. The different size fractions were immediately transferred to separate buckets, filled with SoG seawater, to carefully transport the live zooplankton to UBC laboratory. Samples were then examined under the microscope and, based on species abundance, calanoid copepods, from the 500 μm fraction, were selected for the dAg uptake experiment.

Twenty copepods were handpicked into acid cleaned holding bottles filled with 100 mL of GFF (0.7 μm pore size) filtered SoG seawater and allowed to depurate overnight. In the meantime, duplicate experimental bottles were prepared by adding 0 pM (control with background dissolved Ag concentration in the SoG seawater), 10 pM, 50 pM, and 200 pM of non-radioactive AgNO_3 solution to 100 mL of filtered SoG seawater. Then a spike of the radiotracer $^{110\text{m}}\text{Ag}$ ($t_{1/2} = 249.9$

days) was added to reach a total activity of ~ 2000 cpm (20 cpm/mL) in each experimental bottle, and the water was allowed to equilibrate overnight. The initial activity in 1 mL aliquot of each uptake bottle was then measured to determine the specific activity of $^{110\text{m}}\text{Ag}$.

Once the water had reached equilibrium with the radiotracer $^{110\text{m}}\text{Ag}$, copepods were filtered onto a 250 μm mesh and transferred immediately into the experimental bottles. The copepods were then exposed for 24 hrs to the $^{110\text{m}}\text{Ag}$ -spiked seawater with varying concentrations of dAg. At the end of the uptake experiment, they were filtered onto a mesh, rinsed with chelexed synthetic ocean water (SOW) to remove extracellular adsorbed $^{110\text{m}}\text{Ag}$, and radio-assayed using a Wallac 1480 Wizard Gamma Counter (PerkinElmer). To determine the exact $^{110\text{m}}\text{Ag}$ specific activity in our experiment, the filtrate was collected into acid-cleaned bottles to determine the precise concentrations of dAg once the $^{110\text{m}}\text{Ag}$ has decayed. Any dAg contamination (from field sampling and laboratory manipulations) in the SoG seawater used for the uptake experiment would be reflected by the final concentrations measured in the filtrate.

Accumulation of dAg in copepods after 24 hrs of exposure was calculated from the measured activities (cpm) in the copepods collected on a mesh and a rough estimate of the Ag specific activity (cpm/mol), assuming a background dAg concentration of 10 pM in ambient SoG seawater, and the concentrations of AgNO_3 added for the different treatments. Silver influx rates (pmol/copepod/hr) were calculated for each treatment. Our results showed a positive linear relationship between dAg concentrations in seawater and Ag uptake rates in copepods (Figure C.1). The uptake rate constant for dAg can be calculated from the slope of the regression line ($2.9\text{E-}6$ L/copepod/hr). Examination of formalin-preserved copepods under the microscope showed that all copepods used in our experiment were *Metridia pacifica* in the copepodid stages IV and V. With a rough estimate of the dry weight of one individual (23 μg ; Kwong, 2016), we calculated a dAg uptake rate constant of 2.9 L/g/d in SoG copepods. Our estimate is lower than the 10 L/g/d reported for the marine copepod *Temora longicornis* (Wang and Fisher, 1998). This could be due to inherent differences between copepod species, or potential efflux of dAg during our long-term uptake (24 hrs) experiment, relative to the short-term experiment (4 hrs) performed by Wang and Fisher (1998). Nevertheless, our results show evidence of dAg uptake in SoG calanoid copepods,

and the uptake rate has not plateaued with the highest addition (200 pM) in our experiment. Our estimated dAg uptake rate constant (2.9 L/g/d) can be used in models to predict accumulation of Ag in the pelagic food web, and to compare toxicity of trace metals to aquatic organisms.

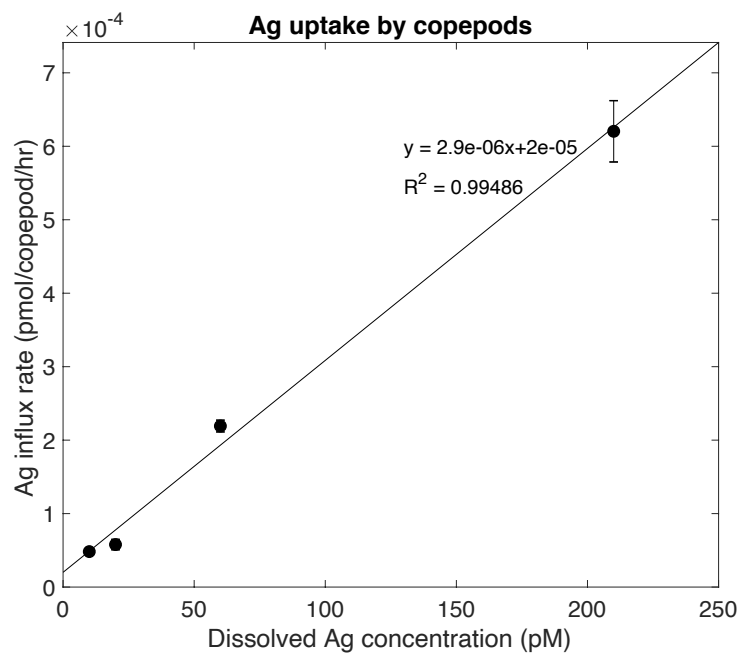


Figure C.1. Influx rates of dissolved Ag in calanoid copepods as a function of ambient dissolved Ag concentration. Error bars represent the range of influx rates from duplicates.

C.2. Uptake of dissolved Ag by marine phytoplankton

Uptake of dAg by marine phytoplankton were conducted on a model oceanic diatom, *Thalassiosira oceanica* (CCMP 1003). Lee et al. (2004) speculated that phytoplankton uptake of Ag^+ in the dissolved phase is likely accidental via membrane transporters for other essential metals ions with an electric charge of +1, such a Cu^+ . Under this premise, we hypothesize that Cu-limited phytoplankton will take up more dAg via the high-affinity Cu^+ transport system, which is upregulated under low Cu conditions (Guo et al., 2010). Since *T. oceanica* can be easily acclimated in Cu-limited media, it was chosen as our study organism. *T. oceanica* was grown in semi-continuous batch cultures using the artificial seawater medium Aquil (Price et al., 1989) at $19 \pm 1^\circ$ under a continuous light intensity of $150 \mu\text{mol quanta m}^{-2} \text{s}^{-1}$ (Maldonado & Price, 2001). Cultures

were acclimated in Cu-replete (10.2 nM) and Cu-limited (1 nM) media, as described by Maldonado et al. (2006). Trace metal clean and sterile techniques were employed for all media and culture manipulations. Cell growth was monitored daily by measuring in vivo chlorophyll a fluorescence with a 10-AU fluorometer (Turner Designs). Cell density and size (μm) were determined using a Coulter Z2 Particle Count and Size Analyzer (Beckman Coulter). Cell surface area and volume were calculated assuming a spherical cell shape. *T. oceanica* was inoculated in June 2017 and cultures were routinely transferred when cells reached the exponential phase of growth. Daily fluorescence measurements showed a reduction in growth rates from $1.34 \pm 0.09 \text{ d}^{-1}$ (n=10) in Cu-replete cells to $0.90 \pm 0.05 \text{ d}^{-1}$ (n=3) in Cu-limited cells.

250 mL Cu-replete cultures of *T. oceanica* were grown to mid-exponential phase ($\sim 175,000$ cells/mL; cell size: $5 \mu\text{m}$) and then harvested to undergo a short-term dAg uptake experiment. Cells were collected onto acid-cleaned 47 mm polycarbonate filters with a pore size of $2 \mu\text{m}$ by gentle vacuum, and then rinsed with 10 mL of SOW. The filter was immediately resuspended into 250 mL of chelexed SOW spiked with the radiotracer $^{110\text{m}}\text{Ag}$ with an initial activity of 30 cpm/mL. Initial sampling time was 10 minutes after resuspension, followed by 15 – 30 minutes intervals and up to 2 hours. At each time point, 25 mL of culture was subsampled and filtered onto a $2 \mu\text{m}$ polycarbonate membrane (25mm diameter). The cells were soaked in 1 mM of DTPA wash solution for 5 minutes to remove extracellular adsorbed $^{110\text{m}}\text{Ag}$, then rinsed with 5 mL of chelexed SOW to remove any loosely associated tracer. The filters were radioassayed using a Gamma Counter.

Our results from the uptake experiment showed that nutrient-replete cells took up dAg steadily for 45 minutes (Figure C.2), and intracellular $^{110\text{m}}\text{Ag}$ activity plateaued after 85 minutes of exposure. The last time point (2 hr) was discarded due to inconsistent activities measured in duplicate samples, resulting in large analytical uncertainties. Based on the 3 data points collected within the first hour, an uptake rate of $0.0058 \text{ zmol} \cdot \text{cell}^{-1} \cdot \text{hr}^{-1}$ ($\text{zmol} \cdot \text{cell}^{-1} \cdot \text{hr}^{-1} = 10^{-21} \text{ mol} \cdot \text{cell}^{-1} \cdot \text{hr}^{-1}$) was determined by the linear regression of intracellular Ag as a function of time. In comparison with the measured dissolved Cu uptake rate by *T. oceanica* ($26 \pm 8 \text{ zmol} \cdot \text{cell}^{-1} \cdot \text{h}^{-1}$, Guo et al., 2010) grown in the same nutrient conditions, our dAg uptake rate was 3 orders of magnitude slower.

Although a small dAg uptake rate was expected for Cu-replete cells based on our hypothesis, this rate is likely underestimated because we did not take into account the background dAg concentration present in the uptake media, hence the calculated specific activity (cpm/mol) based solely on the added spike of ^{110m}Ag was inaccurate. The next step forward is to measure the concentration of dAg in the uptake media and focus on collecting data within 1 hour of exposure in order to confirm the linear trend of Ag uptake. Once we have gained more confidence in the dAg uptake rate of Cu-replete cells, the experiment can be repeated for Cu-limited cells, which we would expect a higher dAg uptake rate.

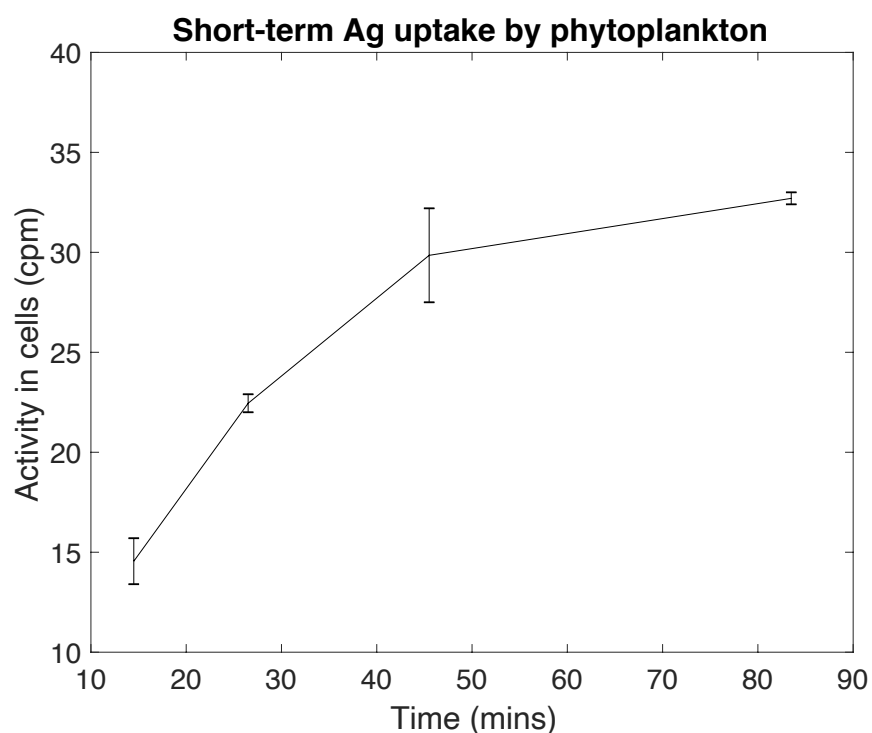


Figure C.2. Ag accumulated in a marine diatom species *Thalassiosira oceanica* as a function of time. Error bars represent the range of counts in cpm from duplicates.